Polysiloxane-Based Liquid Crystal Block Copolymers for Piezoelectric and Mechano-Optical Applications

by

LaRuth C. McAfee

B.S.E. Chemical Engineering
The University of Michigan
(1999)

Submitted to the Department of Chemical Engineering
In Partial Fulfillment of the
Requirements for the Degree of

DOCTOR OF PHILOSOPHY

At the

MASSACHUSETTS INSTITUTE OF TECHNOLOGY
June 2005

© Massachusetts Institute of Technology (2005)

MASSACHUSETTS INSTITUTE OF TECHNOLOGY
JUN 0 1 2005
LIBRARIES

Signature of Author .....
LaRuth C. McAfee
May 16, 2005

Certified by .....
Paula T. Hammond
Mark Hyman, Jr., Associate Professor of Chemical Engineering

Accepted by.....
Daniel Blankschtein
Department of Chemical Engineering
Chairman, Committee for Graduate Students

ARCHIVES

Abstract

Liquid crystal research has gained interest in a wide range of applications that go beyond displays. Some of these applications include memory devices, sensors, and variable light valves. Currently, liquid crystals in the form of small molecules are capable of exhibiting fast response times; however, there are many advantages to using block copolymers in these applications, such as the surface stabilization caused by the block copolymer morphology, and recent research has increased in the area of LC block copolymers. In this group, LC block copolymer research has focused on diblock copolymers with one amorphous block and one side-chain LC block, and examined fundamental phase behavior of these complex systems, and the interplay between liquid crystal and block copolymer ordering.

This research seeks to examine the potential use of ferroelectric and nematic LC block copolymer elastomers as actuators. These devices can be used as artificial muscles, in microrobotics, in micromachinery, in MEMS, and in other applications that require gates or valves. Artificial muscles have previously been prepared using multilayer composites of conducting polymers and non-conducting materials that may or may not be polymers. Similar functionality could also be accomplished by preparing an amorphous-LC block copolymer with cylindrical morphology. The proposed polymers for this research offer unique processing, mechanical, and electrical advantages over the current technologies because they are both block copolymers and elastomers. The main issues that need to be examined when designing such a material are the response time after an electrical pulse has been applied, the amount of strain achievable, and, if used in biological applications, the biocompatibility of the materials.

This project specifically studies the first two issues. In order to do this, block copolymers with side-chain liquid crystal mesogens have been synthesized and their properties are currently being studied. Initially, a polystyrene-b-polyvinylmethylsiloxane diblock copolymer backbone with side-chain LC mesogens was studied. Diblock studies are useful as model systems and have potential for electro-optic applications. However, studies on PS-b-PVMS-b-PS triblock copolymers allow us to make a true elastomer. The mesogens were chosen such that the nematic or smectic C* phase will be present at the desired operating temperature and electromechanical actuation can be obtained.

Mesogens were attached to homopolymer and BCP backbones. DSC indicated that there was phase mixing in all BCP samples because the PS T_g is lowered or absent upon attachment of the mesogen. Nematic mesogens with long alkyl spacers exhibited significant phase mixing and no PS T_g unless the polymer backbone was initially more than 50wt% PS. SAXS data showed strong smectic LC order (d=35-55Å), but weak (d=225-480Å) or no BCP order in films at room temperature. TEM and AFM indicated poorly ordered segregated morphologies in samples, which agreed well with the SAXS data. Mesogens with short spacers strengthened BCP phase segregation, as indicated by well-defined block copolymer peaks in SAXS and well-defined interfaces in TEM images. At room temperature, some samples did not exhibit liquid crystalline textures or birefringence until sheared or stretched when viewed in the polarized optical microscope, indicating mechano-optical properties.

Initial attempts to orient the liquid crystal mesogens have been successful using mechanical stretching in the DMA. Also, a new setup has been developed and preliminary studies have begun to measure the electromechanical properties of these materials.

Acknowledgements

Many people have supported me throughout my time at MIT. First, I would like to acknowledge my advisor, Prof. Paula Hammond. She has consistently provided excellent advice and motivation for me. Additionally, she has a wonderful ability to see the good in all results, which helped to keep me excited when my research was not progressing as quickly as I wanted it to. My committee members, Prof. Robert E. Cohen and Prof. T. Alan Hatton, have also been especially supportive and have offered excellent guidance during my research and my job search.

I would also like to acknowledge the members of the Hammond Research Group for their support during my thesis research. When I first joined the group, Dr. Aaron Moment, Dr. Mitch Anthamatten, Dr. Cathy Santini, and Dr. Mark Johnson helped teach me the syntheses techniques and trained me on many pieces of equipment. Throughout my research, Ms. LaShanda James-Korley and Mr. Greg Pollock have been great people with whom I could discuss ideas. Recently, Dr. Bruce Yu, Mr. Keith Reed (UROP), Mr. Eric Verploegen, and Dr. Lu Tian have been of great help with synthesizing mesogens and working to develop new polymerization techniques.

Staff in the Center for Materials Science and Engineering (NSF Award DMR-9400334) and researchers in the Institute for Soldier Nanotechnologies have been extremely helpful in training me on many pieces of equipment. At the CMSE, Mr. Peter Kloumann and Mr. Joe Adario helped with SAXS training and support, Mr. Mike Frongillo and Mr. Patrick Boisvert helped with my TEM and cryotome research, and Mr. Tim McClure on the low-temperature DSC. All of these staff members were willing to give their time to answer questions and help when machines did not work as I expected them to. Without their support and immense amounts of knowledge from years of experience, my project would have been much more difficult.

In the ISN, many researchers have supported my research. In addition to members of the Hammond Group, I would like to acknowledge Ms. Rachel Pytel and Dr. Brian Pate for their support with the x-ray scattering equipment. Rachel was also very helpful as we considered methods in which to measure actuator properties of our materials by explaining techniques used in the Hunter Lab (Mechanical Engineering). In addition, for general chemistry lab support with setup and techniques, Dr. Brad Holliday should be acknowledged. I would also like to acknowledge the ISN and the NSF for financial support of this research.

During my time at MIT I have been involved in various groups and the friendships developed there have made my experience at MIT a positive one. The student groups include the Black Graduate Students Association, the Tang Hall Residents Association, the Graduate Student Council, and the residents of McCormick Hall $4^{th}/5^{th}$ West Floors. Additionally, administrators and staff in the Graduate Students Office, the Division of Student Life, the Office of the Provost, and the School of Engineering have supported me as friends and coworkers on many projects. Charles Shultz once said, "Try not to have a good time ... this is supposed to be educational." These people have demonstrated that fun and education can definitely go hand-in-hand.

Finally, I would like to acknowledge the many people outside of MIT who have supported me during my experience at MIT. My family and friends have always been supportive and encouraging, and they always knew how to cheer me up. My church families in Ann Arbor (Bethel AME) and Cambridge (St. Paul AME) have also been outstanding supporters and helped to remind me that God will never put more on us that we can bear.

This Thesis is Dedicated to

My Parents, Leo Jr. and Sandra,

and

My Brothers, Leo III and Lawrence.

They have provided an immense amount of
encouragement and support during this doctoral process.
For that and other support throughout my life,
I will forever be grateful.

"Education is simply the soul of a society
as it passes from one generation to another."
– Gilbert Keith Chesterton

Table of Contents

List of Figures

List of Tables

Chapter 1 – Introduction and Background

Project Overview

Liquid crystal research has gained interest due to the usefulness of liquid crystals in many applications other than displays. These materials are part of the family of "soft materials" that have been studied in nanotechnology[1]. Some of these applications include displays, memory devices, sensors, and variable light valves. Currently, liquid crystals are in the form of small molecules or LC homopolymers due to the fast response time that these molecules or polymers can achieve. However, there are many advantages to using block copolymers in these applications, such as surface stabilization caused by the block copolymer morphology, and recent research has increased in the area of LC block copolymers[2-12]. In this group, LC block copolymer research has focused on diblock copolymers with one amorphous block and one side-chain LC block[3, 4, 8, 9, 13-16]. The main drawback of these block copolymers is that the block copolymer interface and high viscosity of the smectic phase increase their response time.

This research seeks to examine the potential use of ferroelectric LC block copolymer elastomers as actuators. These devices can be used as artificial muscles, in microrobotics, in micromachinery, in MEMS devices, and in other applications that require gates or valves. More recently, such materials have been studied for use in defense applications related to soldier survivability. Artificial muscles have previously been prepared using multilayer composites of conducting polymers and non-conducting materials that may or may not be polymers[17-19]. This structure could also be accomplished by preparing an amorphous-LC block copolymer with lamellar or cylindrical morphology. One group has studied the possibility of using elastomeric main-chain LC polymers as actuators[20] due to the ability to mechanically orient ferroelectric

materials using an electric field. The proposed polymers for this research offer unique processing, mechanical, and electrical advantages over the current technologies because they are both thermoplastic block copolymers and elastomers.

By being thermoplastic elastomers, these materials will allow for unique processing opportunities through heating and physical crosslinks. Many groups that study LC polymers use chemical crosslinks to make elastomers[21]. Therefore, those materials cannot be reprocessed once prepared. However, in the materials studied in this research, reprocessing opportunities exist through the use of physical crosslinks. Additionally, many materials studied for ferroelectric and piezoelectric applications are quite rigid, such as ceramics[22]. In such materials the achievable strain is very low (<1%) due to the rigidity. However, in the materials studied in this research, larger strains will be possible owing to the elastomeric flexibility.

The main issues that need to be examined when designing such a material are the response time after an electrical pulse has been applied, the amount of strain achievable, and, if used in biological applications, the biocompatibility of the materials[19]. This project will specifically study the first two issues. In order to do this, block copolymers that exhibit ferroelectric properties were prepared and their properties were studied. Polymers studied include polystyrene-b-polyvinylmethylsiloxane diblock copolymer backbones with side-chain LC mesogens. One PS-PVMS-PS triblock copolymer backbone was also used for comparison. Diblock studies were useful as model systems and may have some potential for electro-optic applications. However, studies on PS-b-PVMS-b-PS triblock copolymers allow us to make a true elastomer. Ideally, the LC block should have mesogens such that the smectic C* phase is present at the desired operating temperature and ferroelectric properties can be accessed. However, LCPs that exhibit the nematic phase have also been studied because they can also be

used as actuators. Various processing techniques were studied in order to determine to what extent processing affects the material properties.

Background

A. Small Molecule Liquid Crystals

Liquid crystals are small molecules that exhibit order when in the liquid state. This order can be one- or two-dimensional and is temperature-dependent. LC's were first described by the Austrian botanist Friedrich Reinitzer in 1888 and the term "liquid crystal" was coined in 1889 by the German scientist Otto Lehmann. LC small molecules must be rigid, and they often have aromatic groups in order to achieve that rigidity. Although there are many acknowledged LC mesophases, for this research, the main mesophases are the nematic (N), smectic A (S_A), and smectic C (S_C) phases.

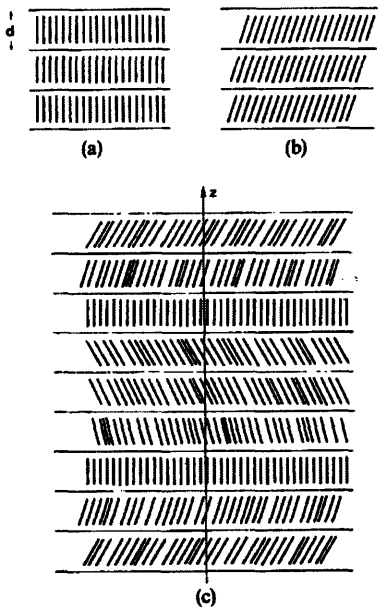

Fig. 2.8. Schematic representation of molecular arrangements in (a) smectic A, (b) smectic C and (c) chiral smectic C phases.

Figure 1.1: Smectic A, smectic C, and chiral smectic C LC mesophases[23]

In the S_A mesophase, the LC molecules are aligned in two dimensions because they are generally positioned parallel to the LC director and arranged in layers. The S_C phase is similar, except that the molecules in this phase are tilted at an angle θ from the director. A diagram of the S_A and S_C mesophases is shown in Figure 1. In chiral molecules, the angle θ will remain constant, but will rotate around the director in order to obtain an overall zero polarization in the system. This brings about the chiral smectic C (S_C*) phase. In the S_C* phase, the distance it takes to make one full rotation around the director is called the pitch of the molecule.

In the nematic phase, the LC molecules are again primarily aligned perpendicular to the director, but they are not arranged in layers. Therefore, this phase only has one dimension of order. As in the smectic phase, the nematic phase can occur with chiral molecules. In the chiral nematic (cholesteric) phase, the director will again rotate throughout the sample and a similar

definition of LC pitch applies. Figure 1.2 shows diagrams of the nematic (Fig. 1.2a) and chiral nematic (Fig. 1.2b) mesophases.

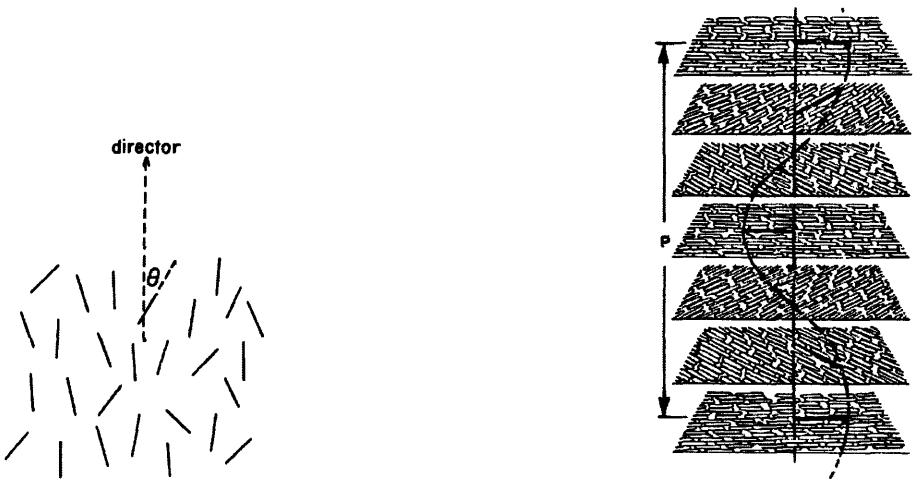

(a) (b)

Figure 1.2: a. Nematic LC arrangement[24]

b. Chiral nematic (cholesteric) LC arrangement[25]

As one would expect, as temperature increases the liquid crystal sample generally will go from the solid state to the smectic mesophase, followed by the nematic mesophase, then finishing with the isotropic liquid phase. This progression is reasonable due to the level of orientation observed in the various phases.

Since all the molecules are not perfectly aligned in any LC phase, an order parameter can be defined to give an idea of the level of order in a particular sample. Mathematically, this parameter is defined as:

$$S = \tfrac{1}{2}\left\langle 3\cos^2\theta - 1 \right\rangle \in [-\tfrac{1}{2}, 1] \qquad (1.1)$$

In this definition, the value of zero corresponds to a sample that is completely randomly oriented (isotropic liquid), while a value of one is a sample that is perfectly oriented. This value is only well defined for a well-ordered material, but it is still useful in giving an idea of the level of order in other systems.

Small molecule LC's can also be attached to polymer chains in order to combine the polymer properties with small molecule LC properties. The small molecules can be incorporated into the polymer main chain or connected as side chains off the polymer main chain using a spacer. There are also studies in which LC polymers have been synthesized with both main-chain LC's and side-chain LC's[26]. A diagram showing possibilities for structures of LC polymers follows in Figure 1.3.

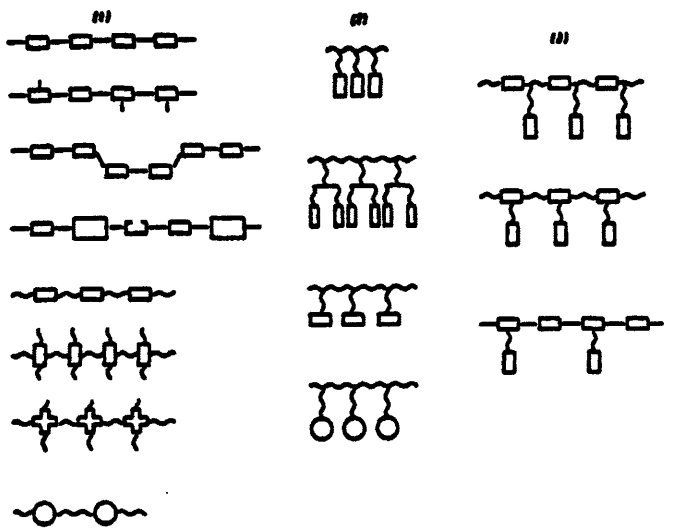

Schematic representation of various possible arrangements of mesogens in polymer chain structures (1) main chain, (2) side chain, and (3) combinations of main and side chain. (Adapted from D. Sek (1988) with permission from Akademie-Verlag).

Figure 1.3: Various polymer LC arrangements[25]

The use of side-chain LC polymers has many benefits over main-chain polymers including increased backbone flexibility and a decoupling of the polymer and LC properties. This type of polymer will be discussed in Section D. Main-chain polymers, however, do have advantages in some applications due to their enhanced electromechanical response.

When studying LC polymers, it is important to keep in mind that the polymer and the mesogen will impact the final properties. The mesogen, including terminal substituents and spacer, will primarily determine mesophases, while the polymer backbone, including tacticity and polydispersity, is secondary. Therefore, the polymer choice will mainly enhance, alter, or disrupt any mesogenic tendency. These tendencies are caused by the competition between the mesogens, which want to orient anisotropically, and the polymer, which wants to adopt a random coil conformation. Studies on LC polymers have shown that increasing the mesogen density in the polymer generally will not affect the T_g. However, it will affect the clearing point, especially using longer spacers[27]. Increasing mesogen density will also help the mesogens obtain smectic ordering. The LC spacer has been shown to impact final LCP properties. Finkelmann introduced the concept of a spacer in 1978[28] in order to decouple the mesogen movement from that of the polymer backbone. Studies have shown that some LCPs with short or no spacers will not exhibit LC properties. Further, shorter spacers generally induce nematic order due to the close coupling with the backbone, while longer spacers tend to allow for smectic order due to decoupling of the mesogen and backbone orientations[27]. Therefore, the choice of mesogen spacer length is quite important in such research

While phase transitions can be affected by the polymer, studies have shown that the transition temperatures generally level out at ~25-30 repeat units for ionically-polymerized materials[27]. Some mesophases are also dependent on molecular weight. Generally higher

molecular weight materials will exhibit the smectic phase, while lower molecular weight materials will have a tendency to align in the nematic phase. Larger molecular weight materials also have tendencies toward higher clearing points[27].

The polymer tacticity will generally impact the liquid crystal phases, as it does in crystallization in general. Studies have shown that greater tacticity in polymers will cause narrower transition ranges. On the other hand, higher polydispersities tend to cause broader phase transitions. Finally, more flexible backbones, such as the ones used in this study often have monotropic LC phases[27] (i.e. a phase that only exists upon heating or cooling, but not both).

B. Ferroelectricity

Ferroelectricity is the ability of a molecule to display an electrical response (polarization) in the absence of an externally applied field[29]. The polarization that persists when there is no applied field is called the spontaneous polarization. This polarization should be reversible when the opposite field is applied. Since both polarization states are stable, this type of material is said to exhibit bistable switching. A diagram of the standard polarization vs. electric field graph is shown in Figure 1.4. In this figure, the value of the polarization at point A is the spontaneous polarization.

In 1975, Meyer et al.[30] demonstrated that LC molecules are ferroelectric in the chiral smectic C and H phases. These materials naturally exhibit a helical structure and this structure must be unwound using an electrical field in order to produce a permanent dipole. It is also necessary to confine the LC phase in a layer no thicker than a few microns. Therefore, these LC's are generally sandwiched between two surfaces in order to preserve a thin spacing of 3-5mm.

By definition, ferroelectric materials are also piezoelectric. The direct piezoelectric effect means that electrical polarization can be produced by a strain. There is also a converse, or indirect, piezoelectric effect. This effect causes an electrical field to produce a deformation in the material. Piezoelectricity makes materials suitable for use as sensors and transducers. This quality of ferroelectric materials is the basis for their use in actuator applications because the applied electrical field should produce a deformation in the material so that it can flex or deform.

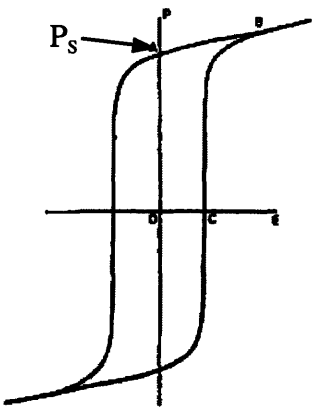

Figure 1.4: Ferroelectric hysteresis loop[29]. The spontaneous polarization is indicated.

Another important property that is seen in ferroelectric materials is the electro-optical effect. This occurs when the material's refractive index changes linearly with the applied electrical field. This property makes many LC materials suitable for use in electro-optical switches, sensors, and displays. Since these materials have a connection between the electrical and mechanical properties (piezoelectricity), as well as a relationship between the electrical and optical properties, there is also a tie between the mechanical and optical properties. This makes ferroelectric materials mechano-optic.

One very important quantity in ferroelectric materials is the response time. For this research, the response time is defined as the time it takes for the material to go from 10% to 90% of its

maximum polarization. Mathematically, it can be related to viscosity (μ), spontaneous polarization (P_S), and applied field (E) as shown in Equation 1.2:

$$\tau \sim \frac{\mu}{P_S E} \tag{1.2}$$

As one can see, the response time is directly proportional to the viscosity of the material. Therefore, small molecules will generally have faster response times than similar larger molecules. These times are generally on the order of microseconds for small molecules, while they are on the order of milliseconds for larger molecules such as small polymers. Although most applications desire the fastest response time achievable, it is sometimes acceptable to use polymer LCs instead of small molecule LCs for reasons that will be discussed later. The Kornfield group[31] has used blends of LC BCPs with liquid crystal monomers to increase response time. However, this creates a gel with mechanical properties lower than in the polymer.

Another characteristic of ferroelectric molecules that will affect their usefulness in applications is something known as the pyroelectric response. This is the ability of molecules to reorient with changes in temperature, causing an electrical charge to build up at the ends of the material. The quality of pyroelectricity is useful in certain detectors and imaging devices. While this will not be studied in this research, pyroelectricity is something that would affect a LC polymer when used in certain actuator applications because there will be fluctuations in the biological or ambient temperature with time.

C. Actuators as Artificial Muscles

While actuators have many applications, one that is gaining interest is that of artificial muscles. Current polymer research with potential applications as artificial muscles includes studies on multilayer composites of conducting polymer/non-conducting material[18], main-chain elastomers[20], and polymer metal composites[19]. Three main considerations must be taken into account when studying materials that could be used as artificial muscles[32]:

1. **The response time of the material when the electrical field is applied**

   Response times of natural muscles are on the order of milliseconds, while those of artificial muscles are on the order of seconds. This is not fast enough for biological applications, however it may be suitable for other actuator devices. Generally, electrical pulses of 100-200mV are applied in natural muscles. Current artificial muscles require at least 200-500mV in order to obtain a response, with some requiring up to tens of Volts.

2. **The amount of strain achievable**

   An artificial muscle must be able to stretch and bend just as natural muscles do. Therefore, it is important to design a material that can achieve a noticeable strain when an electric field is applied.

3. **The biocompatibility and durability of the material**

   Any material used in biological applications must be able to withstand the environment as well as be harmless to the body.

While all three of these issues ultimately must be considered when designing an artificial muscle, the proposed research will only focus on the first two.

As mentioned previously, artificial muscles based on multilayer composites of a conducting polymer with a non-conducting material have been studied. Much of this research has been done by Otero and Sansiñena at La Universidad del País Vasco in Spain[17, 18]. A diagram of the bilayer material they have tested is shown in Figure 1.5. This material uses a conducting polymer that expands and contracts based on its oxidation state. The other layer of material is not affected by the flow of ions, so the composite flexes upon adding ions.

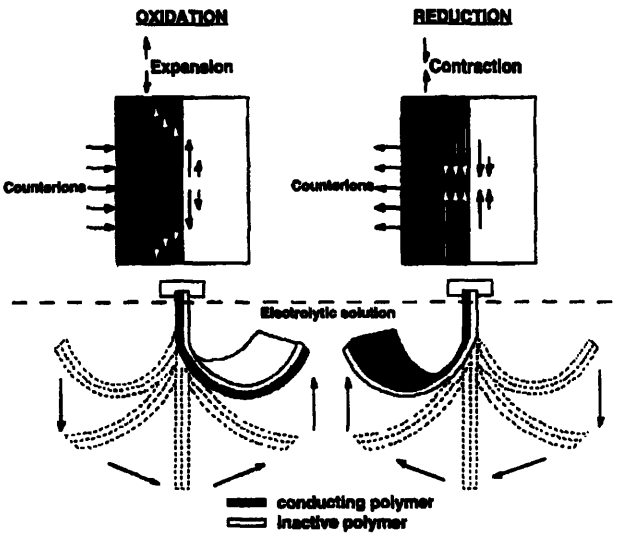

Scheme 3. Movements of a (polypyrrole/non-conducting polymer) bi-layer (down) produced by the stress gradients originated at the two layers interface (upper) owing to reverse conformational changes in polypyrrole during oxidation or reduction processes.

Figure 1.5: Bilayer artificial muscle design[18]

More recently, Frecker and Aguilera[33] have examined using a layered structure with individually-controlled segments of active materials to allow for novel actuation opportunities. Figure 1.6 shows the structure of this material.

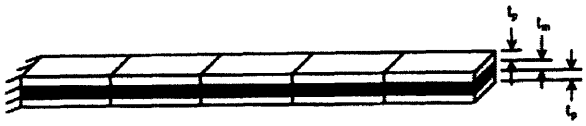

Figure 1. Segmented actuator.

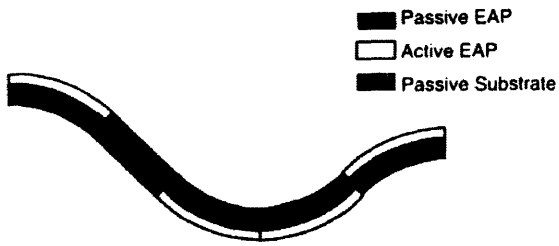

Figure 2. Varying the curvature by activating certain EAP segments.

Figure 1.6: Segmented actuator materials[33]

In this system, each segment can bend independently of the other segments. This allows the user to "steer" the material during actuation.

Researchers have also studied the potential to use main-chain elastomeric LC polymers as artificial muscles. Finkelmann et al. reported studies they did on a main-chain LC elastomer[20]. A picture of the polymer they used is shown in Figure 1.7. The rigid core of this elastomeric polymer is shown in Figure 1.8.

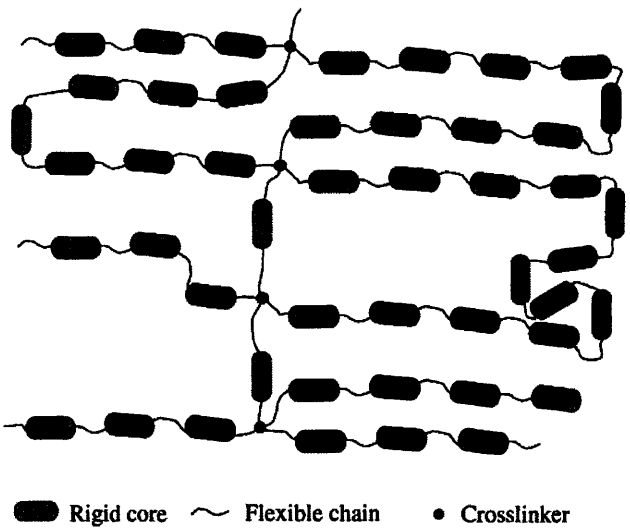

Figure 1.7: Main-chain LC Elastomer[20]

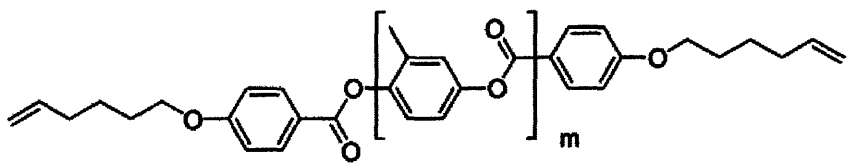

Figure 1.8: Rigid core of the LC polymer[20]

As one can see, the elastomeric properties in this polymer come from permanent chemical crosslinks. However, as previously mentioned, in the polymers for this proposed research the elastomeric properties will come from a physically crosslinked network in order to allow for flexibility in processing.

D. Side-Chain LC Polymers

As mentioned in the previous section on small molecule LCs, LC mesogens have been incorporated into polymers by attaching them to a polymer chain via a short alkyl spacer. This spacer allows the polymer properties and the LC mesogen properties to be decoupled while still

being attached to each other. Although these polymer LCs do exhibit ferroelectric properties, they respond more slowly than their small molecule analogues due to a much higher viscosity (see Equation 1.2). LC homopolymers are favored in certain applications due to their greater durability, processibility, and chemical resistance compared to small molecule LCs. Common LC polymer backbones include polysiloxanes and polyacrylates. Polysiloxane LC polymers generally have T_g values below room temperature while polyacrylate LC polymers have T_g values around room temperature and above. The triangular relationship in Figure 1.8 illustrates the relationship between the spontaneous polarization, stress and strain, and mesogen orientation.

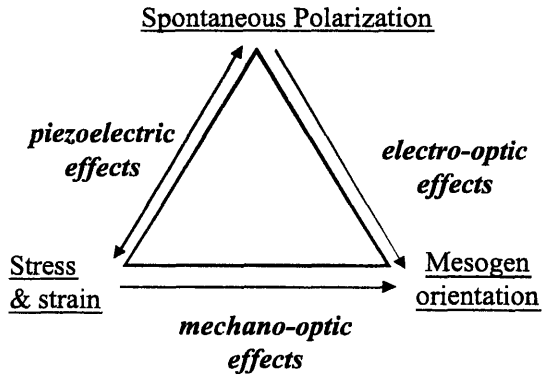

Figure 1.9: Triangular relationship in LC polymers[34]

E. Side-Chain LC Block Copolymers

As the name implies, the side-chain LC block copolymer is an extension of the side-chain LC homopolymer. A schematic of the polymers studied in this group is shown in Figure 1.10.

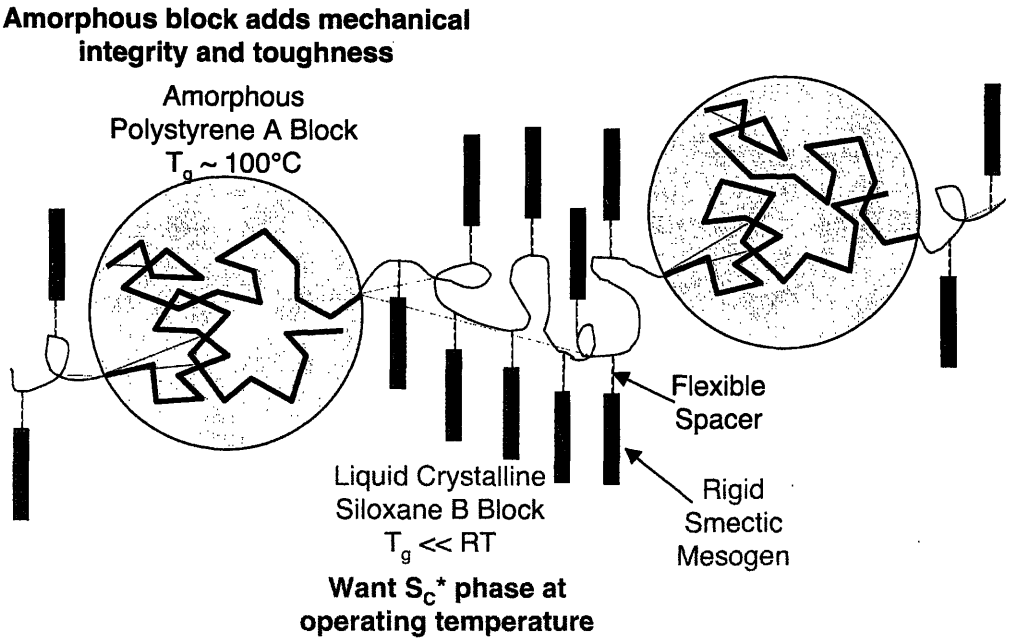

Figure 1.10: PS-PVMS-PS side-chain LC block copolymer

In this case, there is one amorphous block (polystyrene) connected to the flexible LC polymer (polysiloxane). It is also possible to synthesize triblock copolymer in which there are two amorphous blocks connected by a LC block, or vice-versa. As with other block copolymers, the morphology will change with molecular weight and the composition of the block copolymer (LCP volume fraction). A diagram showing the most common morphologies follows in Figure 1.11.

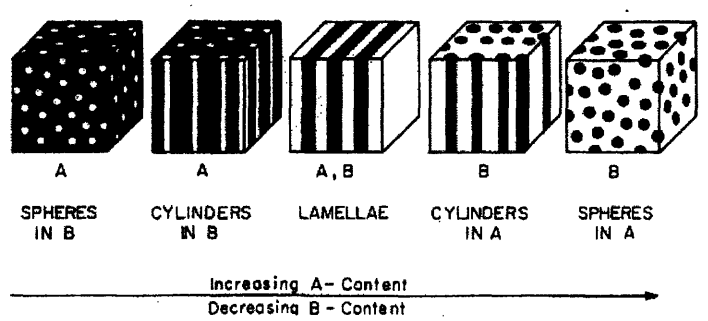

Figure 1.11: Block copolymer morphologies[35]

A sample MW-ϕ phase diagram is shown in Figure 1.12 for the PS-b-PMA LC block copolymer system studied in this group.

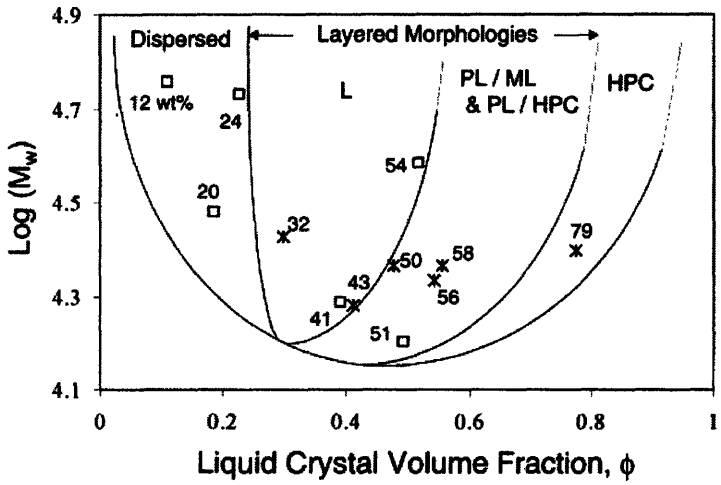

Figure 1.12: PS-PMA side-chain LC block copolymer phase diagram[9]

In this system, the following four different microstructure morphologies were observed: dispersed (D), lamellar (L), predominately lamellar (PL), and cylinders (CYN). Anthamatten et al. in this group have attempted to mathematically model amorphous-LC diblock copolymer phase diagrams[8]. This model is useful in determining the expected morphology of a side-chain LC block copolymer system. It uses free energy expressions and can predict the order-order transitions (OOT) and order-disorder transitions (ODT) of a particular system.

In general for LC block copolymers, depending on the value of the interaction parameter χ_{AB}, there can be very sharp transitions from one region to another or there can be very broad interfacial regions. The amount of phase mixing is also dependent on the polydispersity index of

the block copolymer. Studies have shown that polymers with high PDI values generally have broad transitions from one phase to the other and may only weakly phase segregate. However, samples with small PDI values have sharper transitions and higher transition temperatures. Therefore, when synthesizing a side-chain LC block copolymer, it is very important to obtain a polymer with a low PDI.

The dimensions of the lamellae, cylinders, or spheres in these morphologies are generally on the order of several hundred Ångstroms. When unprocessed, the grains of these materials can be on the order of microns. However, by using a processing technique such as roll-casting[4, 36, 37], it is possible to orient the grains and obtain a well-oriented, almost grainless sample.

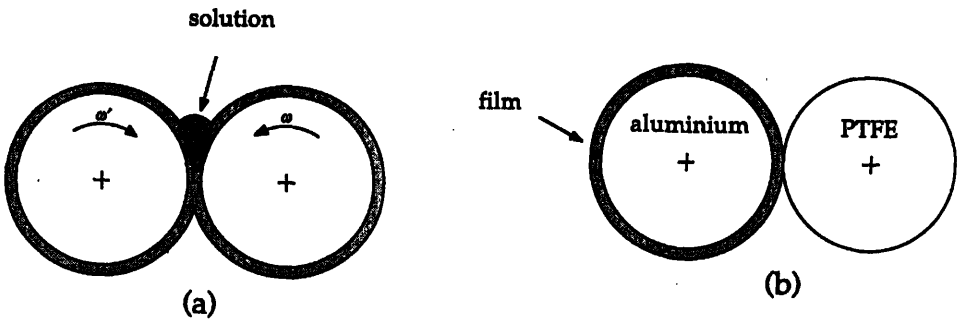

Figure 1.13: Diagram of the roll-cast technique[36]

As mentioned previously, in order to obtain ferroelectric properties in a LC sample, the S_C^* phase must be confined to a region smaller than a few microns. Therefore, the block copolymer morphology ensures that the sample will be ferroelectric by containing the LC mesogens within a region on the nanometer scale.

It is important to note that other groups have studied amorphous-LC diblock copolymers. Some of the well-known researchers are Finkelmann[20, 21, 28, 38-41], Fischer[6, 42-44], Gronski[10, 45],

Hikmet[46], Thomas and Ober[5, 7, 36, 37, 43, 47-50], and Watanabe[2]. Gronski's group was the first to report studies on this type of diblock copolymer in 1989[45]. Hikmet as well as Thomas and Ober have been successful at preparing copolymers that exhibit switching at voltages of 60 to 75V/μm. However, they used quite different materials. Hikmet was able to use a low T_g amorphous block and obtained electro-optic switching. Thomas and Ober used a block copolymer with two high T_g blocks and used a high voltage (±75V/μm) in order to obtain switching. Finally, Watanabe has done a significant amount of research in this area and even did a study on the impact on transition temperatures when the amorphous block is varied to another amorphous block with a higher or lower T_g value.

One important class of block copolymers is thermoplastic elastomers. These polymers are generally triblock or multiblock copolymers with an ABA or $(AB)_n$ structure with an amorphous A block (hard segment) and a flexible B block (soft segment). One common example is the styrene-butadiene-styrene (SBS) triblock copolymer. As the name implies, thermoplastic elastomers combine the properties of rubber elasticity and thermoplasticity. Therefore, they can be reversibly deformed by applying a stress and they can be processed, set, and reprocessed by heating, cooling, and reheating. In most cases, the size of the amorphous block is much smaller than the size of the flexible block. Gronski reported synthesis of polystyrene-b-polybutadiene-b-polystyrene thermoplastic liquid crystal elastomers[10]. It should be noted that it is not necessary to use a triblock copolymer in order to obtain a LC elastomer. Finkelmann and his group have successfully prepared a main-chain liquid crystal elastomer. This novel material was discussed in the section on Actuators as Artificial Muscles.

Studies have shown that the amorphous block in LC BCPs can affect the LC phases observed[44]. Also, transition temperatures in such materials may be estimated using the Gibbs-Thomson relation[42] shown in Equation 1.3:

$$T = T^0\left(1 - \frac{V\sigma}{I\Delta H}\right) \tag{1.3}$$

In this equation, T is actual phase transition, T^0 is the phase transition temperature for an infinite size of the material, V is the specific volume, σ is the mean surface free energy, I is the dimension of the LC phase, and ΔH is heat of fusion per unit mass.

Although this project will focus on side-chain LC polymers, there is also a considerable amount of research happening on other types of LC polymers. Shashidhar and his group at the Naval Research Lab have studied cyclic siloxane LC polymers[51]. Figure 1.14 is a picture illustrating the polymer they designed.

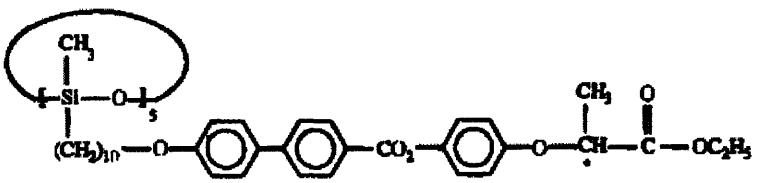

Figure 1.14: Cyclic LC siloxane polymer[51]

This polymer was shown to exhibit better ferroelectric properties compared to linear siloxane polymers with the same mesogen attached.

Summary of Previous Progress

Moment et al.[34] studied systems with a polystyrene-b-polyvinylmethylsiloxane backbone, the same one that will initially be studied in this research. Figures 1.15 and 1.16 showing the molecular structure of the polymer backbone and the LC mesogens that Moment used are below. As one can see, the polymer backbone is actually a triblock, however the middle polydimethylsiloxane block should be very short in order to obtain what is essentially a diblock copolymer. The synthesis scheme for the copolymer will be discussed later in this proposal. It also should be noted that Moment's mesogens are chiral and have dipole moments such that LC ferroelectric properties can be obtained. Both Mesogen A and Mesogen B are quite similar in structure. However, Mesogen A is more flexible owing to the longer alkyl spacer near the siloxane end and the lack of a biphenyl group as in Mesogen B. Mesogen A LC blocks had T_g values ranging from –35°C to –24°C while Mesogen B LC blocks had values of -9 °C to -5°C.

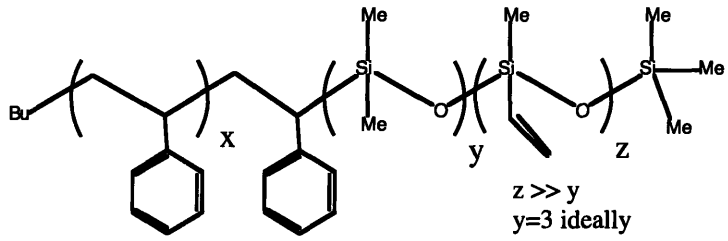

Figure 1.15: Structure of PS-b-PVMS block copolymer[34]

mesogen A

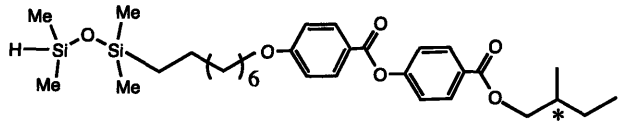

mesogen B

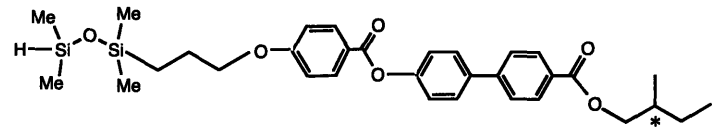

Figure 1.16: Structures of Mesogen A and Mesogen B[34]

Moment et al. found that siloxane homopolymers with these mesogens exhibited electro-optic properties. However, the block copolymers did not. Moment did find that the block copolymers with mesogen A exhibited mechano-optic properties when the LC block was much larger than the PS block. These samples were also rubbery in nature. The block copolymers with mesogen B attached did not show mechano-optic properties and were glassy solids.

It was noted that there seemed to be some level of phase mixing between the blocks in the polymers with mesogen A. This became obvious because the amorphous-LC phase boundaries were not very distinct and the size of the LC block affected the T_g of the PS block. Block copolymers with mesogen B had very distinct phase boundaries and the PS T_g did not change with LC content. This indicates that the interaction parameter between the two blocks was larger for PS-LCPB polymers than for PS-LCPA polymers. This difference was attributed to the more rigid structure of Mesogen B compared to that of Mesogen A.

The overall conclusion from Moment's research was that it is important to obtain a better mesogen (i.e. one with a higher spontaneous polarization and one that allows for strong phase segregation) in order to obtain ferroelectric properties in the block copolymers. P_S values for the

mesogens used in Moment's research were less than 10nC/cm^2, while some groups have synthesized LC mesogens that achieved higher P_S values (greater than100nC/cm^2) in PVMS homopolymer or PDMS-b-PVMS block copolymer studies. Quite often these mesogens have strong electron withdrawing groups (halogens, NO_2, etc.) or in some way possess a large dipole moment.

Thesis Outline

The rest of this thesis is organized as follows:

Chapter	Topic
2	Materials Design and Synthesis
3	Thermal Properties and Morphology of Polymers for Use as Nematic Actuators
4	Thermal Properties and Morphology of Polymers for Use as Ferroelectric Actuators
5	Processing of Polymers Studied for Use as Ferroelectric Actuators
6	Summary and Future Project Directions

References

1. Hamley, I. W., Nanotechnology with Soft Materials. *Angewandte Chemie, International Edition* **2003,** 42, 1692-1712.

2. Yamada, M.; Itoh, T.; Hirao, A.; Nakahama, S.-I.; Watanabe, J., Side-chain LC block copolymers with well defined structures prepared by living anionic polymerization. 2: Effect of

the glass transition temperature of amorphous segments on the phase behavior and structure of the LC segment. *High Performance Polymers* **1998,** 10, 131-138.

3. Moment, A. J.; Miranda, R.; Hammond, P. T., Synthesis of polystyrene-polysiloxane side-chain liquid crystalline block copolymers. *Macromolecular Rapid Communications* **1998,** 19, 573-579.

4. Zheng, W. Y.; Albalak, R. J.; Hammond, P. T., Mesogen Orientation within Smectic C* Side Chain Liquid Crystalline Diblock Copolymers. *Macromolecules* **1998,** 31, (8), 2686-2689.

5. Mao, G.; Wang, J.; Ober, C. K.; Brehmer, M.; O'Rourke, M. J.; Thomas, E. L., Microphase-Stabilized Ferroelectric Liquid Crystals (MSFLC): Bistable Switching of Ferroelectric Liquid Crystal-Coil Diblock Copolymers. *Chemistry of Materials* **1998,** 10, 1538-1545.

6. Omenat, A.; Lub, J.; Fischer, H., Liquid-Crystalline Diblock Copolymers Produced by Living Cationic and Anionic Polymerizations. *Chemistry of Materials* **1998,** 10, 518-523.

7. Merenga, A.; Shilov, S. V.; Kremer, F.; Mao, G.; Ober, C. K.; Brehmer, M., Molecular Orientation and Dynamics in Ferroelectric Diblock Copolymers Monitored by FT-IR Spectroscopy. *Macromolecules* **1998,** 31, (25), 9008-9012.

8. Anthamatten, M. L.; Hammond, P. T., Free-energy model of asymmetry in side-chain liquid-crystalline diblock copolymers. *Journal of Polymer Science Part B-Polymer Physics* **2001,** 39, (21), 2671-2691.

9. Anthamatten, M. L.; Zheng, W. Y.; Hammond, P. T., A Morphological Study of Well-Defined Smectic Side-Chain LC Block Copolymers. *Macromolecules* **1999,** 32, 4838-4848.

10. Figueriedo, P.; Geppert, S.; Brandisch, R.; Bar, G.; Thomann, R.; Spontak, R. J.; Gronski, W.; Samlenski, R.; Müller-Buschbaum, P., Ordering of Cylindrical Microdomains in

Thin Films of Hybrid Isotropic/Liquid Crystalline Triblock Copolymers. *Macromolecules* **2001,** 34, (2), 171-180.

11. Sentenac, D.; Demirel, A. L.; Lub, J.; de Jeu, W. H., A New Lamellar Morphology of a Hybrid Amorphous/Liquid Crystalline Block Copolymer Film. *Macromolecules* **1999,** 32, (10), 3235-3240.

12. Kihara, H.; Kishi, R.; Miura, T.; Kato, T.; Ichijo, H., Phase behavior of Liquid-crystalline copolymer/liquid crystal blends. *Polymer* **2001,** 42, 1177-1182.

13. Anthamatten, M. L. Massachusetts Institute of Technology, Cambridge, MA, 2001.

14. Anthamatten, M. L.; Hammond, P. T., A SAXS Study of Microstructure Ordering Transitions in Liquid Crystalline Side-Chain Diblock Copolymers. *Macromolecules* **1999,** 32, 8066-8076.

15. Zheng, W. Y.; Hammond, P. T., Phase Behavior of New Side Chain Smectic C* Liquid Crystalline Block Copolymers. *Macromolecules* **1998,** 31, (3), 711-721.

16. Anthamatten, M. L.; Wu, J. S.; Hammond, P. T., Direct observation of a smectic bilayer microstructure in side-chain liquid crystalline diblock copolymers. *Macromolecules* **2001,** 34, (24), 8574-8579.

17. Otero, T. F.; Sansiñena, J. M., Artificial muscles based on conducting polymers. *Bioelectrochemistry and Bioenergetics* **1995,** 38, 411-414.

18. Otero, T. F.; Sansiñena, J. M., Bilayer dimensions and movement in artificial muscles. *Bioelectrochemistry and Bioenergetics* **1997,** 42, 117-122.

19. Kucernak, A. R.; Muir, B., Analysis of the electrical and mechanical time response of solid polymer-platinum composite membranes. *Electrochimica Acta* **2001,** 46, 1313-1322.

20. Donnio, B.; Wermter, H.; Finkelmann, H., A Simple and Versatile Synthetic Route for the Preparation of Main-Chain, Liquid-Crystalline Elastomers. *Macromolecules* **2000,** 33, (21), 7724-7729.

21. Lehmann, W.; Hartmann, L.; Kremer, F.; Stein, P.; Finkelmann, H.; Kruth, H.; Diele, S., Direct and inverse electrmechanical effect in ferroelectric liquid crystalline elastomers. *Journal of Applied Physics* **1999,** 86, (3), 1647-1652.

22. Bhattacharya, K.; Ravichandran, G., Ferroelectric perovskites for electromechanical actuation. *Acta Materialia* **2003,** 51, 5941-5960.

23. Collyer, A. A., *Liquid Crystal Polymers: From Structures to Applications.* Elsevier Applied Science: New York, 1992.

24. Collings, P. J., *Liquid Crystals: Nature's Delicate Phase of Matter.* Princeton University Press: Princeton, 1990.

25. Cowie, J. M. G., *Polymers: Chemistry and Physics of Modern Materials.* 2nd ed.; Blackie Academic and Professional: London, 1991.

26. Cooray, N. F.; Fujimoto, H.; Kakimoto, M.-A.; Imai, Y., Synthesis and Characterization of Novel Combined Type Ferroelectric Liquid Crystalline Polymers Having Polyester Main Chains. *Macromolecules* **1997,** 30, (11), 3169-3174.

27. Pugh, C.; Kiste, A. L., Molecular Engineering of Side-Chain Liquid Crystalline Polymers by Living Polymerizations. *Progress in Polymer Science* **1997,** 22, 601-691.

28. Finkelmann, H.; Ringsdorf, H.; Wendorff, J. H., Model COnsiderations and Examples of Enantiotropic Liquid-Crystalline Polymers - Polyreactions in ordered Systems. *Makromolekulare Chemie-Macromolecular Chemistry and Physics* **1978,** 179, (1), 273-276.

29. Megaw, H., *Ferroelectricity in Crystals.* Methuen & Co. Ltd.: London, Methuen, 1957.

30. Meyer, R. B.; Liébert, L.; Strzelecki, L.; Keller, P., Ferroelectric Liquid Crystals. *Journal de Physique* **1975,** 36, L69-L71.

31. Kempe, M. D.; Scruggs, N. R.; Verdusco, R.; Lal, J.; Kornfield, J. A., Self-assembled liquid-crystalline gels designed from the bottom up. *Nature Materials* **2004,** 3, (3), 177-182.

32. Pelrine, R.; Kornbluh, R.; Joseph, J.; Heydt, R.; Pei, Q.; Chiba, S., High-field deformation of elastomeric dielectrics for actuators. *Materials Science and Engineering C* **2000,** 11, 89-100.

33. Frecker, M. I.; Aguilera, W. M., Analytical modeling of a segmented unimorph actuator using electrostrictive P(VDF-TrFE) copolymer. *Smart Materials and Structures* **2004,** 13, (1), 82-91.

34. Moment, A. The Synthesis and Characterization of Polystyrene Liquid Crystalline Siloxane Block Copolymers. Doctoral, Massachusetts Institute of Technology, Cambridge, MA, 2000.

35. Argon, A. S.; Cohen, R. E.; Gebizlioglu, O. S.; Schwier, C. E., Crazing in Block Co-polymers and Blends. *Advances in Polymer Science* **1983,** 52, (3), 275-334.

36. Albalak, R. J.; Thomas, E. L., Roll-Casting of Block-Copolymers and of Block Copolymer-Homopolymer Blends. *Journal of Polymer Science Part B-Polymer Physics* **1994,** 32, (2), 341-350.

37. Albalak, R. J.; Thomas, E. L., Microphase Separation of Block Copolymer Solutions in a Flow Field. *Journal of Polymer Science Part B-Polymer Physics* **1993,** 31, (1), 37-46.

38. Stein, P.; Aßfalg, N.; Finkelmann, H.; Martinoty, P., Shear modulus of polydomain, mono-domain and non-mesomorphic side-chain elastomers: Influence of the nematic order. *The European Physics Journal E* **2001,** 4, 255-262.

39. Camacho-Lopez, M.; Finkelmann, H.; Palffy-Muhoray, P.; Shelley, M., Fast liquid-crystal elastomer swims into the dark. *Nature Materials* **2004,** 3, (5), 307-310.

40. Lehmann, W.; Gattinger, P.; Keck, M.; Kremer, F.; Stein, P.; Eckert, T.; Finkelmann, H., The inverse electromechanical effect in mechanically oriented S-C* elastomers examined by means of an ultra-stable Michelson interferometer. *Ferroelectrics* **1998,** 208, (1-4), 373-383.

41. Walther, M.; Finkelmann, H., Structure Formation of Liquid Crystalline Block Copolymers. *Progress in Polymer Science* **1996,** 21, 951-979.

42. Poser, S.; Fischer, H.; Arnold, M., LC Side Group Block and Graft Copolymers - Synthesis and Structure/Property Relationships. *Progress in Polymer Science* **1998,** 23, 1337-1379.

43. Xiang, M.; Li, X.; Ober, C. K.; Char, K.; Genzer, J.; Sivaniah, E.; Kramer, E. J.; Fischer, D. A., Surface Stability in Liquid-Crystalline Block Copolymers with Semifluorinated Monodendron Side Groups. *Macromolecules* **2000,** 33, (16), 6106-6119.

44. Zaschke, B.; Frank, W.; Fischer, H.; Schmutzler, K.; Arnold, M., Synthesis and Characterization of LC Side-Chain AB Blockcopolymers. *Polymer Bulletin* **1991,** 27, (1), 1-8.

45. Adams, J.; Gronski, W., LC Side-Chain AB-Block Copolymers with an Amorphous A-Block and a Liquid-Crystalline B-Block. *Makromolekulare Chemie-Rapid Communications* **1989,** 10, (10), 553-557.

46. Omenat, A.; Hikmet, R. A. M.; Lub, J.; van der Sluis, P., Synthesis, Characterization, and Physical Properties of New Ferroelectric Liquid Crystalline Materials: Block Copolymers. *Macromolecules* **1996,** 29, (21), 6730-6736.

47. Clingman, S. R.; Mao, G.; Ober, C. K.; Colby, R. H.; Brehmer, M.; Zentel, R.; Bignozzi, M.; Laus, M.; Angeloni, A.; Gillmor, J. R., Effect of polymer architecture on self-diffusion of LC polymers. *Journal of Polymer Science Part B-Polymer Physics* **1999,** 37, (5), 405-414.

48. Wang, J.; Mao, G.; Ober, C. K.; Kramer, E. J., Liquid Crystalline, Semifluorinated Side Group Block Copolymers with Stable Low Energy Surfaces: Synthesis, Liquid Crystalline Structure, and Critical Surface Tension. *Macromolecules* **1997,** 30, (7), 1906-1914.

49. Chao, C.-Y.; Li, X.; Ober, C. K.; Osuji, C.; Thomas, E. L., Orientational Switching of Mesogens and Microdomains in Hydrogen-Bonded Side-Chain Liquid-Crystalline Block Copolymers Using AC Electric Fields. *Advanced Functional Materials* **2004,** 14, (4), 364-370.

50. Osuji, C.; Ferreira, P. J.; Mao, G.; Ober, C. K.; Vander Sande, J. B.; Thomas, E. L., Alignment of Self-Assembled Hierarchical Microstructures in Liquid Crystalline Diblock Copolymers Using High Magnetic Fields. *Macromolecules* **2004,** 37, (26), 9903-9908.

51. Gruneberg, K.; Naciri, J.; Shashidhar, R., Ferroelectric Properties of a Fast Switching Cyclic Siloxane Oligomer. *Chemistry of Materials* **1996,** 8, 2486-2490.

Chapter 2 – Materials Design and Synthesis

Introduction and Motivation

In this chapter, the choice of polymer and mesogen systems, and synthetic techniques used in this project are described. Techniques are provided for the polyvinylmethylsiloxane homopolymer, the polystyrene-PVMS diblock copolymer, the PS-PVMS-PS triblock copolymer, the mesogen attachment to the polymer backbones, and the six mesogens (4 without chiral centers, 2 with chiral centers). When functionalized with the mesogens, these polymers are expected to be useful as nematic or ferroelectric actuators.

The polymer systems used in this study will rely on the PS-PVMS backbone that a previous group member, Dr. Aaron Moment, developed[1]. This backbone was chosen to combine the flexibility of PVMS, a low-T_g polymer, with the rigidity of PS, a high-T_g polymer. Other researchers have studied diblock systems with two high-T_g blocks[2] or two low-T_g blocks[3]. In the high-T_g studies, ferroelectricity was not observed, while low-T_g studies were able to obtain materials that exhibited ferroelectric properties. However, in low-T_g studies, rigidity was lacking. Therefore, the combination of a high-T_g block with a low-T_g block allows for ferroelectricity and rigidity, as demonstrated by Moment[1], and was the combination chosen for the current studies.

Mesogens were chosen to exhibit the chiral smectic C phase or a transition to or from the nematic phase at the desired operating temperature. During the initial stages of this project, there was a collaboration between this group and the Shashidhar group at the Naval Research Lab. Through this collaboration, we were sent samples of chiral mesogens they developed and had

tested for ferroelectricity. Therefore, additional chiral mesogens synthesized were similar to those from the NRL so that a reasonable comparison could be made.

Nematic mesogens were chosen based on previous studies by Dr. Bindu Nair[4] in this group. Both types of mesogens are also quite common in research done by other groups[5-7]. Therefore, the synthetic techniques are well-known and the other studies can serve as a source of comparison with the results in these studies.

Materials Design

A. Mesogens

Since the block copolymers that Moment studied did not exhibit electro-optic properties, new chiral mesogens were chosen based on previous studies indicating high P_S values. For instance, Shashidhar and Naciri at the Naval Research Laboratory[8-10] and Cooray et al. at the Tokyo Institute of Technology[11, 12] have synthesized mesogens that exhibit very favorable ferroelectric properties in PVMS homopolymers or PDMS-b-PVMS block copolymers. Examples of these mesogens and their properties are given in Figures 2.1 and 2.2.

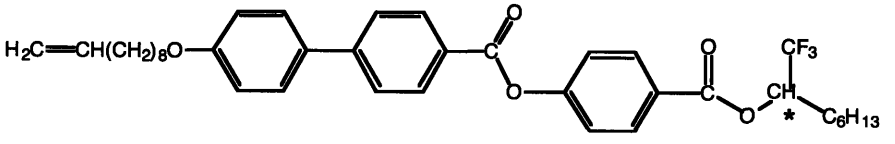

Siloxane Homopolymer Studies:

M_n=7000 PDI=1.1 τ=0.51ms (T=T_c-10°C=90.3°C)

Phases observed: P_s=122nC/cm^2 (T=T_c-30°C=70.3°C)

I 134.8 S_A 100.3 S^*_C <20

Figure 2.1: Cooray ferroelectric mesogen[12]

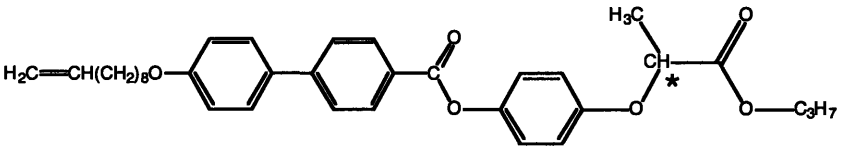

PDMS-b-PVMS Copolymer Studies:

DP_n=30 $n_{PVMS}/(n_{PVMS}+n_{PDMS})$=0.3

P_s=80nC/cm^2 (T=T_{AC*}-30°C=91°C)

Phases observed:

I 141 S_A 121 S^*_C

Figure 2.2: Naciri ferroelectric mesogen[13]

Both P_S values are much higher than the values of the mesogens used in Moment's study. Therefore, it was expected that using these mesogens would result in more desirable switching and response times. However, the Cooray synthesis was much more challenging than initially expected. Also, through a literature search, another Naciri-like mesogen with an even higher P_S was found. Therefore, this similar mesogen was ultimately used and will be described in Section F of Synthesis Techniques.

In addition to studying polymers that are functionalized with chiral mesogens and are desirable for use in ferroelectric actuation, polymers functionalized with achiral mesogens were examined. When using achiral mesogens, ferroelectric actuation is not an option. However, nematic actuation is. In nematic actuation, the mechanical deformation is caused by the transition from the nematic phase to an isotropic phase or from the nematic phase to a smectic phase. Therefore, the choice of mesogen is based on the proximity of the use temperature to the LC transition temperatures.

B. Polymers

Another important consideration in this project was the polymer backbone that was used. Previously PS-b-PVMS diblock copolymers were studied and rubbery samples were obtained, but studying the PS-PVMS-PS triblock copolymer system was necessary in order to obtain a true elastomer. In both cases, it is desirable to have a much larger LC block compared to the PS block to allow for flexibility in both the polymer and the LC mesogens. For diblock copolymers, Moment obtained rubbery samples for polymers with mesogen A, large molecular weights, and large LC blocks (~80-90wt% of the polymer)[14]. Since the goal in this study was to obtain elastomeric BCPs, the initial block copolymers that were synthesized had approximately the same LC to amorphous weight ratio. In the synthesis, the PVMS block was planned to be 35-60wt% of the total BCP molecular weight. However, once the mesogens were attached, the LC block molecular weight was generally in the targeted 80-90wt% of the total functionalized polymer.

Studies on the polystyrene-b-polyvinylmethylsiloxane diblock copolymer system followed the reactant purification and synthesis techniques that were developed by Moment et al.[1]. The procedure will be described in more detail later in this chapter. However, as mentioned previously, for the goals of this project, it is necessary to have a triblock copolymer. Therefore, one of the important pieces in the project was to synthesize a triblock LC BCP. Three methods were initially considered in order to prepare this type of triblock copolymer. They are summarized below:

1. Difunctional Initiator

In this method, the PVMS block is made using a difunctional initiator and endcapped with amine groups. The PS blocks are generally made with the anionic polymerization

method and endcapped with an acid group. The amine groups and the acid groups will react to form a link between the PS block and the PVMS block. Other end groups that react with each other can also be used. By having the α,ω-terminated PVMS block, two PS blocks can add to it in order to form a triblock copolymer. Previous researchers have been able to achieve 92-100% coupling efficiency[15]. In this group, a preprint was recently written about a consistent method to synthesize difunctional PVMS[16].

The advantage to this method is that it requires the researcher to develop no significant additional polymer synthesis techniques. However, the choice of terminal groups for the PVMS and the PS blocks is very important. The terminating agents must be chosen to properly couple the blocks, to allow for a coupling reaction that will not damage the polymers, and to withstand the hydrosilylation technique used to attach the mesogens. Since a suitable pair could not be determined, this method was not used in the current studies.

Recently a new technique was developed to synthesize a difunctional PVMS macroterminating agent. This macroterminating agent could then be used to terminate two living polystyryl anions. Studies on this technique are still limited and will be discussed in Chapter 6.

2. Coupling Two Diblock Copolymers

This method, as the name suggests, couples two living PS-b-PVMS diblock copolymers using a difunctional compound such as dichlorodimethylsilane or 1,1,3,3-tetramethyl-1,3-dichlorodisiloxane. Some groups have successfully used the coupling technique in the synthesis of PS-b-PDMS-b-PS triblocks[15, 17]. Therefore, coupling techniques from such studies were attempted in this research. However, the PVMS and

PDMS reactivities are significantly different, and such techniques were only moderately successful for the current systems.

The primary advantage to this method is that it requires no new chemistry compared to the diblock synthesis. However, the researcher must be careful to obtain proper stoichiometry and conditions in the coupling reaction. Studies in the Knauss group[17] have shown that extremely slow coupling agent addition rates are necessary and the coupling agent should be added at a specific time during the polymerization reaction. Therefore, while the coupling method was successful once in obtaining a PS-PVMS-PS triblock copolymer, future studies should be done in order to make the technique consistently successful.

3. Atom Transfer Radical Polymerization

This method was initially reported by Wang and Matyjaszewski in 1995[18]. In ATRP, a polysiloxane macroinitiator is formed that is strong enough to radically-initiate the styrene polymerization. While previous studies on using ATRP to synthesize a PS-b-PVMS-b-PS copolymer in this group were not successful, ATRP has been used to prepare PS-b-PDMS-b-PS triblock copolymers by other groups[13, 19]. Therefore, that method could be modified to work in this system. The synthesis considered is shown below in Figure 2.3:

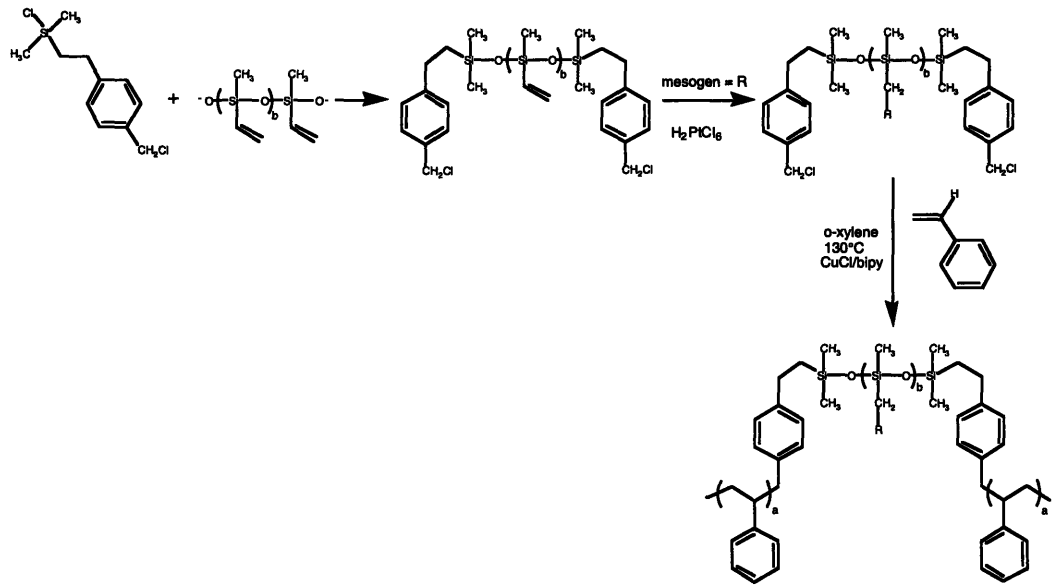

Figure 2.3: ATRP synthesis technique (modified from [20])

ATRP produces copolymers with very low PDI values (<1.1) and high conversion, so it was seriously considered for this research. However, ATRP requires all vinyl groups along the PVMS backbone to be removed before the polystyrene reaction occurs so that the vinyl groups are not polymerized. Since the mesogen attachment will not remove all vinyl groups, a subsequent reaction must be used to remove any remaining vinyls. Even then, it is difficult to ensure that all vinyl groups have been removed and even a few vinyls can cause undesired crosslinking in the polymer.

Synthesis Techniques

A. Anionic Polymerization

As previously mentioned, the PS-b-PVMS diblock copolymer synthesis will follow the scheme developed by Moment et al.[1, 14]. This scheme is shown below in Figure 2.4.

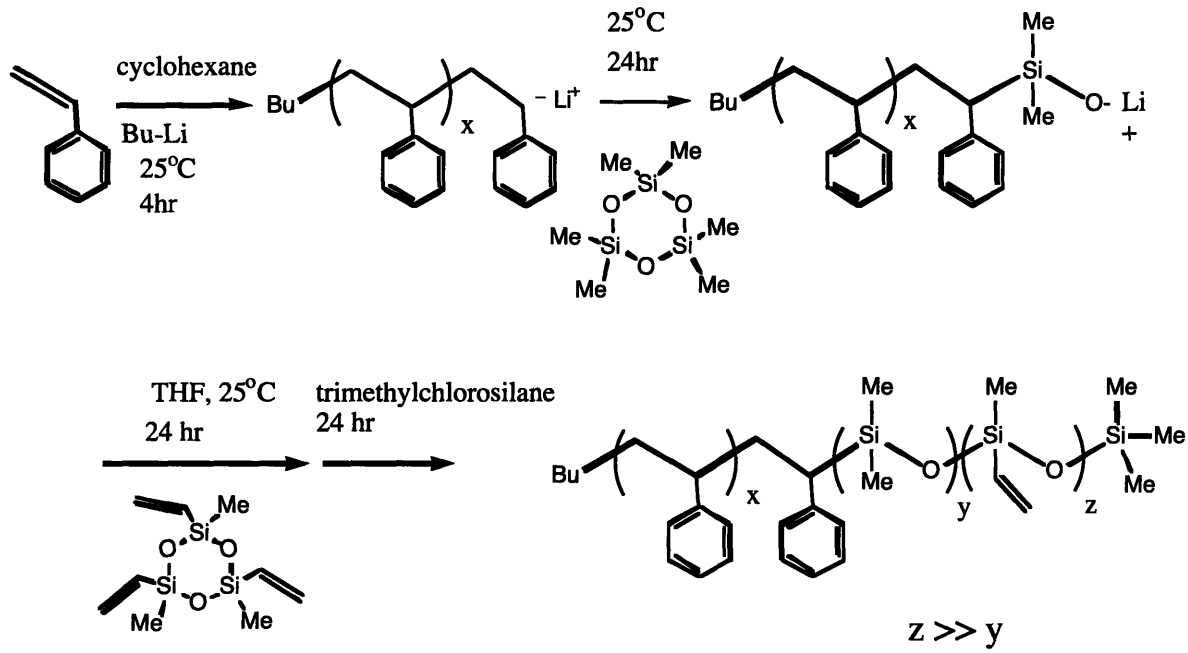

Figure 2.4: PS-b-PVMS copolymer synthesis[14]

All anionic polymerization reactions were carried out in an inert atmosphere glovebox. Therefore, all materials had to be purified before placing them in the glovebox. Specific purification procedures can be found in Moment's thesis[14] and are repeated below.

Polymerization procedure: 6mL cyclohexane was added to a flask with stirring, followed by 101μL butyl lithium. After stirring for about 1 minute, 2.2mL styrene was added. After 4 hours of reaction, a portion of the reaction mixture was taken and precipitated in methanol for

analysis of the polystyrene homopolymer molecular weight and molecular weight distribution. In a separate flask, 0.452g hexamethyltrisiloxane was dissolved in 2mL cyclohexane and this mixture was added to the living polystyryl anion solution. After 24 hours, the color of the living polystyryl anion had cleared, indicating the conversion of the living polystyryl anion to a siloxanolate anion. In a separate flask, 2mL 1,3,5-trimethyl-1,3,5-trivinylcyclotrisiloxane and 6mL THF were mixed, and this mixture is added to the polymerization flask. 24 hours after this addition, 0.2mL trimethylchlorosilane was added to terminate the polymerization. The reaction mixture was allowed to stir for an additional 24 hours to ensure complete termination. The solvents were removed by vacuum, and the product was then re-dissolved in a minimal quantity of THF and precipitated into methanol. A white polymer powder was filtered from this solution.

GPC: PS homopolymer – M_n = 27329g/mol, M_w = 39150, PDI = 1.43

PS-PVMS diblock – M_n = 39291g/mol, M_w = 53895, PDI = 1.37

^{1}H NMR dH: 0.02-0.17 [m, Si-C**H**$_3$], 1.70-2.22 [m,br, -C**H**Ph-], 1.44-1.57 [m,br, -C**H**$_2$CHPh-], 5.79-6.06 [m,Si-C**H**=C**H**$_2$], 6.30-6.80 [m, Ar-**H**], 6.90-6.73 [m, Ar-**H**]

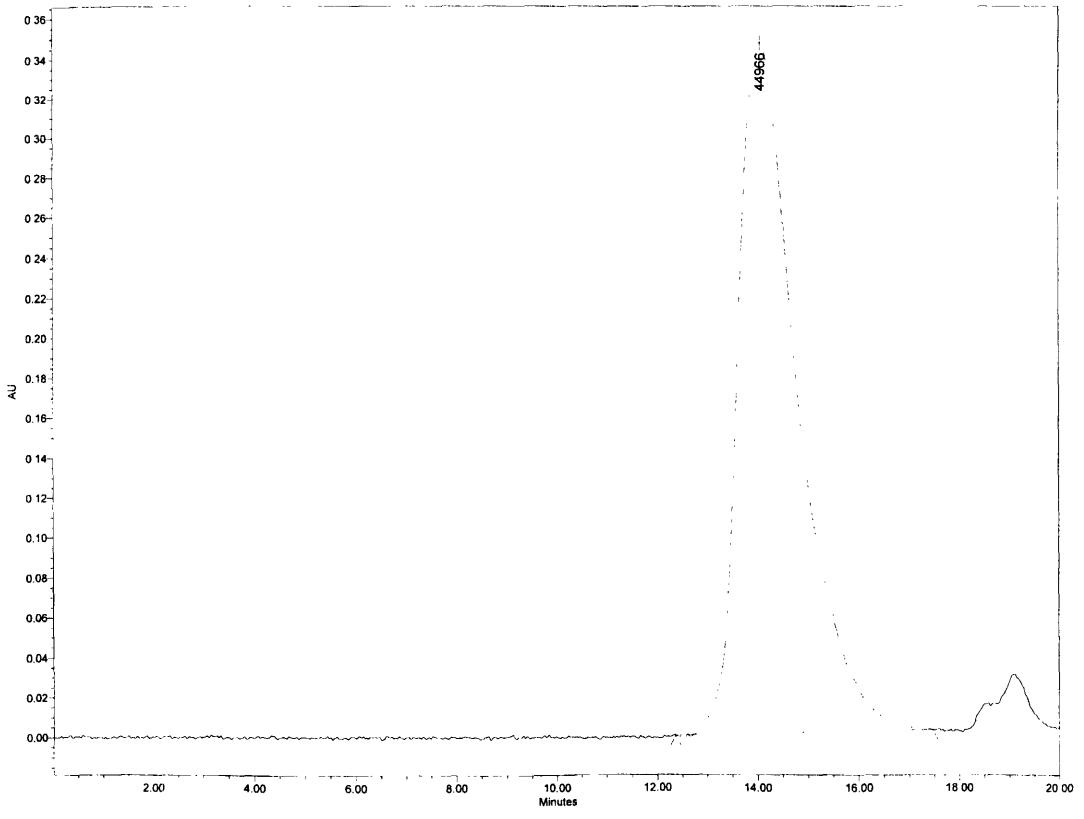

Figure 2.5: GPC of PS intermediate

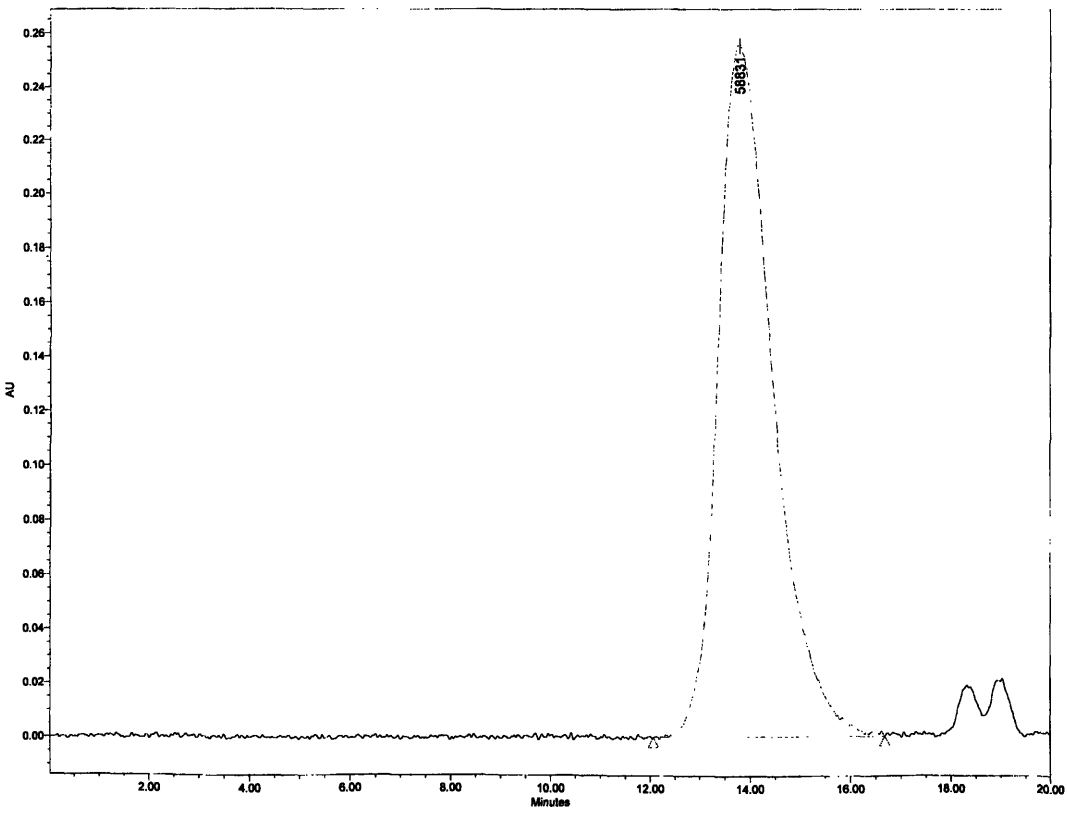

Figure 2.6: GPC of PS-PVMS diblock

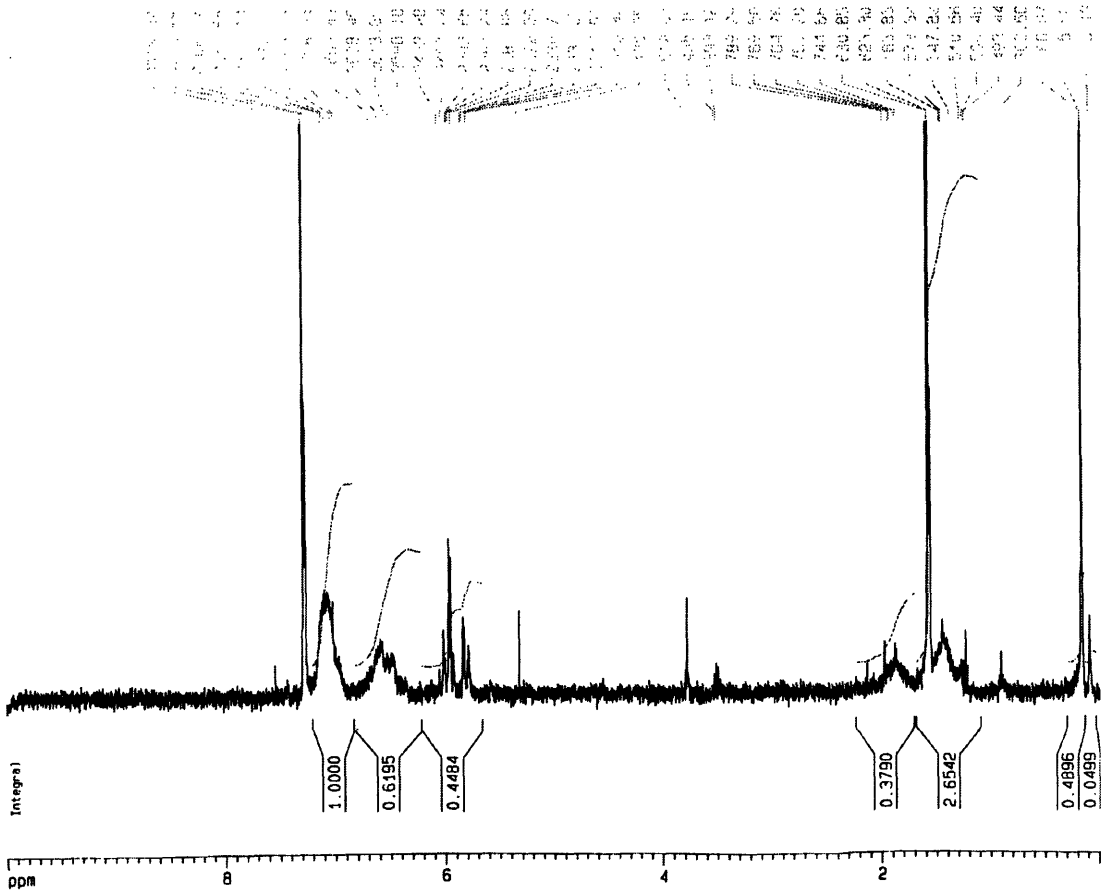

Figure 2.7: NMR of PS27-PVMS60. The PVMS molecular weight was calculated to be 69900g/mol knowing the PS molecular weight from GPC and using NMR to do endgroup analysis by comparing the PS phenyl peaks to the PVMS methyl and vinyl peaks.

After the polymer was recovered the desired mesogen was attached using hydrosilylation, described in Section G of Synthesis Techniques.

B. PS-b-PVMS-b-PS Triblock Copolymers

As previously discussed, there were three methods initially considered to produce a triblock copolymer of this type. However, the diblock coupling method emerged as the most reasonable one taking into account the synthetic expertise of the group. As mentioned already, this

technique involved coupling two living PS-b-PVMS diblock copolymers. Therefore, the diblock could be prepared as discussed in Section A. However, instead of using trimethylchlorosilane to terminate the polymerization, 1,1,3,3-tetramethyl-1,3-dichlorodisiloxane was used in order to couple two diblocks. PDI values for this method are generally around 1.3[13]. Previous studies[15] have used elevated temperatures to increase the polymerization rate without adversely affecting the polymer quality. This modification was used to successfully make one triblock copolymer and the synthetic scheme is shown in Figure 2. 8.

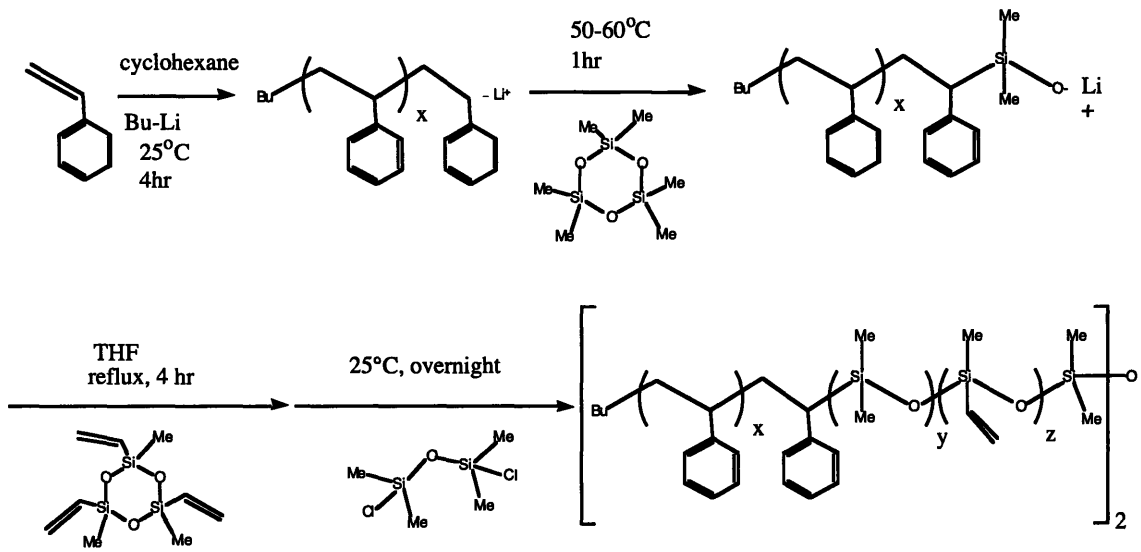

Figure 2.8: Scheme used to synthesize a PS-PVMS-PS triblock copolymer

Polymerization procedure: 3mL cyclohexane was added to a flask with stirring, followed by 90μL butyl lithium. After stirring for about 1 minute, 1mL styrene was added. After 4 hours of reaction, a portion of the reaction mixture was taken and precipitated in methanol for analysis of the polystyrene homopolymer molecular weight and molecular weight distribution. The temperature was increased to 60°C. In a separate flask, 0.184g hexamethylcyclotrisiloxane was

dissolved in 0.8mL cyclohexane and this mixture was added to the living polystyryl anion solution. After 1 hour, the color of the living polystyryl anion cleared, indicating the conversion of the living polystyryl anion to a polydimethylsiloxanolate anion. In a separate flask, 1.15mL trimethyltrivinylcyclotrisiloxane, 1.4mL THF, and 2.8mL cyclohexane were mixed. This mixture was added to the polymerization flask. 4 hours after this addition, 5.05μL 1,1,3,3-tetramethyl-1,3-dichlorodisiloxane was added to terminate the polymerization. The reaction mixture was allowed to stir for overnight to ensure complete coupling. The solvents were then removed by vacuum. The product was re-dissolved in a minimal quantity of THF and precipitated into methanol. A white polymer powder was filtered from this solution.

GPC: PS homopolymer – M_n=17578g/mol, M_w=30632g/mol, PDI=1.743

PS-PVMS diblock – M_n=21636g/mol, M_w=38750g/mol, PDI=1.79

PS-PVMS-PS triblock – M_n=31983g/mol, M_w=43014g/mol, PDI=1.345

^{1}H NMR dH: 0.02-0.17 [m, Si-C**H**$_3$], 1.70-2.22 [m, br, -C**H**Ph-], 1.44-1.57 [m,br, -C**H**$_2$CHPh-], 5.79-6.06 [m,Si-C**H**=C**H**$_2$], 6.30-6.80 [m, Ar-H], 6.90-6.73 [m,Ar-H]

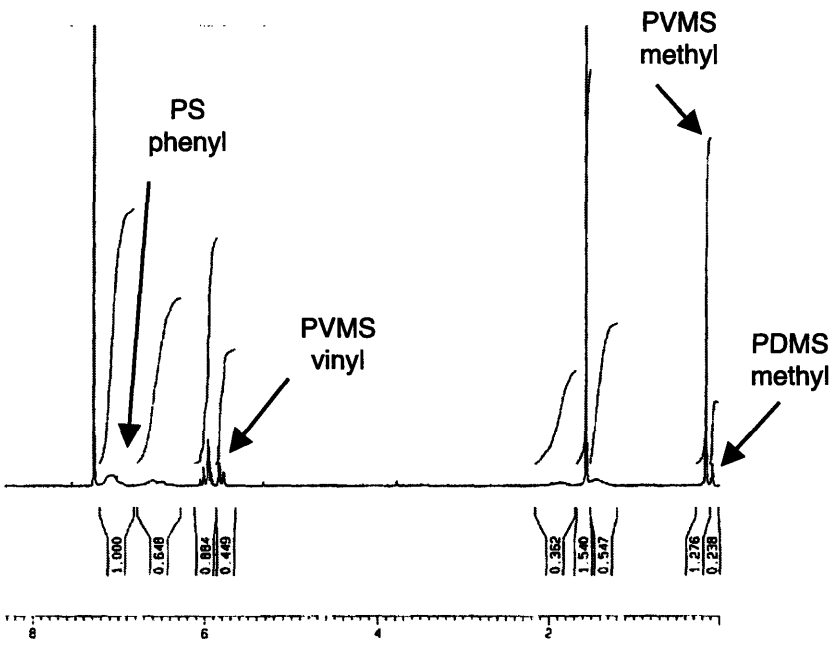

Figure 2.9: NMR of PS18-PVMS41-PS18 triblock copolymer indicating the peaks used for molecular weight calculations. Since the size of the PS block is known from GPC, ratios of the PS phenyl peak with the other peaks can be used to calculate PVMS and PDMS molecular weights.

After the polymerization, the mesogens could be attached using the standard hydrosilylation technique described in Section G.

C. PVMS Homopolymer

In addition to BCP studies, homopolymers were used to compare with small molecule LC data and with the BCP data. The synthesis of a PVMS homopolymer, including the mesogen attachment, was given in Moment's thesis[14] and is shown in Figure 2.10.

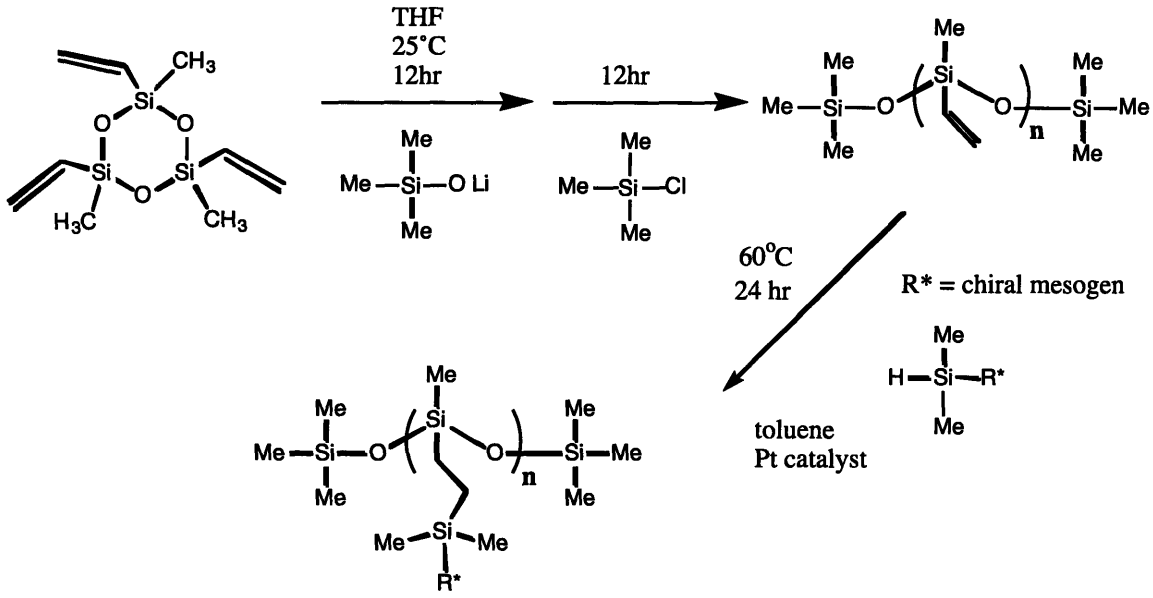

Figure 2.10: Synthesis of PVMS homopolymer[14]

Synthesis: 0.101g lithium trimethylsilanolate was mixed with 20mL tetrahydrofuran. In a separate flask, 10mL 1,3,5-trimethyl-1,3,5-trivinylcyclotrisiloxane was mixed with 20mL tetrahydrofuran. The contents of the second flask were added dropwise to the first flask over 10min. A light yellow color is observed. This reaction mixture was allowed to react for 12hr at room temperature. 0.15mL trimethylchlorosilane was added to the polymerization flask to terminate the reaction. The solution turned clear. After 12hr, the termination was complete and the polymer was recovered by precipitating into 50mL methanol with 0.5mL triethylamine. The polymer precipitated as a second liquid phase. 0.273 g product. GPC: M_w = 9360, M_n = 13420, PDI =1.4.

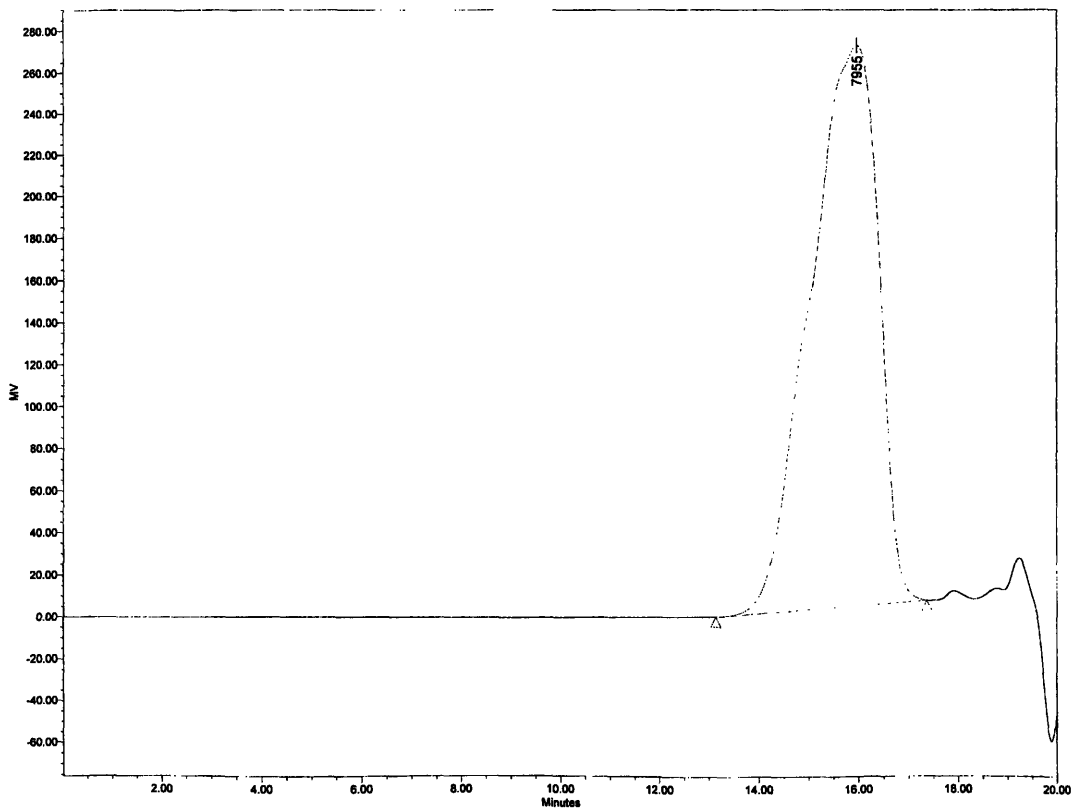

Figure 2.11: GPC of PVMS homopolymer

D. 8CB Mesogen

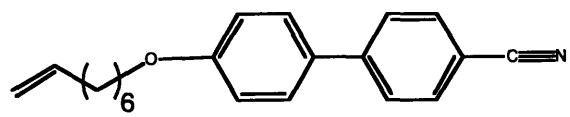

Figure 2.12: Chemical structure of 8CB mesogen

Materials: 4'-hydroxy-4-biphenylcarbonitrile was purchased from Sigma-Aldrich and recrystallized in hexane at 50°C. All other materials were used as received.

Synthesis: The synthesis of this mesogen was outlined in Dr. Bindu Nair's thesis[4]. In this reaction, 4.88g 4'-hydroxy-4-biphenylcarbonitrile was combined with 1.59g KOH in 5mL H_2O and 48mL ethanol in a flask. 4.3mL 8-bromo-1-octene was added to the flask and allowed to

reflux at 60°C overnight. The reaction solution was neutralized using hydrochloric acid and washed in a solution of 120mL dichloromethane and 80mL H_2O. The organic phase was dried over $MgSO_4$. The product was recovered using column chromatography (13:1 hexane:ethyl acetate). White crystals were recovered. ^{1}H NMR dH: 1.409-1.594 [m, 6 secondary H], 1.820-1.857 [m, 2 secondary H], 2.087-2.104 [m, 2H, $CH_2CH=CH_2$], 4.014-4.047 [m, 2H, CH_2OPh], 4.955-5.056 [m, 2H, $CH=CH_2$], 5.75-5.92 [m, 1H, $CH=CH_2$], 7.004-7.026 [m, 2H, Ar-H], 7.540-7.562 [m, 2H, Ar-H], 7.652-7.726 [m, 4H, Ar-H]

Si-H-tipped 8CB – 6.5mL toluene was mixed with 15mL tetramethyldisiloxane and heated to 60°C. In a separate flask, 2.28g vinyl-terminated 8CB was mixed in 8mLtoluene with 4drops 0.12M hexachloroplatinic acid in a dry flask. The contents of the second flask were added dropwise over a 10-15min period to the reaction flask. After 1day of reaction, the toluene and excess siloxane were removed at room temperature by vacuum. An oily yellow substance remained. The final product was isolated using column chromatography with 13:1 hexane:ethyl acetate as the mobile phase. 95% yield. ^{1}H NMR dH: 0.065-0.557 [m, 15 Si-CH_3], 1.349-1.581 [m, 12 secondary H], 1.816-1.836 [m, 2 secondary H], 4.013-4.046 [m, 2H, CH_2OPh], 4.955-5.056 [m, 2H, $CH=CH_2$], 5.75-5.92 [m, 1H, $CH=CH_2$], 7.005-7.027 [m, 2H, Ar-H], 7.539-7.561 [m, 2H, Ar-H], 7.652-7.727 [m, 4H, Ar-H]

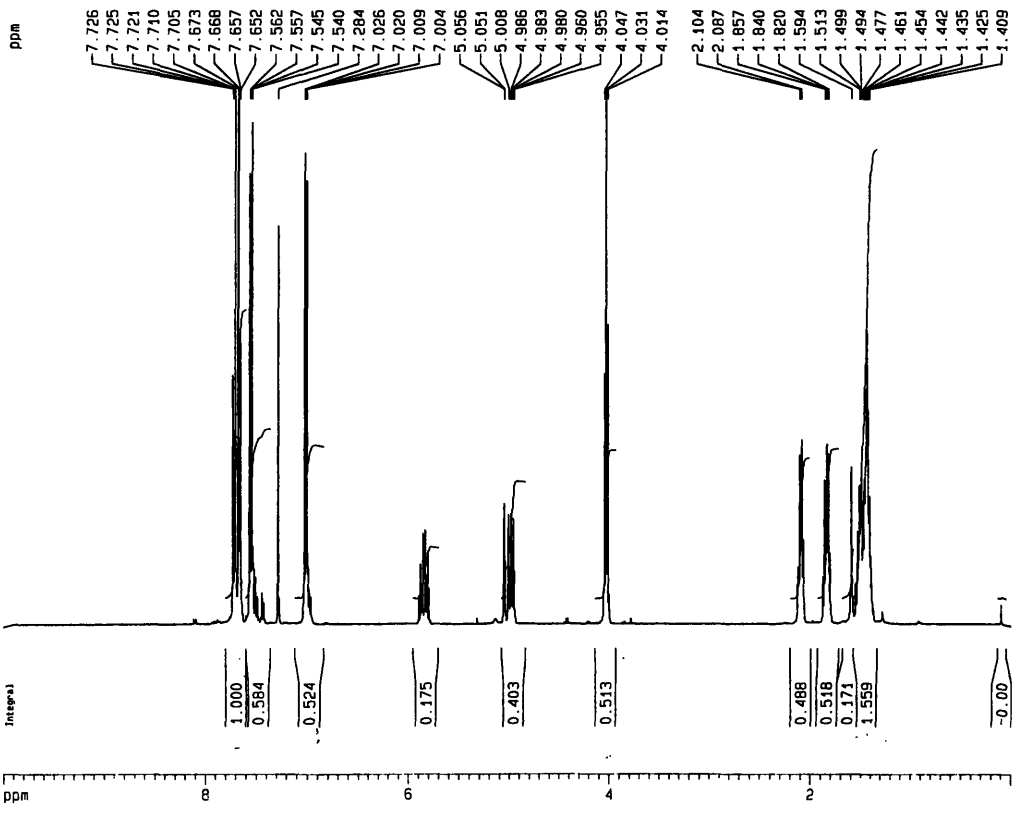
ppm
7.726
7.725
7.721
7.710
7.705
7.673
7.668
7.657
7.652
7.562
7.557
7.545
7.540
7.284
7.026
7.020
7.009
7.004
5.056
5.051
5.008
4.986
4.983
4.980
4.960
4.955
4.047
4.031
4.014
2.104
2.087
1.857
1.840
1.820
1.594
1.513
1.499
1.494
1.477
1.461
1.454
1.442
1.435
1.425
1.409
Integral
1.000
0.584
0.524
0.175
0.403
0.513
0.488
0.518
0.171
1.559
-0.00
ppm
8
6
4
2

(a)

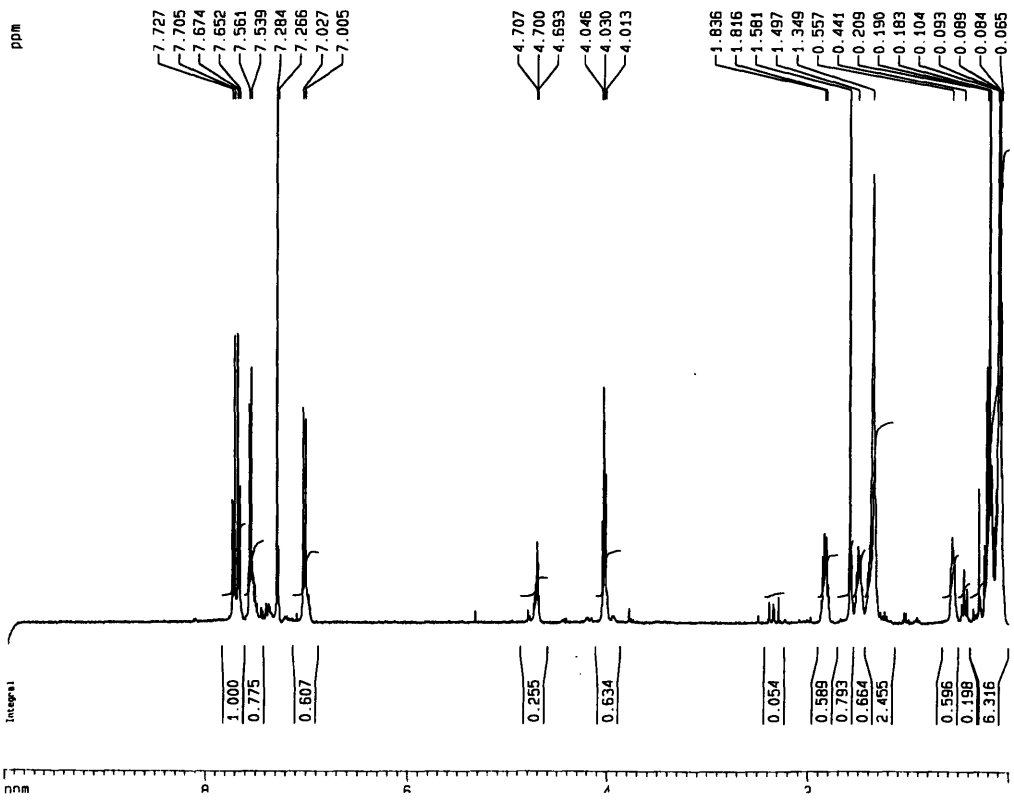

Figure 2.13: NMR of 8CB mesogen. (a) vinyl-tipped and (b) Si-H-tipped.

E. nMPOB Mesogen

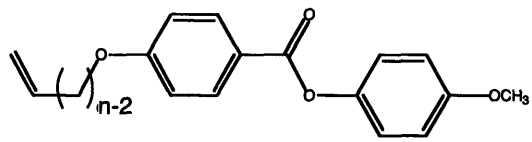

Figure 2.14: Chemical structure of nMPOB mesogen

The synthesis of this mesogen was outlined in an article by Yu, et al.[16].

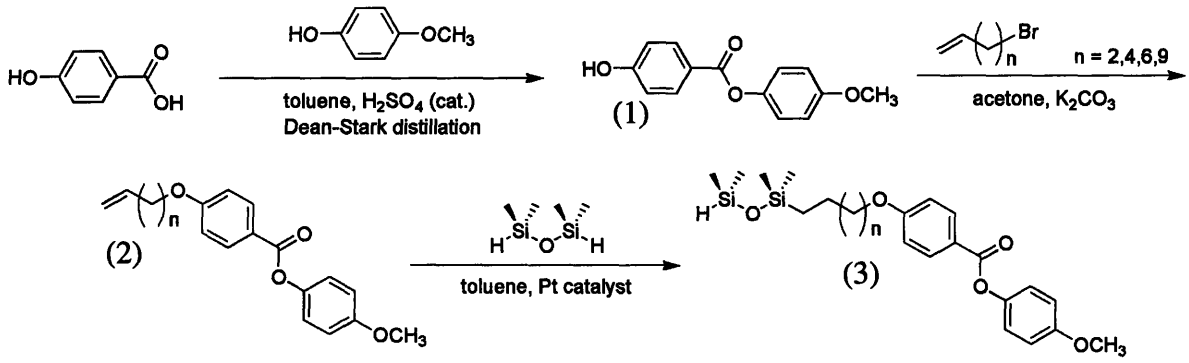

Figure 2.15: Synthesis of nMPOB mesogen, including hydrosilylation step

Materials: 4-methoxyphenol, 4-hydroxybenzoic acid, 11-bromo-1-undene, 8-bromo-1-octene, 1,1,3,3-tetramethyldisiloxane, and the platinum catalyst (platinum-divinyl tetramethyl disoloxane complex in xylene, Gelest SIP6831.0) were used without further purification.

Synthesis: *Intermediate 1* – 13.65g 4-methoxyphenol and 13.81g 4-hydroxybenzoic acid were combined in 60mL toluene in a reaction flask. 30drops sulfuric acid were added to the flask and the temperature was raised to 145°C. This solution was reacted overnight using a Dean-Stark distillation apparatus. A precipitate formed as the reaction was cooled to room temperature. This precipitate was filtered, redissolved in ethyl ether, then washed in $NaHCO_3$ followed by brine. The product in ethyl ether solution was dried using $MgSO_4$ before the ethyl ether was partially removed using rotary evaporation. Hexanes was added to the solution, causing a precipitate to form. The precipitate (Intermediate 1) was dried under vacuum. ^1H NMR dH: 3.8 [m, -OCH_3], 6.99-7.01 [m, 2H, Ar-H], 7.30-7.32 [m, 2H, Ar-H], 8.03-8.10 [m, 4H, Ar-H]

11MPOB Mesogen (Product 2a) – 2.44g of Intermediate 1 was dissolved in 50mL acetone with 1.27g K_2CO_3. $N_2(g)$ was bubbled through the mixture for 30min to remove O_2. 2.4mL 11-bromo-1-undecene was added to this mixture and the reaction was allowed to reflux for 4days.

At the end of this time, the acetone was removed using rotary evaporation. The solid was redissolved in ethyl acetate followed by the addition of 1M hydrochloric acid, which caused a precipitate to form. The organic layer was separated and washed in hydrochloric acid again. The solution was dried over $MgSO_4$ and the solvent was removed by vacuum. The final 11MPOB product (2) was isolated using a packed column with a mobile phase of 1:8 hexane:ethyl acetate, followed by a column using 1:2 hexane:dichloromethane solution. A 90% yield was achieved. ^{1}H NMR dH: 0.917-1.06 [m, 6 primary H], 1.21-1.54 [m, 8 secondary H], 1.88-1.90 [m, 1 tertiary H, 2 secondary H], 2.07-2.09 [m, 2H, $CH_2CH=CH_2$], 4.05-4.09 [m, 2H, CH_2OPh], 4.22-4.24 [m, 2H, CH_2OCOPh], 4.95-5.08 [m, 2H, $CH=CH_2$], 5.81-5.92 [m, 1H, $CH=CH_2$], 6.99-7.01 [m, 2H, Ar-H], 7.30-7.32 [m, 2H, Ar-H], 8.03-8.10 [m, 4H, Ar-H]

Si-H-tipped 11MPOB (Product 3a) – 0.792g 11MPOB and 2.67g 1,1,3,3-tetramethyl-disiloxane were dissolved in 10mL anhydrous toluene. Nitrogen gas was bubbled through the solution for 10 minutes. 2drops platinum catalyst was added and the solution temperature was increased to 65°C. The reaction mixture was stirred for 2 days. The solvent and excess tetramethyldisiloxane were removed by rotary evaporator and the crude product was further purified by column chromatography (13:1 hexane:ethyl acetate). 95% yield. ^{1}H NMR dH: 0.10-0.19 [m, 12 Si-CH_3], 0.4-0.5 [m, 2 Si-CH_2], 1.34-1.59 [m, 12 aliphatic CH_2], 1.80-1.98 [m, 1 tertiary H, 2 secondary H], 4.05-4.09 [m, 2H, CH_2OPh], 4.14-4.70 [m, 2H, CH_2OCOPh], 4.71 [s, 1 Si-H], 6.99-7.01 [m, 2H, Ar-H],7.30-7.32 [m, 2H, Ar-H], 8.13-8.18 [m, 4H, Ar-H]

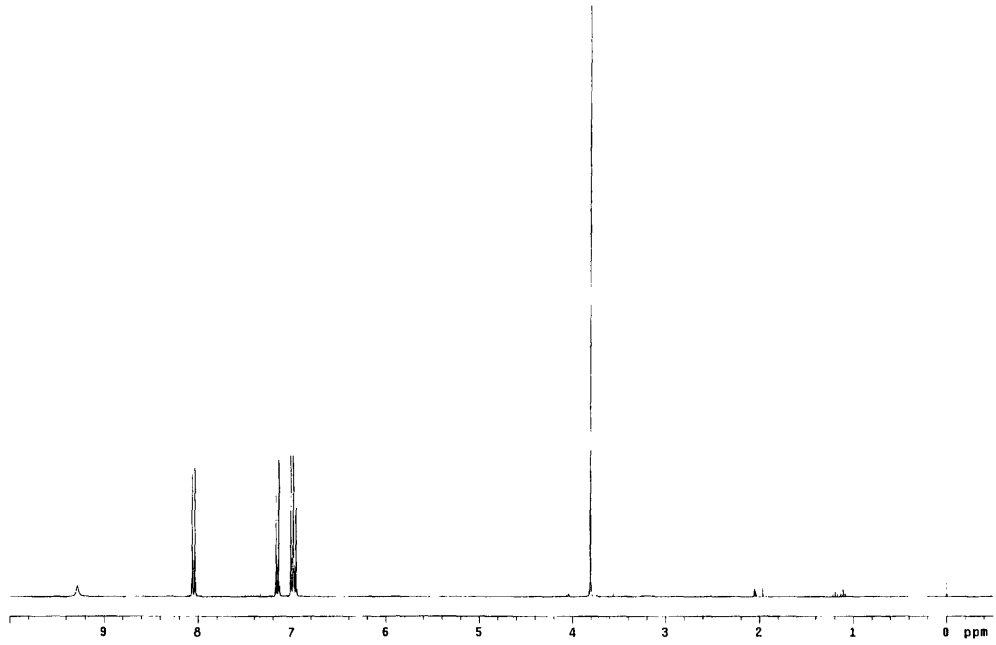

(a)

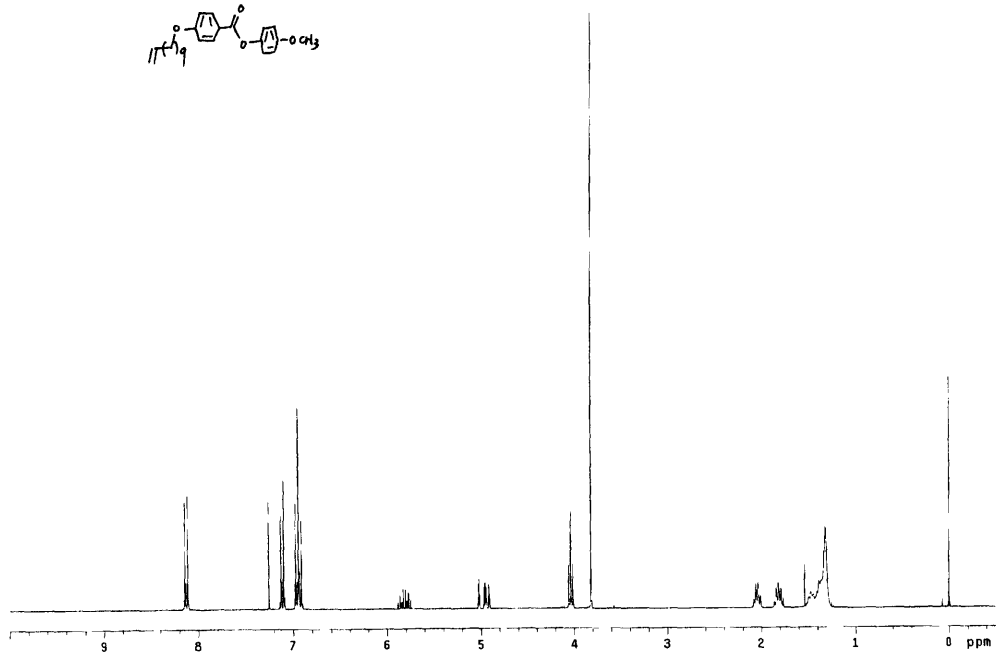

(b)

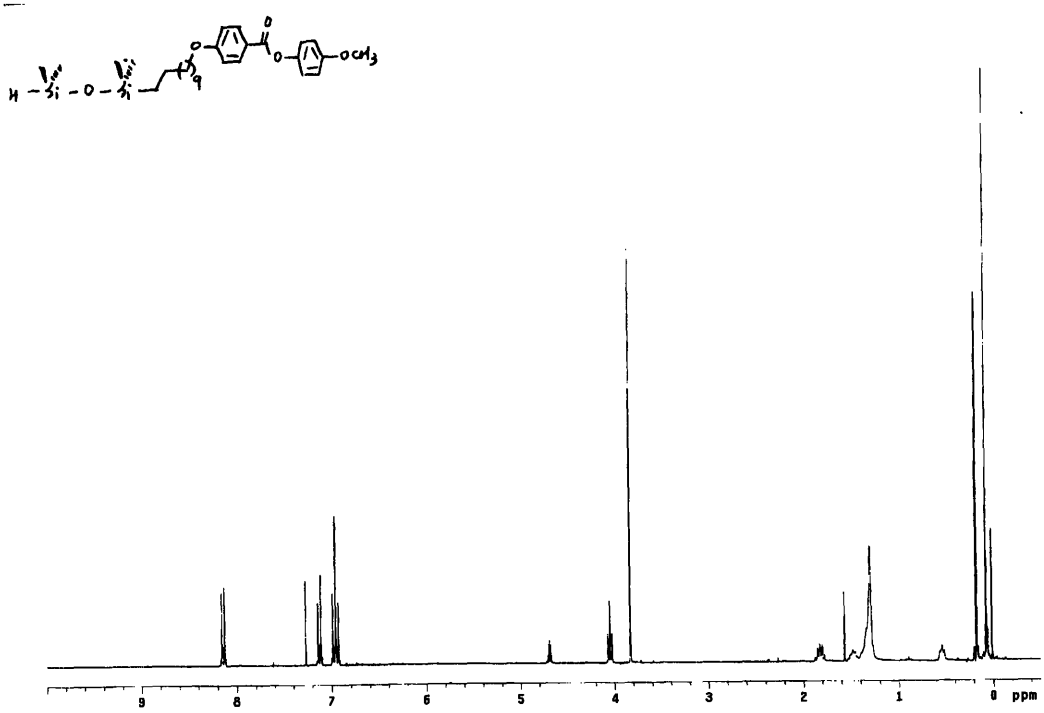

(c)

Figure 2.16: NMR of (a) Intermediate 1, (b) 11MPOB mesogen, and (c) Si-H-tipped 11MPOB

8MPOB Mesogen (Product 2b) – 2.44g of Product 1 was dissolved in 50mL acetone with 1.16g K_2CO_3. N_2(g) was bubbled through the mixture for 15min to remove O_2. 1.84mL 8-bromo-1-octene was added to this mixture and the reaction was allowed to reflux for 4days. The product was recovered using the same procedure as for 11MPOB (Product 2a). A 90% yield was achieved. ^{1}H NMR dH: 0.917-1.06 [m, 6 primary H], 1.21-1.54 [m, 8 secondary H], 1.88-1.90 [m, 1 tertiary H, 2 secondary H], 2.07-2.09 [m, 2H, $CH_2CH=CH_2$], 4.05-4.09 [m, 2H, CH_2OPh], 4.22-4.24 [m, 2H, CH_2OCOPh], 4.95-5.08 [m, 2H, $CH=CH_2$], 5.81-5.92 [m, 1H, $CH=CH_2$], 6.99-7.01 [m, 2H, Ar-H], 7.30-7.32 [m, 2H, Ar-H], 8.13-8.18 [m, 4H, Ar-H]

Si-H-tipped 8MPOB (Product 3b) – 2.47g 8MPOB and 9.36g 1,1,3,3-tetramethyl-disiloxane were dissolved in 50mL anhydrous toluene. Nitrogen gas was bubbled through the solution for 10 minutes. 14drops platinum catalyst was added and the solution temperature was increased to

65°C. The reaction mixture was stirred for 2 days. The final product was isolated using column chromatography with 13:1 hexane:ethyl acetate as the mobile phase. 95% yield. ^{1}H NMR dH: 0.10-0.19 [m, 12 Si-C**H**$_3$], 0.4-0.5 [m, 2 Si-C**H**$_2$], 1.34-1.59 [m, 12 aliphatic C**H**$_2$], 1.80-1.98 [m, 1 tertiary H, 2 secondary H], 4.05-4.09 [m, 2H, C**H**$_2$OPh], 4.14-4.70 [m, 2H, C**H**$_2$OCOPh], 4.71 [s, 1 Si-**H**], 6.99-7.01 [m, 2H, Ar-H],7.30-7.32 [m, 2H, Ar-H], 8.13-8.18 [m, 4H, Ar-H]

4MPOB Mesogen (Product 2c) – 2.44g of Product 1 was dissolved in 50mL acetone with 1.27g K_2CO_3. N_2(g) was bubbled through the mixture for 15min to remove O_2. 1.12mL 4-bromo-1-butene was added to this mixture and the reaction was allowed to reflux for 4days. The product was recovered as discussed for 11MPOB (Product 2a). A 90% yield was achieved. ^{1}H NMR dH: 0.917-1.06 [m, 6 primary H], 1.21-1.54 [m, 8 secondary H], 1.88-1.90 [m, 1 tertiary H, 2 secondary H], 2.07-2.09 [m, 2H, C**H**$_2$CH=CH$_2$], 4.05-4.09 [m, 2H, C**H**$_2$OPh], 4.22-4.24 [m, 2H, C**H**$_2$OCOPh], 4.95-5.08 [m, 2H, CH=C**H**$_2$], 5.81-5.92 [m, 1H, C**H**=CH$_2$], 6.99-7.01 [m, 2H, Ar-H], 7.30-7.32 [m, 2H, Ar-H], 8.13-8.18 [m, 4H, Ar-H]

Si-H-tipped 4MPOB (Product 3c) – 0.652g 11MPOB and 2.67g 1,1,3,3-tetramethyl-disiloxane were dissolved in 10mL anhydrous toluene. Nitrogen gas was bubbled through the solution for 10 minutes. 2drops platinum catalyst was added and the solution temperature was increased to 65°C. The reaction mixture was stirred for 2 days. The final product was isolated using column chromatography with 13:1 hexane:ethyl acetate as the mobile phase. 95% yield. ^{1}H NMR dH: 0.10-0.19 [m, 12 Si-C**H**$_3$], 0.4-0.5 [m, 2 Si-C**H**$_2$], 1.34-1.59 [m, 12 aliphatic C**H**$_2$], 1.80-1.98 [m, 1 tertiary H, 2 secondary H], 4.05-4.09 [m, 2H, C**H**$_2$OPh], 4.14-4.70 [m, 2H, C**H**$_2$OCOPh], 4.71 [s, 1 Si-**H**], 6.99-7.01 [m, 2H, Ar-H],7.30-7.32 [m, 2H, Ar-H], 8.13-8.18 [m, 4H, Ar-H]

F. nBPP4 Mesogen

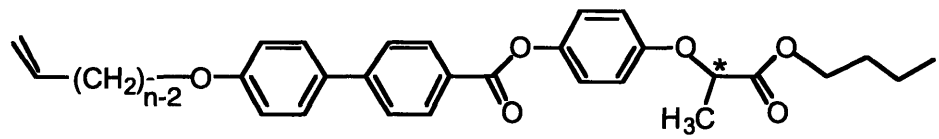

Figure 2.17: Chemical structure of nBPP4 mesogen

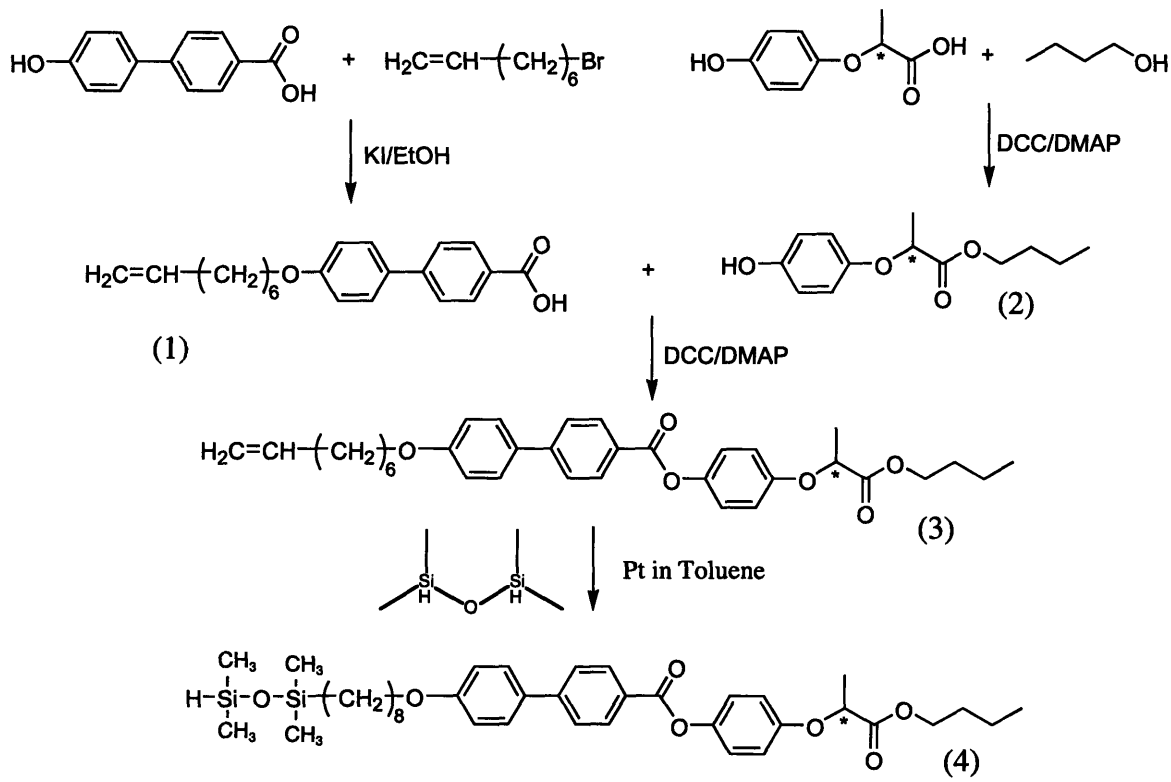

Figure 2.18: Synthesis scheme for 8BPP4 mesogen (modified from Svensson, et al.[21])

Synthesis: *Intermediate 1a (8-carbon spacer)* – 15.1mL 8-bromo-1-octene is combined with 9.65g 4'-hydroxy-4-biphenylcarboxylic acid in 750mL hot ethanol, 37.5mL H_2O, 5.75g KOH, and a few crystals of KI. This mixture is stirred at 70°C under argon gas for 1day. Hydrochloric acid was added to cause the product to precipitate. The solid was then dissolved in acetic acid and stirred overnight. The remaining salts were filtered and the solution with product was

concentrated. This concentrated product was precipitated in ethanol to isolate the Intermediate 1 from the starting materials that are soluble in ethanol. This solid was filtered and dried under vacuum to obtain Intermediate 1a. 60% yield. ^{1}H NMR dH: 1.26-1.34 [m, 6 secondary H], 1.65-1.75 [m, 2 secondary H], 1.98-2.04 [m, 2 secondary H], 4.01-4.07 [m, 2 Ar-OC**H**$_2$], 4.91-5.05 [m, 2H, CH=C**H**$_2$], 5.75-5.9 [m, 1H, C**H**=CH$_2$], 6.97-7.09 [d, 2 aromatic H], 7.6-7.7 [d, 2 aromatic H], 7.75-7.82 [d, 2 aromatic H], 7.9-7.98 [d, 2 aromatic H]

Intermediate 2 – Separately, 10g (R)-(+)-2-(4-hydroxyphenoxy)propionic acid was combined with 60mL n-butyl alcohol, 18.81g DMAP, and 100mL methylene chloride under argon with positive pressure. When the compounds were dissolved, 9.086g diisopropylcarbodiimide (DIPC) was added to the flask. The reaction was allowed to run overnight. The solution was concentrating under vacuum, then dissolved in 80mL methylene chloride. This solution was then washed three times with 0.1M HCl, the four times with brine. The solution was dried over $MgSO_4$, then concentrated under vacuum. The product was dissolved in 4:1 hexane:ethyl acetate, which allowed urea to be filtered out. The solution was reconcentrated before isolating Intermediate 2 using column chromatography (4:1 hexane:ethyl acetate). 90% yield. ^{1}H NMR dH: 0.95-1.02 [m, 3 primary H], 1.2-1.3 [m, 2 secondary H], 1.55-1.7 [m, 2 secondary H, 3 primary H], 4.03-4.2 [m, 2H, C**H**$_2$O], 4.6-4.7 [m, 1H, OC**H**CO], 6.7-6.85 [m, 4 Ar-H]

8BPP4 Mesogen (Product 3a) – 7.5g Intermediate 1 was combined with 7.9g Intermediate 2 in 100mL methylene chloride with 3.09g DMAP. 140mL methylene chloride was added and the solution stirred. 10mL DMF was added with 60mL methylene chloride and 6mL DIPC to start the reaction. The reaction was allowed to stir overnight under argon. Excess reactants were filtered from this solution while leaving the product in the solution. The solution was washed three times with 0.1M HCl, then four times with brine. It was dried over $MgSO_4$ to remove any

residual water from the wash steps. The product solution was concentrated under vacuum and Product 3 was isolated using column chromatography. 90% yield. ^{1}H NMR dH: 0.95-1.02 [m, 3 primary H], 1.1-2 [m, 14 secondary H, 3 primary H], 4.01-4.1 [m, 2 Ar-OC**H**$_2$], 4.2-4.3 [m, 2H, COOC**H**$_2$], 4.6-4.7 [m, 1H, OC**H**CO], 4.91-5.05 [m, 2H, CH=C**H**$_2$], 5.75-5.9 [m, 1H, C**H**=CH$_2$], 6.7-6.85 [m, 4 Ar-H], 6.97-7.09 [d, 2 aromatic H], 7.6-7.7 [d, 2 aromatic H], 7.75-7.82 [d, 2 aromatic H], 7.9-7.98 [d, 2 aromatic H]

Si-H-tipped 8BPP4 (Product 4a) – 6.5mL toluene was mixed with 15mL tetramethyldisiloxane and heated to 60°C. In a separate flask, 2.28g vinyl-terminated 8BPP4 was mixed in 8mLtoluene with 4drops 0.12M hexachloroplatinic acid in a dry flask. The contents of the second flask were added dropwise over a 10-15min period to the reaction flask. After 3days of reaction, the toluene and excess siloxane were removed at room temperature by vacuum. An oily and grainy white substance remained. The final product was isolated using column chromatography with 13:1 hexane:ethyl acetate as the mobile phase. 95% yield. ^{1}H NMR dH: 0.05-0.25 [m, 12 Si-C**H**$_3$], 0.95-1.02 [m, 3 primary H], 1.2-1.35 [m, 14 secondary H], 1.6-1.75 [m, 2 secondary H, 3 primary H], 1.85-2.95 [m, 2 secondary H], 4.01-4.1 [m, 2 Ar-OC**H**$_2$], 4.2-4.3 [m, 2H, COOC**H**$_2$], 4.6-4.7 [m, 1H, OC**H**CO], 6.7-6.85 [m, 4 Ar-H], 6.97-7.09 [d, 2 aromatic H], 7.6-7.7 [d, 2 aromatic H], 7.75-7.82 [d, 2 aromatic H], 7.9-7.98 [d, 2 aromatic H]

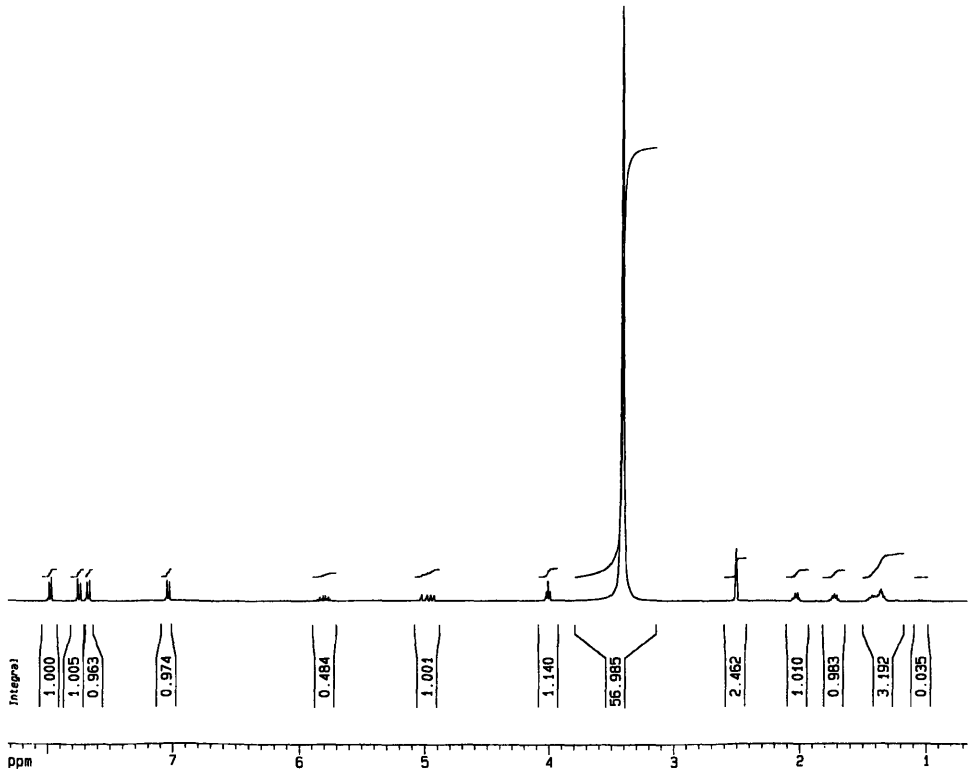
Integral
1.000
1.005
0.963
0.974
0.484
1.001
1.140
56.985
2.462
1.010
0.983
3.192
0.035
ppm
7
6
5
4
3
2
1

(a)

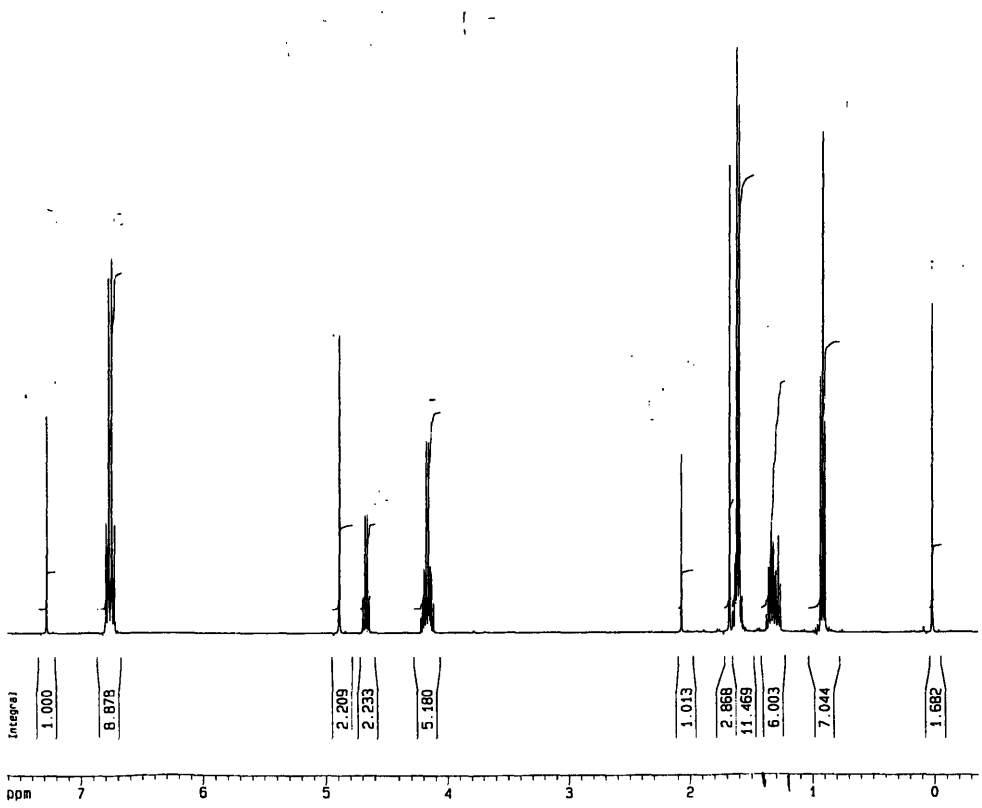
Integral
1.000
8.878
2.209
2.233
5.180
1.013
2.868
11.469
6.003
7.044
1.682
ppm
7
6
5
4
3
2
1
0

(b)

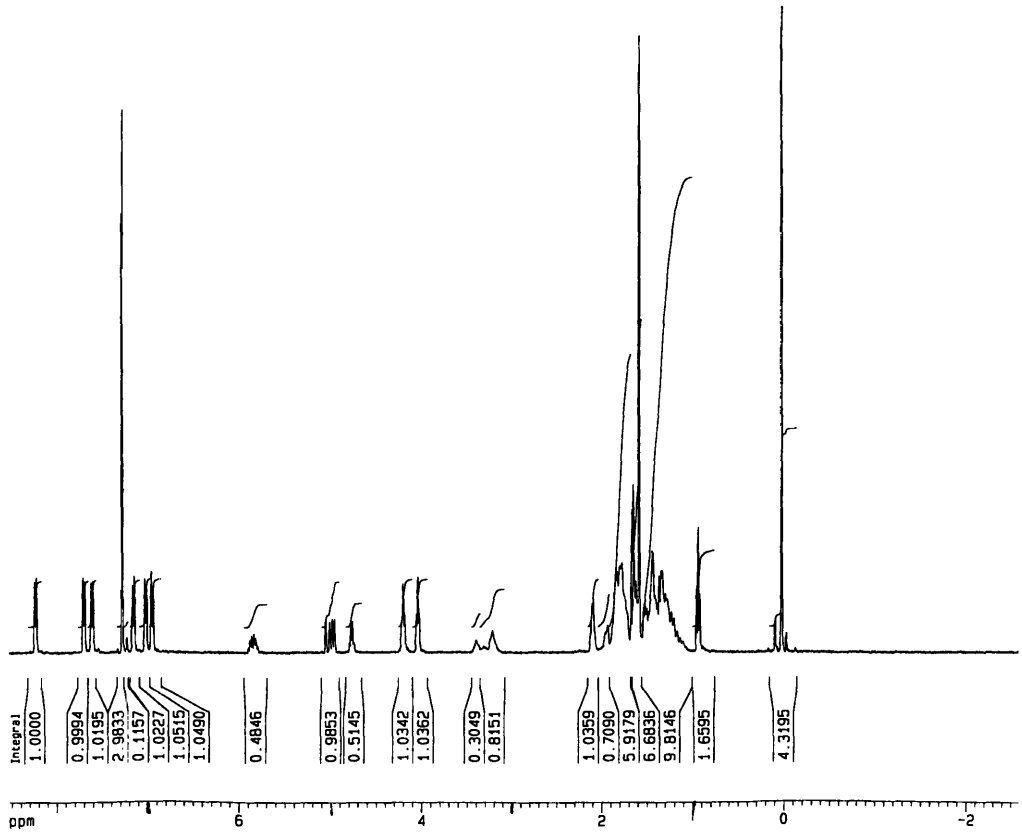
Integral
1.0000
0.9994
1.0195
2.9833
0.1157
1.0227
1.0515
1.0490
0.4846
0.9853
0.5145
1.0342
1.0362
0.3049
0.8151
1.0359
0.7090
5.9179
6.6836
9.8146
1.6595
4.3195
ppm
6
4
2
0
-2

(c)

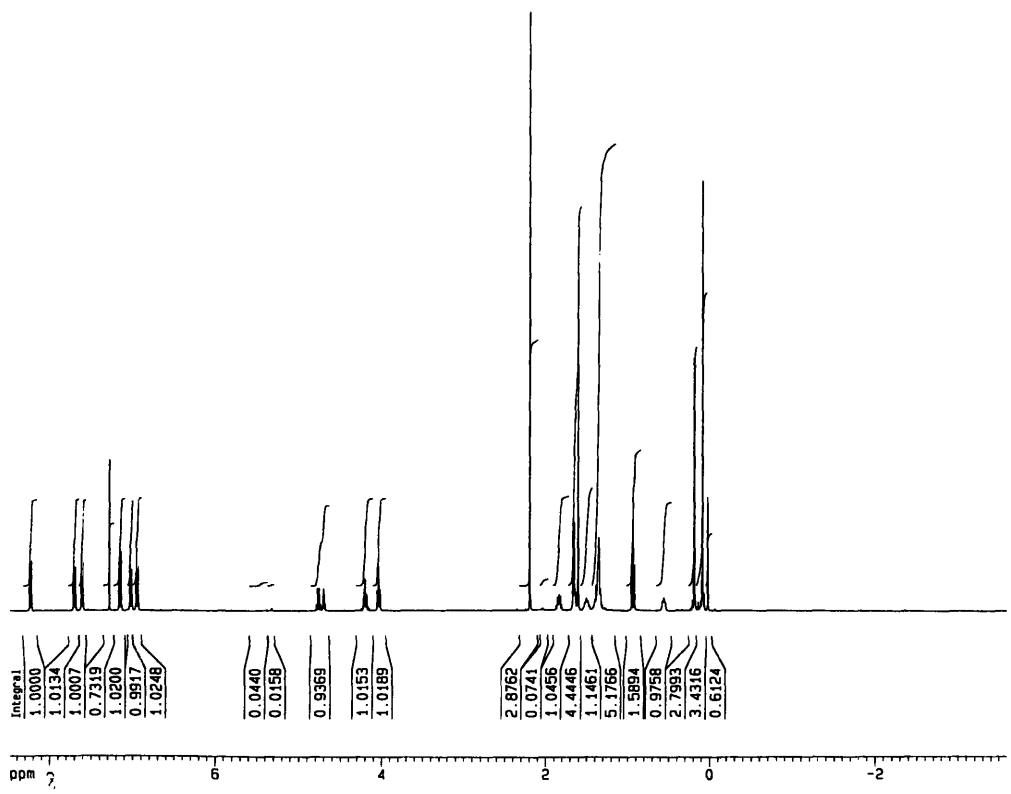
Integral
1.0000
1.0134
1.0007
0.7319
1.0200
0.9917
1.0248
0.0440
0.0158
0.9369
1.0153
1.0189
2.8762
0.0741
1.0456
4.4446
1.1461
5.1766
1.5894
0.9758
2.7993
3.4316
0.6124
ppm
6
4
2
0
-2

(d)

Figure 2.19: NMR for (a) Intermediate Product (1), (b) Intermediate Product 2, (c) 8BPP4 mesogen, and (d) Si-H-tipped 8BPP4 mesogen

Intermediate 1b (4-carbon spacer) – 13.4mL 4-bromo-1-butene is combined with 10g 4'-hydroxy-4-biphenylcarboxylic acid in 750mL hot ethanol, 37.5mL H_2O, 5.75g KOH, and a few crystals of KI. This mixture is stirred at 70°C under argon gas for 1day. The product was recovered as described in Intermediate 1a. 50% yield. ^{1}H NMR dH: 2.45-2.53 [m, 2 secondary H], 4.01-4.07 [m, 2 Ar-OC**H**$_2$], 4.91-5.05 [m, 2H, CH=C**H**$_2$], 5.75-5.9 [m, 1H, C**H**=CH$_2$], 6.97-7.09 [d, 2 aromatic H], 7.6-7.7 [d, 2 aromatic H], 7.75-7.82 [d, 2 aromatic H], 7.9-7.98 [d, 2 aromatic H]

4BPP4 Mesogen (Product 3b) – 4.06g Intermediate 1b was combined with 3.68g Intermediate 2 in 100mL methylene chloride with 0.4g DMAP. 140mL methylene chloride was added and the solution stirred. 10mL DMF was added with 60mL methylene chloride and 2.58mL DIPC to start the reaction. The product was recovered as described for 8BPP4 mesogen (Product 3a). 40% yield. ^{1}H NMR dH: 0.95-1.02 [m, 3 primary H], 1.1-2 [m, 2 secondary H, 3 primary H], 4.01-4.1 [m, 2 Ar-OC**H**$_2$], 4.2-4.3 [m, 2H, COOC**H**$_2$], 4.6-4.7 [m, 1H, OC**H**CO], 4.91-5.05 [m, 2H, CH=C**H**$_2$], 5.75-5.9 [m, 1H, C**H**=CH$_2$], 6.7-6.85 [m, 4 Ar-H], 6.97-7.09 [d, 2 aromatic H], 7.6-7.7 [d, 2 aromatic H], 7.75-7.82 [d, 2 aromatic H], 7.9-7.98 [d, 2 aromatic H]

Si-H-tipped 4BPP4 (Product 4b) – 6.5mL toluene was mixed with 15mL tetramethyldisiloxane and heated to 60°C. In a separate flask, 2.5g vinyl-terminated 4BPP4 was mixed in 8mL toluene with 0.05mL 0.12M hexachloroplatinic acid in a dry flask. The contents of the second flask were added dropwise over a 10-15min period to the reaction flask. 80% yield. ^{1}H NMR dH: 0.05-0.25 [m, 12 Si-C**H**$_3$], 0.95-1.02 [m, 3 primary H], 1.2-1.35 [m, 4

secondary H], 1.6-1.75 [m, 2 secondary H, 3 primary H], 1.85-2.95 [m, 2 secondary H], 4.01-4.1 [m, 2 Ar-OC**H**$_2$], 4.2-4.3 [m, 2H, COOC**H**$_2$], 4.6-4.7 [m, 1H, OC**H**CO], 6.7-6.85 [m, 4 Ar-H], 6.97-7.09 [d, 2 aromatic H], 7.6-7.7 [d, 2 aromatic H], 7.75-7.82 [d, 2 aromatic H], 7.9-7.98 [d, 2 aromatic H]

G. Hydrosilylation

Hydrosilylation is used in order to attach Si-H-terminated mesogens to the vinyl groups along the polymer backbone. This technique is described in Moment's thesis[14] and repeated in Figure 2.20.

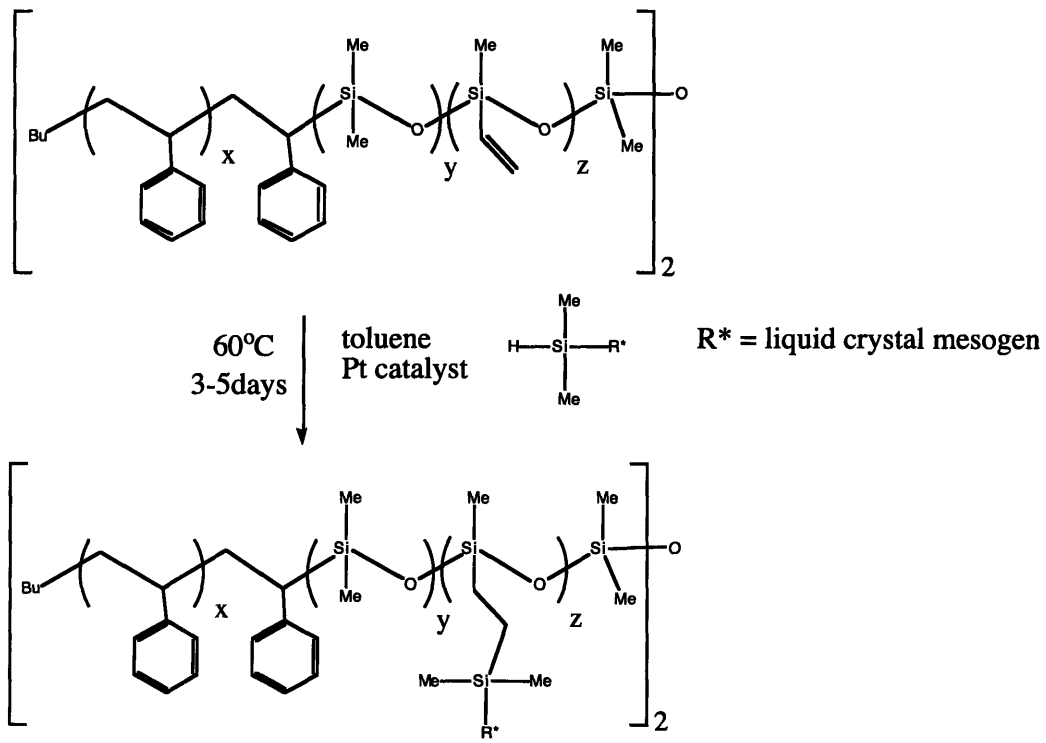

Figure 2.20: Hydrosilylation technique[14]

Synthesis: 0.251g PS27-PVMS16 was dissolved in 1mL toluene with stirring at 60°C. 4drops of hexachloroplatinic acid was added to this mixture, which was stirred for 15min. Finally, 1.03g Si-H-tipped 8BPP4 (~1:3 molar equivalents of vinyl groups to Si-H mesogens) was added drop-wise in 2mL toluene. The reaction mixture was stirred for 5days at 60°C. The toluene was removed at room temperature by vacuum, and the product was then dissolved in a minimal amount of THF and precipitated into methanol until no residual mesogen remains as determined by TLC. A soft white product was recovered. NMRs of the mesogen and functionalized polymer are shown in Figure 2.19. 1H NMR dH: 0.05-0.11 [m, Si-CH_3], 0.40-0.60 [m, Si-CH_2], 0.95-1.05 [m, CH_3-C], 1.22-1.70 [m, aliphatic], 1.72-2.10 [m, aliphatic], 4.01-4.11 [m, CH_2OPh], 4.14-4.24 [m, CH_2OCOPh], 5.70-6.10 [m, Si-CH=CH_2], 6.30-6.80 [m, Ar-H], 6.94-6.99 [m, Ar-H], 7.01-7.10 [m, Ar-H], 7.26-7.30 [d, Ar-H], 8.12-8.15 [m, Ar-H]

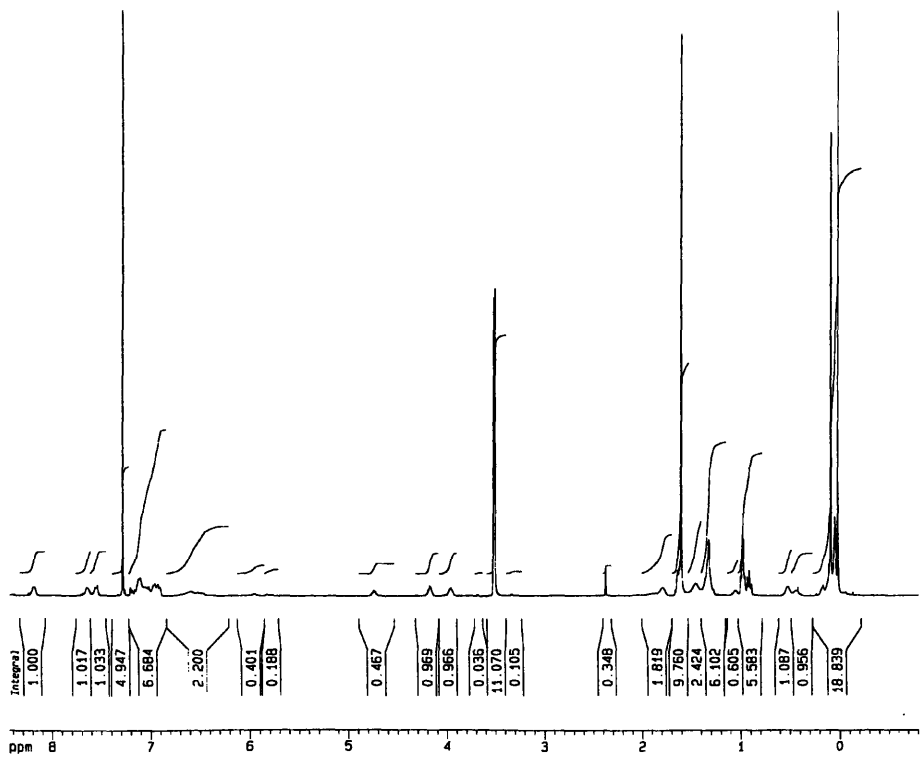

Figure 2.21: NMR data for 8BPP4 attached to PS27-PVMS16 (PS27-LCP_{8BPP4}108)

The mesogen attachment percentage can be determined using end group analysis on the NMR data for the functionalized polymer. In these calculations, the ratio of PS phenyl peaks to PVMS vinyl peaks in the polymer backbone can be compared to the ratio in the functionalized polymer. Since the number of PS phenyl groups is unaffected by the mesogen attachment, this is the control peak. In the case of PS27-LCP_{8BPP4}108, comparing Figures 2.19d with 2.21, the mesogen substitution was determined to be 73%.

Summary of Materials Synthesized

While many polymer samples were synthesized, Table 2.2 lists the polymer backbones that were used in the current research and the functionalized polymers studied are listed in Table 2.3.

Table 2.1: Summary of polymer backbones used

Polymer	PS block	PS PDI	PDMS block	PVMS block	Polymer MW	Polymer PDI	PVMS wt%
PVMS10	--	--	--	10000	10000	1.76	100
PS16-PVMS29	16197	1.44	1486	29395	47078	1.03	62.4
PS18-PVMS41-PS18	17578	1.74	1071	19603	76504	1.34	51.2
PS27-PVMS16	26956	1.17	445	15507	42908	1.06	36.1

Table 2.2: Summary of functional polymers studied

Polymer Name	PS MW	PS T_g (°C)	LC Attachment	LCP MW	LCP T_g (°C)	Total MW	LCP wt%
LCP_{11MPOB}62	-	-	85	62400	-35	62400	100
PS16-LCP_{11MPOB}183	16200	-	85	183300	-35	199500	92
PS18-LCP_{8CB}153-PS18	17600	59	53	153200	-41	188300	81
PS18-LCP_{4MPOB}218-PS18	17600	-	85	217800	-27	253000	86
PS18-LCP_{8MPOB}248-PS18	17600	76	88	247800	-22	283000	87
PS18-LCP_{11MPOB}258-PS18	17600	-	85	257900	-35	293000	88

PS18-LCP$_{10BPB4}$297-PS18	17600	76	67	297500	-31	332600	89
PS27-LCP$_{4BPP4}$79	27000	85	55	79400	-20	106300	75
PS27-LCP$_{4MPOB}$84	27000	84	85	84000	-20	111000	76
PS27-LCP$_{11MPOB}$99	27000	61	85	99500	-29	127400	79
PS27-LCP$_{8BPP4}$108	27000	65	73	107700	-10	134700	80

Results from the studies on the polymers functionalized with mesogens that are not chiral (8CB and nMPOB) will be given in Chapter 3. Studies on the polymers functionalized with chiral mesogens (nBPP4 and 10BPB4) will be reported in Chapter 4. Data from processing studies on PS27-LCP$_{4BPP4}$79 will be given in Chapter 5.

References

1. Moment, A. J.; Miranda, R.; Hammond, P. T., Synthesis of polystyrene-polysiloxane side-chain liquid crystalline block copolymers. *Macromolecular Rapid Communications* **1998,** 19, 573-579.

2. Anthamatten, M. L. Massachusetts Institute of Technology, Cambridge, MA, 2001.

3. Omenat, A.; Hikmet, R. A. M.; Lub, J.; van der Sluis, P., Synthesis, Characterization, and Physical Properties of New Ferroelectric Liquid Crystalline Materials: Block Copolymers. *Macromolecules* **1996,** 29, (21), 6730-6736.

4. Nair, B. Massachusetts Institute of Technology, Cambridge, MA, 2001.

5. Stanczyk, W. A.; Ganicz, T.; Gladkova, N. K.; Bialecka-Florjanczyk, E.; Sledzinska, I. In *Liquid Crystals: Chemistry, Physics, and Applications*, Proceedings of SPIE, 2000; Klosowicz, S. J.; Rutkowska, J.; Zielinski, J.; Zmija, J., Eds. 2000; pp 23-29.

6. Wewerka, A.; Floudas, G.; Pakula, T.; Stelzer, F., Side-Chain Liquid Crystalline Homopolymers and Copolymers. Structure and Rheology. *Macromolecules* **2001,** 34, (23), 8129-8137.

7. Zhukov, S.; Geppert, S.; Stühn, B.; Staneva, R.; Gronski, W., Dielectric Relaxation in Isotropic/Liquid Crystalline Block Copolymers: Effect of Nanoscale Confinement on the Local ß and g Dynamics. *Macromolecules* **2003,** 36, (16), 6166-6170.

8. Gruneberg, K.; Naciri, J.; Shashidhar, R., Ferroelectric Properties of a Fast Switching Cyclic Siloxane Oligomer. *Chemistry of Materials* **1996,** 8, 2486-2490.

9. Spector, M. S.; Heiney, P. A.; Naciri, J.; Weslowski, B. T.; Holt, D. B.; Shashidhar, R., Electroclinic liquid crystals with large induced tilt angle and small layer contraction. *Physical Review E* **2000,** 61, (2), 1579-1584.

10. Sprunt, S.; Geer, R. E.; Crawford, G. P.; Naciri, J.; Ratna, B. R.; Shashidhar, R., Large second-order optical nonlinearity in a molecular crystal formed from a chiral smectic liquid crystal. *Journal of Applied Physics* **1998,** 83, (5), 2392-2398.

11. Cooray, N. F.; Fujimoto, H.; Kakimoto, M.-A.; Imai, Y., Synthesis and Characterization of Novel Combined Type Ferroelectric Liquid Crystalline Polymers Having Polyester Main Chains. *Macromolecules* **1997,** 30, (11), 3169-3174.

12. Cooray, N. F.; Kakimoto, M.; Imai, Y., Novel Fluorine-Containing Ferroelectric Side Chain Liquid-Crystalline Polysiloxanes Showing Bistable Fast Switching. *Macromolecules* **1994,** 27, (6), 1592-1596.

13. Naciri, J.; Crawford, G. P.; Ratna, B. R.; Shashidhar, R., Effect of Chiral End Group Variations on the Properties of Ferroelectric Copolymers. *Ferroelectrics* **1993,** 148, 297-310.

14. Moment, A. The Synthesis and Characterization of Polystyrene Liquid Crystalline Siloxane Block Copolymers. Doctoral, Massachusetts Institute of Technology, Cambridge, MA, 2000.

15. Davies, W. G.; Jones, D. P., Styrene-Siloxane ABA Block Copolymer: Synthesis and Dilute Solution Properties. *Industrial Engineering Chemistry, Product Research and Development* **1971,** 10, 168-171.

16. Yu, H.-H.; Reed, K. G.; Moment, A. J.; Hammond, P. T., Liquid Crystalline Triblock Copolymer Actuators: 1. Syntheses of Difunctional Polysiloxane Microinitiators. *Polymer Preprints* **2004,** 45, (1), 529-530.

17. Huang, T. Z.; Knauss, D. M., Synthesis and characterization of (star polystyrene)-block-(linear polydimethylsiloxane)-block-(star polystyrene) triblock copolymers. *Polymer Bulletin* **2002,** 49, (2-3), 143-150.

18. Matyjaszewski, K.; Gaynor, S.; Wang, J. S., Controlled Living Radical Polymerization - Atom-Transfer Radical Polymerization in the Presence of Transition-Metal Complexes. *Journal of the American Chemical Society* **1995,** 117, (20), 5614-5615.

19. Patten, T. E.; Matyjaszewski, K., Atom transfer radical polymerization and the synthesis of polymeric materials. *Advanced Materials* **1998,** 10, (12), 901.

20. Brown, D. A.; Price, G. J., Preparation and thermal properties of block copolymers of PDMS with styrene or methyl methacrylate using ATRP. *Polymer* **2001,** 42, 4767-4771.

21. Svensson, M.; Helgee, B.; Sharp, K.; Andersson, G., Effects of nitro substituents on the properties of a ferroelectric liquid crystalline side chain polysiloxane. *Journal of Materials Chemistry* **1998,** 8, (2), 353-362.

Chapter 3 – Thermal Properties and Morphology of Polymers for Use as Nematic Actuators

Motivation and Background

In these studies a series of polymers functionalized with achiral mesogens is examined. Such materials in homopolymer studies have been found to exhibit large strains (40% or higher). Therefore, they are attractive as materials to consider for use in actuator applications based on nematic actuation. Additionally, recent research by the Kornfield group[1] indicates that large LC BCPs when blended with small molecule LCs can be used in electro-optical applications. These materials may also be used as sensors because certain properties such as chemical diffusivity can change when the material comes in contact with a specific chemical, producing an electrical polarization in the sample that can be used to signal the user(s) of the hazard. Additional opportunities for such materials were discussed in an article by Garg, et al.[2].

Previous research in this area has mainly included crosslinked polymer gels. Since those materials are chemically crosslinked, processing options are limited once the material is prepared. However, the materials examined in the current study take advantage of physical crosslinks to form ordered morphologies and stabilize the LC phase. Therefore, the materials may be reprocessed if necessary in order to obtain the desired morphology. A cylindrical morphology is desired so that both the LC and PS phases will be continuous. Therefore, the PS cylinders will stabilize the LC phase and will aid in obtaining a long-range, uniform nematic director.

Nematic liquid crystal-based materials have been studied for use as actuators. The Finkelmann group[3-7] has done extensive work in studying nematic elastomers and evaluated their

opportunity for use as actuators. Nematic actuation relies on smectic to nematic or nematic to isotropic phase transitions. This means that such actuation is only accessible in small temperature ranges near the transition temperature. However, nematic actuation has been shown to obtain very high strains. In studies by Naciri and coworkers[8], strains of 35-40% were achieved. Other studies have suggested that strains of 200% or higher are possible[6, 9]. In addition to the proper temperature regions, these actuations require large voltages. Therefore, a large energy input is needed for actuation to occur. Further, since nematic actuation is not bistable at zero applied electrical field, much more energy is required to maintain the actuation compared to ferroelectric actuation.

This chapter will examine the thermal properties and morphologies obtained when achiral mesogens are attached to block copolymer backbones. Such an investigation was necessary in order to determine if the materials are useful as nematic actuators. To be used as nematic actuators, materials should have PS cylinders in a LCP matrix and strong phase segregation. TEM and SAXS were used to determine the BCP morphologies, while DSC, temperature-dependent SAXS, and optical microscopy were used to determine thermal transitions. WAXS was also used to study the mesogen spacing when it could not be determined using SAXS.

Experimental

Synthesis – All polymer and mesogen synthetic techniques were described in Chapter 2.

Sample Preparation – All polymer samples were cast from a concentrated (≥10wt%) toluene solution onto a Teflon coated sheet, then air dried for ~1day. Film thickness was approximately 0.25mm.

Gel Permeation Chromatography – GPC was used to determine the molecular weight and polydispersity of the polystyrene block in copolymers. This technique was not used to determine the polysiloxane molecular weight for reasons outlined in Moment's thesis[10]. A Waters Breeze gel permeation chromatography (GPC) system equipped with 2 Polymer Laboratories Plgel 5μm MIXED-C 300x7.5mm columns (200-2,000,000 MW range), a refractive index detector (Waters 2414), and an ultraviolet detector (Waters 2487, λ=254nm) was used for molecular weight measurement relative to polystyrene standards. The system also contains a column heater (T=35°C) and an inline degasser, and uses Waters Breeze software. Tetrahydrofuran (THF) was the mobile phase and a flowrate of 1ml/min was used.

Nuclear Magnetic Resonance – ^{1}H NMR was used to determine the molecular weight of the PDMS and PVMS blocks as well as for general characterization of synthesis products. This was done on a Bruker Avance DPX-400 400MHz NMR Spectrometer.

Optical Microscopy – OM was used to determine the types of LC phases present as well as their transition temperatures. Different LC phases produce characteristic textures when viewed through cross polarizers. A Zeiss Axioskop 2 MAT optical microscope equipped with a Linkam THMS600 hotstage and Linkam TP94 controller was used to observe samples under crossed polarizers at different temperatures. Images of the samples were captured using an AxioCam MRc camera and AxioVision software.

Small Angle X-ray Scattering – SAXS was used to determine the shape and orientation of polymer features with dimensions on the order of 100Å (spheres, cylinders, lamellae, etc.). The shape determination was based on the relative scattering vector ratios of the peaks in the profile, while the LC spacing was based on the *d*-spacing of the first-order peak. SAXS also allowed us to determine how these features were oriented with respect to each other. A Molecular

Metrology 2-D SAXS detector placed 1300mm from the sample was used to detect the scattering of Cu K_α x-rays at 45kV and 0.66mA produced by a Microsource x-ray generator. A Molecular Metrology hotstage with temperature controller was used for heating studies.

Additionally, SAXS equipment was available in the MIT Center for Materials Science and Engineering. This SAXS machine has a different range of q values than the Molecular Metrology SAXS and was used to characterize some samples. For this machine, a Siemens 2-D SAXS detector placed 130cm from the sample was used to detect the scattering of Cu K_α x-rays at 40kV and 24mA. In figures, "ISN" will be used to indicate data taken on the Molecular Metrology SAXS and "CMSE" will be used to indicate samples taken on the Siemens SAXS.

Transmission Electron Microscopy – TEM was used to obtain images of the phase-segregated morphology of the block copolymers. The type of morphology, grain size, and degree of ordering were determined with these images. Samples first were cryotomed before using in the TEM. A RMC MT-X ultramicrotome with CR-X cryo attachment was used to section samples of ~50nm in thickness below room temperature. The diamond knife temperature was set at -75°C and the sample temperature set at -85°C. Films were transferred to copper grids and, unless otherwise stated, stained for 25 minutes with the vapor from OsO_4 4% aqueous solution. OsO_4 preferentially stains the liquid crystal polymer, making these regions appear dark in the TEM images. Samples were observed with a JEOL 200CX electron microscope operating at 200kV.

Wide Angle X-ray Scattering – WAXS was used to determine the types of liquid crystal phases present (S_C*, S_A, N, etc.). LC spacings with dimensions of 40Å and smaller were studied with this method. The same equipment used for SAXS was used for WAXS by moving the detector closer to the sample (sample-to-detector distance = 300mm).

Differential Scanning Calorimetry – DSC was used to determine the transition temperatures of the LC phases and the T_g values of both polymer blocks. Both heating and cooling scans were done in a TA Instruments Q1000 auto modulated DSC. All scans were conducted at heating and cooling rates of 10°C/min, and at least two heating and cooling ramps were done for each sample. Q Series and TA Universal Analysis software were used to control the DSC and analyze data.

Results

Materials Used

Achiral mesogens were attached to the PVMS block of a PVMS homopolymer, a PS-PVMS diblock copolymer, or a PS-PVMS-PS triblock copolymer.

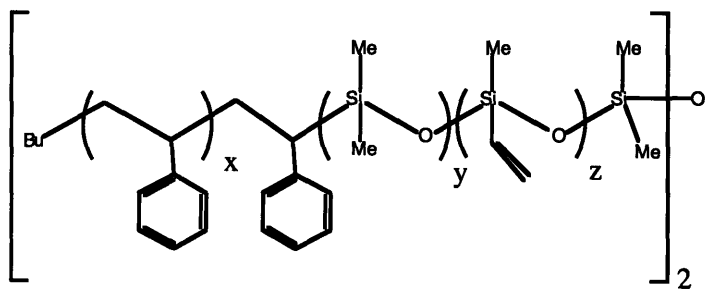

Figure 3.1: Chemical structure of the triblock copolymer. Mesogens were attached to the vinyl group on the PVMS block.

a. 8CB (n=8)

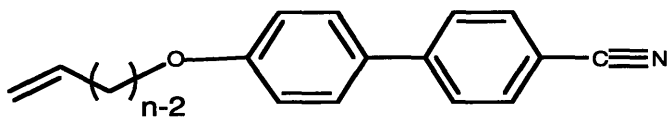

- Thermal Transitions – G <-20 S 60 N 90 I[11]

b. 4MPOB

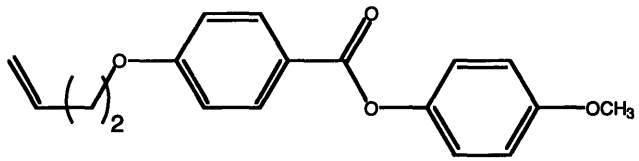

- Thermal Transitions – <-50 N 77 I

c. 8MPOB

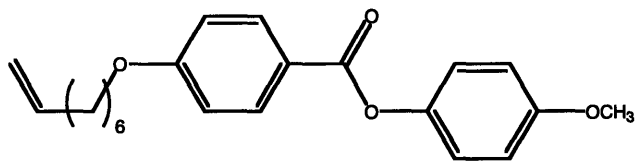

- Thermal Transitions – G 56 LC 63 I

d. 11MPOB

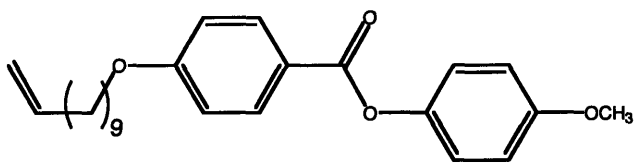

- Thermal Transitions – G 44 N 69 I

Figure 3.2: Mesogens studied for use as nematic actuators

These mesogens were attached to four polymer backbones of varying molecular weight and composition. The calculated molecular weights of the functional polymers that were synthesized were listed in Table 2.3 and the polymers that will be discussed in this chapter are in Table 3.1.

Table 3.1: Summary of polymers synthesized for use as nematic actuators

		POLYMER BACKBONES			
		PS27-PVMS16	**PS18-PVMS41-PS18**	**PS16-PVMS29**	**PVMS10**
MESOGENS	**8CB**		PS18-LCP_{8CB}153-PS18 (53%, 81%)		
	4MPOB	PS27-LCP_{4MPOB}84 (***85%*** , 76%)	PS18-LCP_{4MPOB}218-PS18 (***85%*** , 86%)		
	8MPOB		PS18-LCP_{8MPOB}248-PS18 (88%, 87%)		
	11MPOB	PS27-LCP_{11MPOB}99 (***85%*** , 79%)	PS18-LCP_{11MPOB}258-PS18 (***85%*** , 88%)	PS16-LCP_{11MPOB}193 (***85%*** , 92%)	LCP_{11MPOB}62 (***85%*** , 100%)

Key: Polymer Name (Mesogen attachment percentage, LCP weight percentage)

Notes: Boxes highlighted in grey indicate materials that were viscous liquids. Mesogen attachment percentages given in bold italics are assumed.

As discussed in Chapter 2, NMR was used to calculate mesogen attachment percentages, then that information was used to calculate the full polymer molecular weight for all materials. In some cases, NMR peaks from the mesogen and polymer coincided to the point that a good estimate of the mesogen attachment could not be determined. This was common in samples with the 4MPOB and 11MPOB mesogens. In those cases, the mesogen attachment percentage was assumed to be approximately the same as that of the sample with the 8MPOB mesogen.

Functionalized polymers had total molecular weights of 62000g/mol-284000g/mol, PS blocks of 0g/mol-27000g/mol, PDMS blocks of 400g/mol-1000g/mol, and PVMS-LC blocks of 62000g/mol-248000g/mol. Considering the short PDMS block to be part of the LCP and taking into account the mesogen functionalization percentages of 53%-88%, this created polymers that ranged from 76wt% to 100wt% LCP. Previous studies have shown that the critical degree of polymerization at which thermal transitions are no longer functions of molecular weight is 25-30 repeat units[12]. However, in previous studies on siloxane-based LCPs, a critical value of ~10 was

determined[13]. Therefore, all samples studied are much higher than this critical value and molecular weight should not impact such properties.

Thermal Transitions

DSC and POM were used to determine the transition temperatures of the liquid crystal block copolymers. While certain phase transitions and clearing points were observed in POM, characteristic liquid crystal textures were generally difficult to determine. Therefore, x-ray scattering was also used in some cases to determine liquid crystal phase transitions by monitoring the smectic liquid crystal peak. Table 3.2 shows a summary of the results from these studies. Figures 3.3 and 3.4 also show a characteristic POM image and DSC thermograph.

Table 3.2: Thermal transitions of polymers studied for use as nematic actuators

	LCP T_g	PS T_g	Transitions
PVMS10	-105	-	
$LCP_{11MPOB}62$	-35	-	G -35 LC 59 I
PS16-PVMS27	-60	81	
PS16-$LCP_{11MPOB}183$	-31	-	G -31 LC 62 I
PS18-PVMS41-PS18	-60	82	
PS18-$LCP_{8CB}153$-PS18	-41	59	G -41 S 12 N 59
PS18-$LCP_{4MPOB}218$-PS18	-27	-	G -27 LC 10 I
PS18-$LCP_{8MPOB}248$-PS18	-22	75	G -22 S 36 LC 75 I
PS18-$LCP_{11MPOB}258$-PS18	-33	-	G -33 LC 55 I
PS27-PVMS16	-60	84	
PS27-$LCP_{4MPOB}84$	-20	85	G -20 S 17 N 115 I
PS27-$LCP_{11MPOB}99$	-30	63	G -30 S 63 I

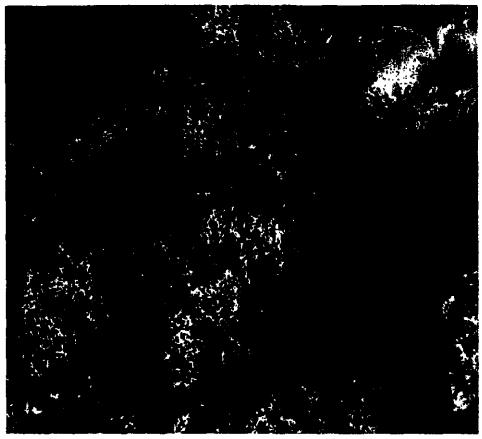

Figure 3.3: POM image of PS27-LCP_{11MPOB}99 at room temperature. Birefringence is observed, but characteristic textures are not.

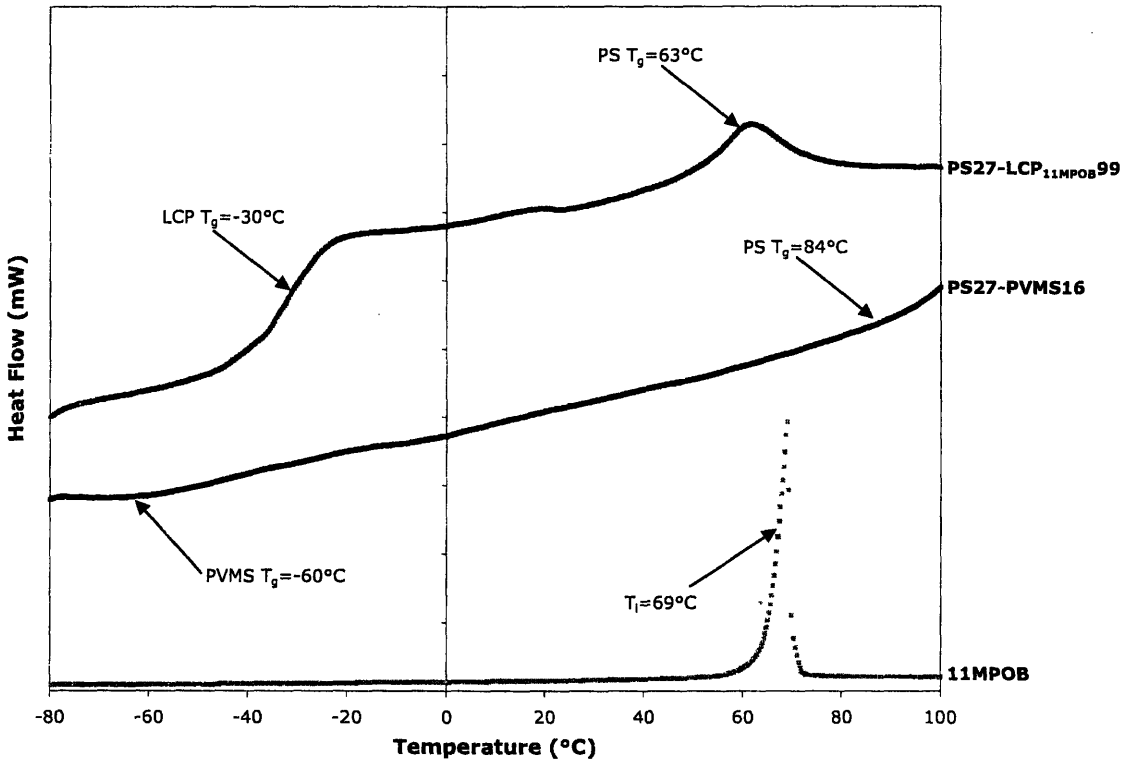

Figure 3.4: DSC thermographs of PS27-LCP_{11MPOB}99, 11MPOB mesogen, and PS27-PVMS16 polymer backbone. Transition temperatures are indicated using arrows.

As shown in Table 3.1, the PS T_g of unfunctionalized BCPs is 81°C-84°C and the PVMS T_g is –60°C. These values indicate phase mixing in the polymer backbone because both values exhibit significant deviations from their values in homopolymers. The T_g for pure PS is 105°C, while the PVMS T_g is –110°C[14]. In a perfectly segregated system, the BCP T_gs would be the same as they are in homopolymers. However, in these unfunctionalized polymer systems, the PVMS T_g is raised by 50°C and the PS T_g is lowered by 20°C, indicating some miscibility between the two blocks.

Further phase mixing is observed in most functionalized samples because the PS T_g is lowered from the PS phase being plasticized by the LCP phase. The only sample that does not exhibit such plasticization is PS27-LCP_{4MPOB}84. In that case, the PS T_g actually increases slightly from the enhanced phase segregation caused by mesogen being more tightly coupled to the polymer backbone. Some phase mixing is still evident, however, because the PS T_g is lower than it would be in a PS homopolymer. The strong phase segregation in PS27-LCP_{4MPOB}84 also leads to a stabilization of the LC phase by ~40°C. None of the other polymers functionalized with achiral mesogens exhibits such a stable LC phase, likely due to the poor phase segregation between the PS and LCP blocks.

It is also observed that the PVMS T_g is higher in the LC-functionalized polymers compared to its value in the unfunctionalized polymer, and significantly higher than it would be in an unfunctionalized PVMS homopolymer. While this also indicates phase mixing, it primarily indicates an increase in backbone rigidity caused by the mesogen attachment. One notes that the LCP T_g increases as the mesogen becomes more closely coupled to the backbone with a shorter spacer length. This agrees with results from studies by other groups on LCPs[15]. In addition, the values are reasonable compared to T_gs obtained in studies on similar LCP homopolymers[16]. The

only exception to this trend is that the LCP T_g in PS18-LCP_{4MPOB}218-PS18 is lower than that of PS18-LCP_{8MPOB}248-PS18. Since this difference is small, it can be attributed to the difference in mesogen attachment and some machine error. The PS18-LCP_{8CB}153-PS18 sample also had a significantly lower T_g compared with the other samples. Since PS18-LCP_{8CB}153-PS18 has a mesogen substitution of 53% while polymers functionalized with nMPOB mesogens have substitution percentages of ~85%, this difference in LCP T_g is primarily caused by the difference in mesogen substitution.

It is observed that two of the block copolymers with the 11MPOB mesogen do not exhibit PS T_gs. The lack of a PS T_g suggests that the PS and LCP regions are co-miscible in these samples. This observation is in agreement with the physical observation that the materials are viscous liquids and cannot form solid films. This result is caused by favorable interactions between the phenyl and biphenyl groups in the mesogen, and the PS block, which also contains phenyl groups. Such observations are similar to what Zheng[17], Anthamatten[18], and Moment[10] observed in their studies on mesogen/polymer miscibility. In those cases, unfunctionalized polymers were completely miscible with unattached small molecule LCs.

In the solid 11MPOB-functionalized polymer, the PS T_g coincides with the LC clearing point. Since the mesogen attachment percentage had to be estimated for most of these samples, it is not possible to determine how that impacted their thermal properties. However, another reason for the trends in the thermal data is the free energy in the LC BCP system, which is influenced by the ordering of the system and the co-miscibility of the two blocks. Previous studies have shown that the domain size, morphology, and interfacial curvature have an impact on LC transitions due to surface energy effects related to the LC confinement[6, 10, 18]. Since the domain size is on the order of tens of nanometers, the polymer translational motion is restricted

and mesogens cannot move freely. The specific mesogen anchoring at the interface will influence the LC alignment and can stabilize or destroy smectic phases. The morphology and interfacial curvature are determined by geometrical packing factors and the elastic energy of the LC phase. The geometrical packing factor encourages the formation of cylindrical and spherical morphology, while the elastic energy is minimized for planar interfaces because planar surfaces lead to minimal LC director deformation.

In a review by Walther and Finkelmann[6] and previous studies by Zheng[17] and Anthamatten[18], it was proposed that the effective χ parameter is actually a composite of the Flory-Huggins χ parameter for block copolymer segmental interactions, representing enthalpic contributions to segmental mixing, and an additional component due to the interactions between the mesogens, for which ordering is favorable, and the amorphous polymer (χ_{LC}). As an equation, this can be written,

$$\chi_{eff} = \chi + \chi_{LC} \tag{3.1}$$

This quantity takes into account enthalpic and excess entropic effects in LC BCP mixing. As temperature increases, the χ_{LC} component will decrease until it is negligible at the LC clearing point. Since the product $\chi_{eff}N$ must exceed a critical value in order for phase segregation to occur and χ_{eff} is a function of temperature, this value can be just above the critical value at lower temperatures to allow for phase segregation and just below the critical value at temperatures about T_i, to create phase mixing. Such an explanation is also not unreasonable considering that most of the nMPOB-functionalized polymers in this study were viscous liquids, already

indicating phase miscibility well below the LC clearing point (i.e. χ for these systems in not that large).

One also notices that all of the samples that were viscous liquids had polymer backbones that initially contained greater than 50wt% PVMS before the mesogen was attached. After the mesogens were attached, these samples were 86wt% or greater LCP. While our initial goal was to make a material with 80wt%-90wt% LCP so as to achieve cylindrical or spherical morphology in the thermoplastic elastomers, these results lead us to believe that such a large LCP block is undesirable with this type of mesogen. Therefore, future studies using similar mesogen/polymer pairs should consider materials that are ~70wt%-85wt% LCP.

A final observation from the thermal data is that functionalized polymers with mesogens with shorter spacers have a greater number of phase transitions compared to those with longer mesogens. Also, the clearing point increases as the spacer length decreases. This agrees with previous studies in this group[10] and in others[19]. However, in some studies using the nMPOB mesogen on a polycarbosilane homopolymers backbone[20], the clearing point actually increases with an increase in spacer length. The reasoning used to explain this is that the longer spacer plasticizes the backbone, causing it to be more flexible. Therefore, in our LC BCP systems, a similar explanation is still reasonable, but the spacer plasticizes the PS block and its T_g is lowered.

Block Copolymer Morphology

In addition to determining phase transitions, x-ray scattering, TEM, and AFM have been used to determine block copolymer morphologies and mesogen spacings in the various systems. A

summary of the results from these studies on the solid functionalized polymers at room temperature is given in Table 3.3 and supporting x-ray data are given in Figures 3.5 through 3.8.

Table 3.3: X-ray scattering data on block copolymer and LC spacings for phase-segregated functional polymers

	BCP Spacing (Å)	Observed LC Spacing (Å)
PS18-LCP$_{8CB}$153-PS18	250[1]	-
PS27-LCP$_{4MPOB}$84	370[2]	-
PS18-LCP$_{8MPOB}$248-PS18	450[2]	34[1]
PS27-LCP$_{11MPOB}$99	525[2]	58[2]

Key: 1 = data obtained on the CMSE SAXS, 2 = data obtained on the ISN SAXS

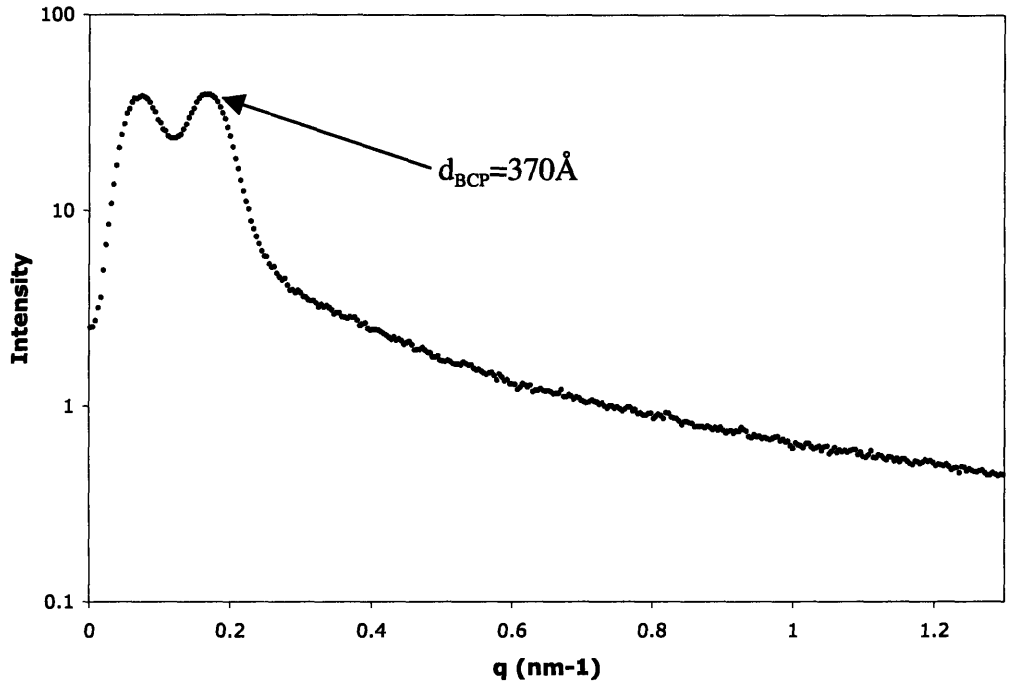

Figure 3.5: SAXS of PS27-LCP$_{4MPOB}$84 (ISN). The arrow indicates a BCP spacing peak at d=370Å.

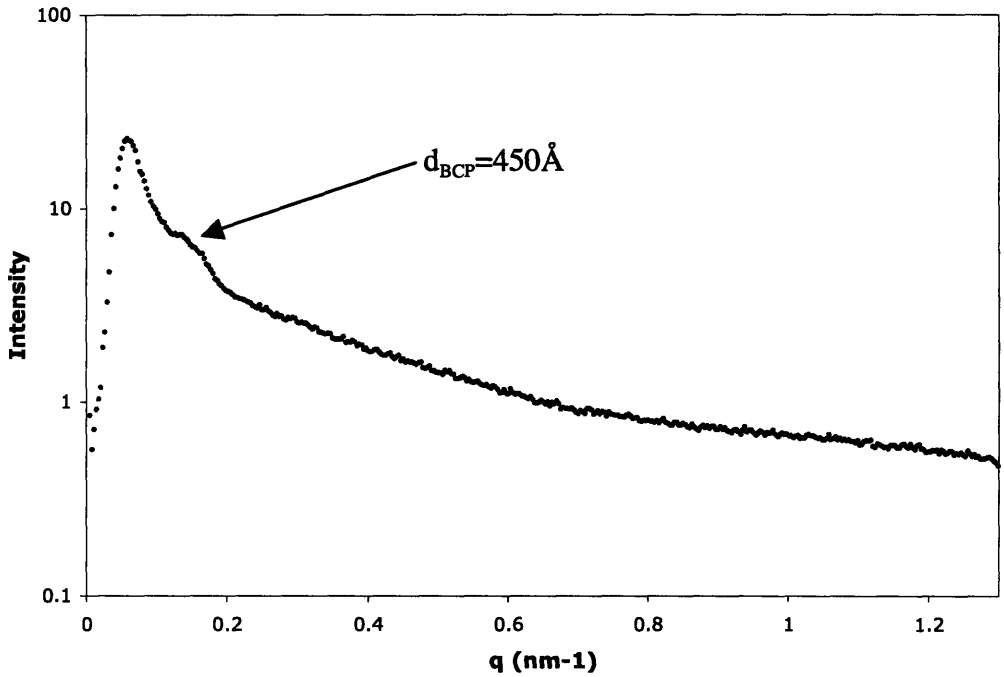

Figure 3.6: SAXS of PS18-LCP_{8MPOB}248-PS18 (ISN). The arrow indicates a BCP spacing peak at d=450Å.

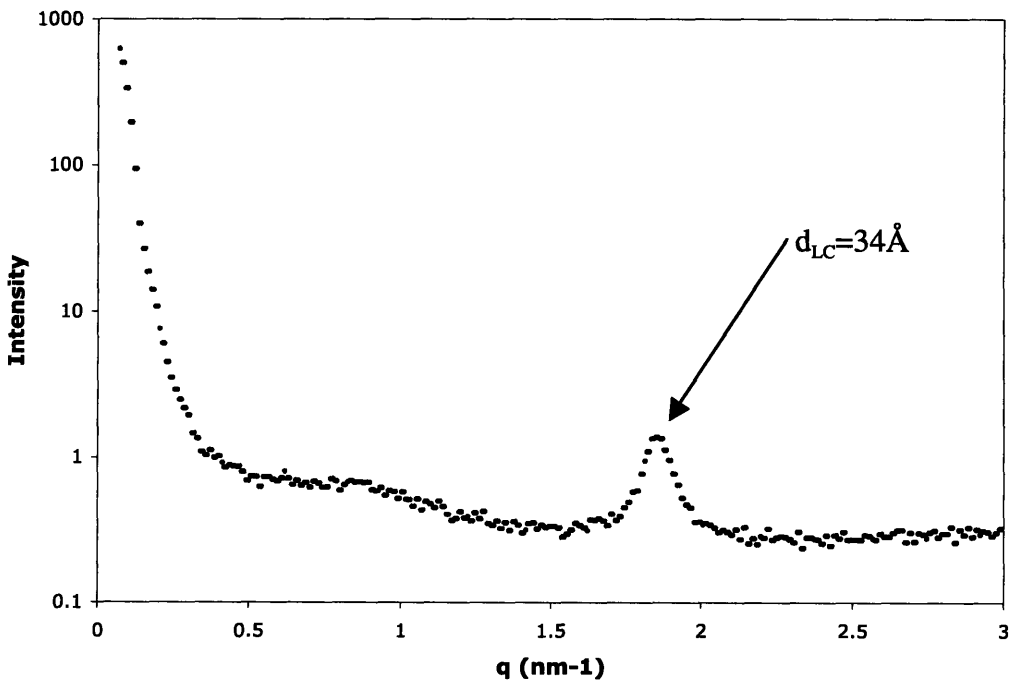

Figure 3.7: SAXS of PS18-LCP_{8MPOB}248-PS18 (CMSE). The arrow indicates a smectic LC spacing peak at d=34Å.

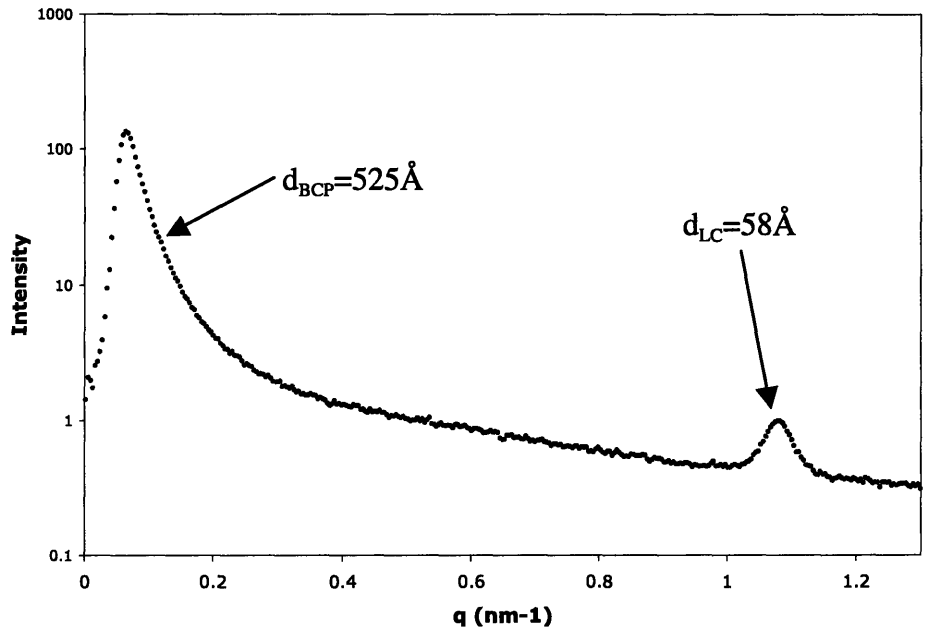

Figure 3.8: SAXS of PS27-LCP_{11MPOB}99 (ISN). The arrows indicate weak BCP spacing (d=525Å) and smectic LC spacing (d=58Å).

As we observe in Figures 3.5 and 3.8, the PS27-LCP_{4MPOB}84 sample has much stronger phase segregation compared to the PS27-LCP_{11MPOB}99 sample. This was determined because the BCP peak in the 4MPOB-functionalized sample is strong and clearly separate from the beamstop. In contrast, the 11MPOB-functionalized sample has a block copolymer peak that is a weak shoulder off the beamstop. As previously discussed, the shorter spacer increases the BCP phase segregation due to the increased LC rigidity and coupling to the PVMS backbone, while the longer spacer enables decoupling of the mesogen from the PVMS backbone, allowing the

mesogen to interact with the PS phase. Stronger phase segregation will enhance the observed scattering.

TEM and AFM have also been used to study the BCP morphologies in these systems. A comparison of the SAXS and TEM morphological determinations are in Table 3.4 and actual TEM micrographs of the samples are in Figures 3.9 through 3.12. PS18-LCP_{8MPOB}248-PS18 did not exhibit well-ordered morphology in microscopy studies. Therefore, no TEM or AFM image is shown.

Table 3.4: Comparison of SAXS and TEM data for functionalized polymers.

	SAXS Spacing (Å)	TEM Spacing (Å)	Notes
PS18-LCP_{8CB}153-PS18	250[1]	300	Large interfacial area
PS18-LCP_{8MPOB}248-PS18	450[2]	-	Ill-defined morphology
PS27-LCP_{4MPOB}84	370[2]	380	Poorly-segregated morphology
PS27-LCP_{11MPOB}99	525[2]	420	AFM: d~550Å, large interfacial area observed

Key: 1 = data obtained on the CMSE SAXS, 2 = data obtained on the ISN SAXS

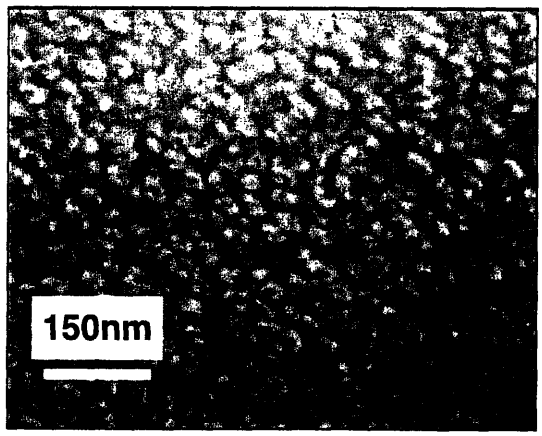

Figure 3.9: TEM micrograph of PS18-LCP_{8CB}153-PS18 (stained with RuO_4 for 15min, which preferentially stained the PS regions). The grey regions are LCP-rich, black regions are PS-rich, and white regions are the interface.

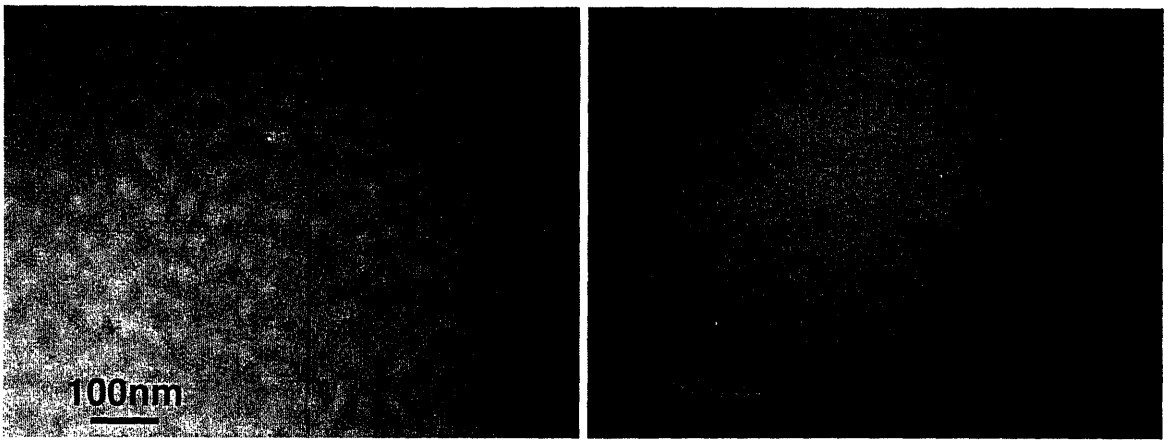

Figure 3.10: TEM micrographs of PS27-LCP$_{4MPOB}$84 (the contrast has been adjusted to make features more visible). Oval-shaped and worm-like features are observed corresponding to cylindrical morphology.

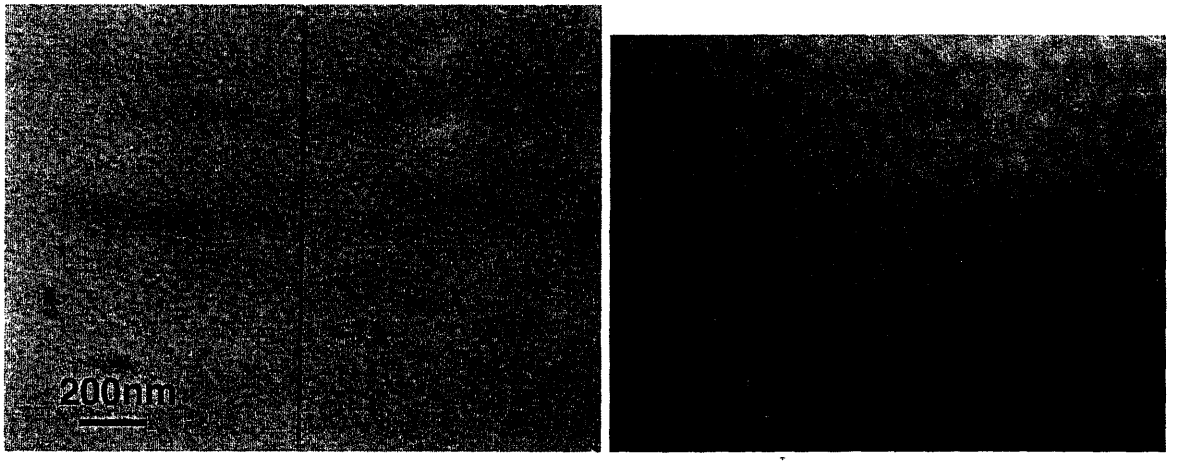

Figure 3.11: TEM micrographs of PS27-LCP$_{11MPOB}$99. Oval-shaped and worm-like features are observed corresponding to cylindrical morphology.

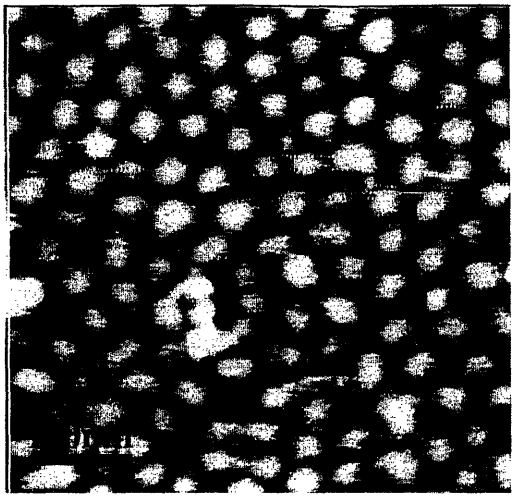

Figure 3.12: AFM micrograph of PS27-LCP_{11MPOB}99. Dark regions are the soft block (LCP) and lighter regions are the hard block (PS). Circle/oval-shaped features are observed, indicating spherical or cylindrical morphology.

The SAXS data and the microscopy data are in good agreement. However, the microscopy studies also allow determination of the ordering of the systems, something that was not evident in SAXS due to the absence of higher order reflection peaks. Other groups studying LC BCP systems have also observed a lack of higher order peaks in SAXS data[21] and relied on TEM to determine BCP morphology. In the materials in this study, the TEM data indicate cylindrical morphology in all samples. While no system has long-range regular order, the observed cylindrical or worm-like morphology in all samples is the desired ordering for these systems, and it is what was expected based on the size and composition of the samples. While the morphology is what is desired, the cylinders are weakly segregated with no regular lattice order. This prevents the coordinated mesogen reorientation necessary for actuation. Therefore, in order to use these materials, processing studies must be done in order to obtain the necessary segregation, morphology, and orientation.

We do, however, also observe a significant interfacial area in two of the systems: PS18-LCP_{8CB}153-PS18 and PS27-LCP_{11MPOB}99. This agrees well with the thermal data because the PS T_g was significantly depressed in both of these samples. In PS18-LCP_{8CB}153-PS18 the interfacial areas are the least stained (i.e. white) regions. Such selective staining has been observed in previous studies[10] and was attributed to fluctuations in density at the interface. Such fluctuations could allow for enhanced or weakened staining. Also, in the SAXS data, a weak shoulder off the beamstop and a lack of higher order reflection peaks can be caused by poor phase segregation and a lack of an ordered morphology in the system. Again, the longer, more flexible spacers contribute to this phenomenon because they increase the miscibility between the PS and PVMS blocks. In the 4MPOB-functionalized polymer, we observe a much smaller interface due to the enhanced phase segregation in that system. However, this sample still does not exhibit long-range BCP order.

The block sizes determined from TEM and AFM micrographs can be compared to the theoretical domain sizes in the desired perfectly segregated hexagonally close-packed cylindrical morphology. Such a morphology is shown in Figure 3.13. If L is the center-to-center distance of the cylinders determined by SAXS, then the expected diameter of the PS cylinders in a perfectly segregated morphology can be calculate using Equation 3.2b.

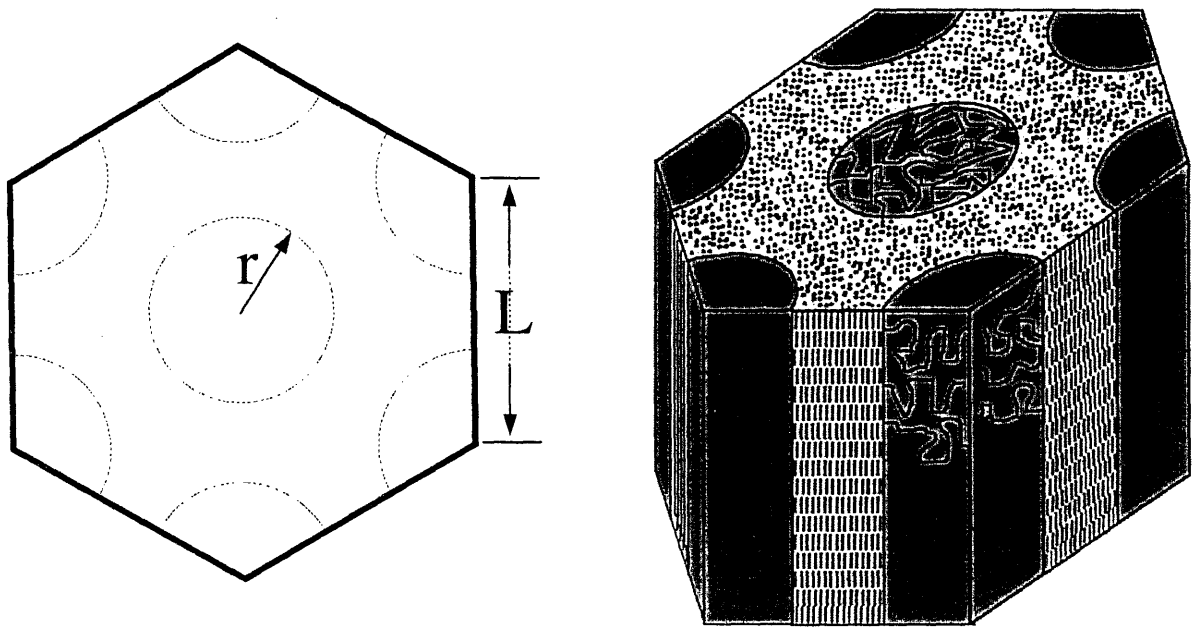

(a) (b)

Figure 3.13: Cross-sectional view (a) and schematic model[22] (b) of perfectly-segregated morphology with PS cylinders in a LCP matrix

$$\frac{V_{PS}}{V_{Total}} = \phi_{PS} = \frac{3A_{cs,PS}}{A_{cs,hex}} = \frac{3\pi r_{PS}^2}{\frac{3\sqrt{3}}{2}L^2} = \frac{2\sqrt{3}\pi r_{PS}^2}{3L^2} \tag{3.2a}$$

$$d_{PS} = 2r_{PS} = \sqrt{\frac{2\sqrt{3}}{\pi}\phi_{PS}L^2} \tag{3.2b}$$

$$L_{LCP} = L - d_{PS} \tag{3.2c}$$

L_{LCP} is the thickness of the LCP region between cylinders.

Assuming that the density of the LCP blocks is 1.12[10] and that of polystyrene is 1.05[14], the volume fractions ϕ_{PS} and ϕ_{LCP} can be calculated based on the weight fractions w_{PS} and w_{LCP}.

$$\phi_{PS} = \frac{\frac{w_{PS}}{\rho_{PS}}}{\frac{w_{PS}}{\rho_{PS}} + \frac{w_{LCP}}{\rho_{LCP}}} \qquad (3.3a)$$

$$\phi_{LCP} = 1 - \phi_{PS} \qquad (3.3b)$$

Results of these calculations are given in Table 3.5. While results for the PS27-LCP_{4MPOB}84 system are in good agreement with the experimental data, the PS27-LCP_{11MPOB}99 system shows significantly different results compared to AFM and TEM data. Since all TEM and AFM distance measurements were done by hand, some error was introduced in those values. Additionally, these results suggest that some LCP has mixed with the PS or the estimate of ϕ_{PS} is too large. As has been discussed, data from other techniques confirm the suggestion that there is incomplete phase segregation in the samples. Also, since the mesogen substitution for PS27-LCP_{11MPOB}99 was estimated, it is not unreasonable to expect actual volume fractions to be different from what was calculated owing to this estimation error. Finally, results from studies by Hashimoto, et al., on lamellar systems[23, 24] indicate that an interfacial region of 20Å is not uncommon even in strongly-segregated BCP systems. Therefore, the results from theoretical calculations based on SAXS data and actual measurements from TEM and AFM images are in reasonable agreement.

Table 3.5: Comparison of TEM and AFM measured domain dimensions with theoretical domain dimensions for perfect segregation in MPOB systems. TEM measurements were done by hand using graphical software.

	PS27-LCP_{4MPOB}84	PS27-LCP_{11MPOB}99 (TEM)	PS27-LCP_{11MPOB}99 (AFM)

PS wt. Frac	0.243	0.214	0.214
LCP wt. Frac	0.757	0.786	0.786
ϕ_{LC}	0.745	0.775	0.775
ϕ_{PS}	0.255	0.225	0.225
L (SAXS)	370	525	525
Theor. L_{LCP} (SAXS)	174	263	263
Theor. d_{PS} (SAXS)	196	262	262
Meas. L (TEM)	380	420	550
Meas. L_{LCP} (TEM)	140	130	225
Meas. d_{PS} (TEM)	220	280	290

Liquid Crystal Properties

In addition to comparing the experimental BCP spacings with the theoretical spacings, we can compare the experimental liquid crystal smectic spacings with the theoretical values. A summary of these results is given in Table 3.6.

Table 3.6: Comparison of experimental LC spacing with theoretical mesogen lengths

	Observed LC Spacing (Å)	**Mesogen Length (Å)**	**Notes**
PS18-LCP$_{8CB}$153-PS18	-[1,2]	18	Nematic phase at RT
PS27-LCP$_{4MPOB}$84	-[2]	17	Nematic phase at RT
PS18-LCP$_{8MPOB}$248-PS18	34[1]	22	Smectic C bilayer, ~20° mesogen tilt
PS27-LCP$_{11MPOB}$99	58[2]	25	Smectic A bilayer

Key: 1 = data obtained on the CMSE SAXS, 2 = data obtained on the ISN SAXS

A diagram of the proposed smectic bilayer in the LCP phase is given in Figure 3.14 and experimental x-ray scattering data were given in Figures 3.5 through 3.8.

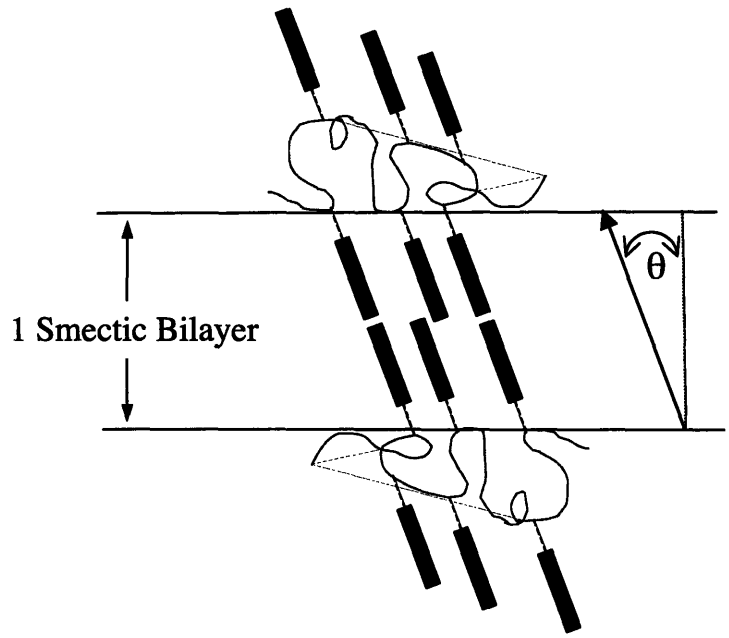

Figure 3.14: Smectic bilayer in LCP region. θ = mesogen tilt angle, which is the angle between smectic director and layer normal.

As expected, the shorter mesogens give smaller LC spacings in the BCP. We also observe that in all cases the observed LC spacing is approximately 1.5-2 times the length of the mesogen. In the case of the spacing being ~2 times the mesogen length, we believe that the mesogens are in the S_A phase with the mesogens fully-extended and the ends abutting each other. However, when the observed spacing is ~1.5 times the mesogen length, the difference is caused by a tilting of the mesogen (i.e. the smectic C phase). The tilt angle is determined to be ~20° for PS18-LCP_{8MPOB}248-PS18. This is similar to the reported tilt angles determined in previous studies[25]. In some systems mesogen interdigitation causes smaller smectic bilayer spacings. However, studies have shown that interdigitation is negligible for mesogens with methyl endgroups, as is the case with the nMPOB mesogen. Therefore, in these studies, the mesogen tilt angle can be considered the primary cause of the deviation from the spacing in a perfect S_A bilayer.

Chapter 3 Summary

This chapter showed a comparison of thermal and morphological properties for a series of liquid crystalline polymers with various polymer backbones, mesogens, and mesogen spacer length. The primary result is that the shorter spacer enhances phase segregation in these systems. Therefore, $\chi_{PS\text{-}LCP11MPOB} < \chi_{PS\text{-}LCP4MPOB}$. In addition, the composition of the functionalized polymer should be no higher than 85wt% LCP for MPOB systems. Systems with higher LCP weight percentages were viscous liquids, and such a material will not be useful for the desired applications. Lowering the LCP composition could be accomplished by synthesizing block copolymers that are less than 50wt% PVMS, adjusting the mesogen attachment percentage to obtain the desired final LCP weight percentage, or using mesogens with shorter spacers. Finally, the polymer size and composition in samples PS27-LCP_{4MPOB}84 and PS27-LCP_{11MPOB}99 are in the correct range to obtain cylindrical morphology. However, processing techniques must be explored in order to obtain a better-ordered morphology to allow for coordinated actuation in the material.

References

1. Kempe, M. D.; Scruggs, N. R.; Verdusco, R.; Lal, J.; Kornfield, J. A., Self-assembled liquid-crystalline gels designed from the bottom up. *Nature Materials* **2004,** 3, (3), 177-182.

2. Garg, D. P.; Zikry, M. A.; Anderson, G. L., Current and potential future research activities in adaptive structure: an ARO perspective. *Smart Materials and Structures* **2001,** 10, 610-623.

3. Donnio, B.; Wermter, H.; Finkelmann, H., A Simple and Versatile Synthetic Route for the Preparation of Main-Chain, Liquid-Crystalline Elastomers. *Macromolecules* **2000,** 33, (21), 7724-7729.

4. Lehmann, W.; Hartmann, L.; Kremer, F.; Stein, P.; Finkelmann, H.; Kruth, H.; Diele, S., Direct and inverse electrmechanical effect in ferroelectric liquid crystalline elastomers. *Journal of Applied Physics* **1999,** 86, (3), 1647-1652.

5. Stein, P.; Aßfalg, N.; Finkelmann, H.; Martinoty, P., Shear modulus of polydomain, mono-domain and non-mesomorphic side-chain elastomers: Influence of the nematic order. *The European Physics Journal E* **2001,** 4, 255-262.

6. Walther, M.; Finkelmann, H., Structure Formation of Liquid Crystalline Block Copolymers. *Progress in Polymer Science* **1996,** 21, 951-979.

7. Camacho-Lopez, M.; Finkelmann, H.; Palffy-Muhoray, P.; Shelley, M., Fast liquid-crystal elastomer swims into the dark. *Nature Materials* **2004,** 3, (5), 307-310.

8. Naciri, J.; Srinivasan, A.; Jeon, H.; Nikolov, N.; Keller, P.; Ratna, B. R., Nematic Elastomer Fiber Actuator. *Macromolecules* **2003,** 36, (22), 8499-8505.

9. Lacour, S. P.; Prahlad, H.; Pelrine, R.; Wagner, S., Mechatronic system of dielectric elastomer actuators addressed by thin film photoconductors on plastic. *Sensors and Actuators A* **2004,** 111, 288-292.

10. Moment, A. The Synthesis and Characterization of Polystyrene Liquid Crystalline Siloxane Block Copolymers. Doctoral, Massachusetts Institute of Technology, Cambridge, MA, 2000.

11. Nair, B. Massachusetts Institute of Technology, Cambridge, MA, 2001.

12. Pugh, C.; Kiste, A. L., Molecular Engineering of Side-Chain Liquid Crystalline Polymers by Living Polymerizations. *Progress in Polymer Science* **1997,** 22, 601-691.

13. Plate, N. A.; Shibaev, V. P., In *Comb-Shaped Polymers and Liquid Crystals*, Cowie, J. M. G., Ed. Plenum: New York, 1987.

14. Brandrup, J.; Immergut, E. H., *Polymer Handbook.* Third ed.; John Wiley & Sons: New York, 1989.

15. Freiberg, S.; Lagugné-Labarthet, F.; Rochon, P.; Natansohn, A., Synthesis and Characterization of a Series of Azobenzene-Containing Side-Chain Liquid Crystalline Polymers. *Macromolecules* **2003,** 36, (8), 2680-2688.

16. Stanczyk, W. A.; Ganicz, T.; Gladkova, N. K.; Bialecka-Florjanczyk, E.; Sledzinska, I. In *Polyvinylsilanes - a novel group of organosilicon liquid crystal systems*, SPIE, 2000; Klosowicz, S. J.; Rutkowska, J.; Zielinski, J.; Zmija, J., Eds. 2000.

17. Zheng, W. Y.; Hammond, P. T., Phase Behavior of New Side Chain Smectic C* Liquid Crystalline Block Copolymers. *Macromolecules* **1998,** 31, (3), 711-721.

18. Anthamatten, M. L. Massachusetts Institute of Technology, Cambridge, MA, 2001.

19. Hsiue, G.-H.; Sha, Y.-A.; Hsieh, S.-J.; Jeng, R.-J.; Kuo, W.-J., Synthesis and characterization of halogen-containing ferroelectric liquid crystals and side chain liquid crystalline polymers. *Liquid Crystals* **2001,** 28, (3), 365-374.

20. Mucha, M.; Grzyb, J.; Schönhals, A., Dielectric Relaxation Phenomena in Side Chain Liquid Crystalline Polycarbosilane of Various Spacer Lengths. *SPIE* 4017, 180-186.

21. Hamley, I. W.; Castelletto, V.; Lu, Z. B.; Imrie, C. T.; Itoh, T.; Al-Hussein, M., Interplay between Smectic Ordering and Microphase Separation in a Series of Side-Group Liquid-Crystal Block Copolymers. *Macromolecules* **2004,** 37, (13), 4798-4807.

22. Xiang, M.; Li, X.; Ober, C. K.; Char, K.; Genzer, J.; Sivaniah, E.; Kramer, E. J.; Fischer, D. A., Surface Stability in Liquid-Crystalline Block Copolymers with Semifluorinated Monodendron Side Groups. *Macromolecules* **2000,** 33, (16), 6106-6119.

23. Hashimoto, T.; Shibayama, M.; Kawai, H., Domain-Boundary Structure of Styrene-Isoprene Block Copolymer Films Cast from Solution. 4. Molecular-Weight Dependence of Lamellar Microdomains. *Macromolecules* **1980,** 13, (5), 1237-1247.

24. Hashimoto, T.; Todo, A.; Itoi, H.; Kawai, H., Domain-Boundary Structure of Styrene-Isoprene Block Copolymer Films Cast from Solutions. 2. Quantitative Estimation of the Interfacial Thickness of Lamellar Microphase Systems. *Macromolecules* **1977,** 10, (2), 377-384.

25. Blinov, L. M.; Chigrinov, V. G., *Electrooptical Effects in Liquid Crystal Materials.* Springer-Verlag: New York, 1994.

Chapter 4 –Thermal Properties and Morphology of Polymers for Use as Ferroelectric Actuators

Motivation and Background

In these studies a series of polymers functionalized with chiral mesogens is examined. Such materials are of interest for use as ferroelectric actuators. When chiral mesogens are attached to BCP backbones, actuation may be achieved using the ferroelectric property of piezoelectricity. Ferroelectric actuators have been studied for use in many applications, including artificial muscles, sensors, and structure damping. Additional opportunities for such materials were discussed in an article by Garg, et al.[1]. Ferroelectric actuator materials in homopolymer studies have been found to exhibit strains on the order of 1%-4%. The materials examined in the current study take advantage of physical crosslinks to form ordered morphologies and stabilize the LC phase. Therefore, the materials may be reprocessed if necessary in order to obtain the desired morphology. A grainless cylindrical morphology is desired so that both the LC and PS phases will be continuous. Therefore, the PS cylinders will stabilize the LC phase and will aid in obtaining a long-range, uniform LC alignment necessary for ferroelectric properties.

As previously discussed, liquid crystals can be used as ferroelectric actuators when they are confined to a space no wider than their pitch and are in the chiral smectic C (S_C*) phase. Other groups have studied the use of smectic homopolymers as actuators in crosslinked networks. Groups that have done extensive work in the area are the Zentel group[2, 3] and the Finkelmann group[4, 5]. In those groups, strains of up to 4% have been reported using voltages of 150MV/m. More recent studies[6] have shown slightly lower strains (2.7%) may be achieved using

significantly lower voltages (1.5MV/m). These strains are greatest when near the S_A* to S_C* transition temperature.

As opposed to nematic actuation, which relies on changes in LC order induced by a thermal phase transition, smectic actuation relies on inducing a torque on the mesogens caused by the applied electrical field interacting with the S_C* polarization. Since the polarization persists throughout the entire S_C* phase, this type of actuation is useful over a wide temperature range. If the LC phase is in the S_A* phase and near the S_A* to S_C* transition temperature, electroclinic switching is accessible by electrically or thermally tilting the mesogens into the S_C* phase. Figure 4.1 shows an example of such actuation.

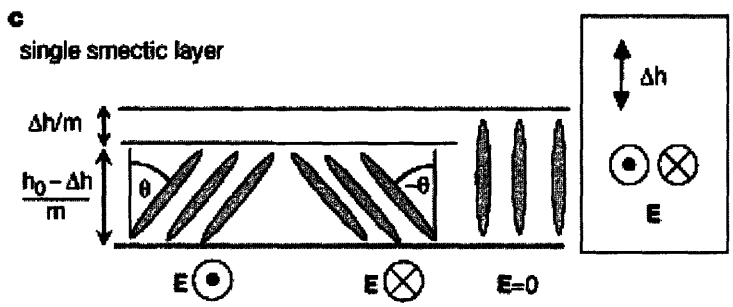

Figure 4.1: Proposed electroclinic actuation mechanism in smectic liquid crystals[5]. The electrical field is in the "Off" state in the middle region, while it is shown in the "On" state to the left and right.

While the strains achieved in ferroelectric actuation are significantly lower than those obtained in nematic actuation, a much smaller voltage is necessary. In addition, switching is bistable due to the P_S quality of ferroelectric materials. Therefore, the voltage can be removed

without losing the macroscopic polarization necessary for ferroelectric properties and actuation. These properties of ferroelectric actuation make it highly desirable for many applications.

This chapter examines the thermal properties and morphologies obtained when chiral mesogens are attached to block copolymer backbones. Such information was necessary to determine if the materials are useful as actuators. As discussed in the Introduction, to be used as actuators, materials should have PS cylinders in a LCP matrix with intercylinder spacings of less than the S_C^* pitch, strong phase segregation, and a broad S_C^* phase. TEM and SAXS were used to determine the BCP morphologies, WAXS was used to study LC smectic spacings, and DSC, temperature-dependent SAXS, and optical microscopy were used to determine thermal transitions.

Experimental

Synthesis – All polymer and mesogen synthetic techniques were described in Chapter 2.

Sample Preparation – All polymer samples were cast from a concentrated (≥10wt%) toluene solution onto a Teflon coated sheet, then air dried for ~1day. Film thickness was approximately 0.25mm.

Gel Permeation Chromatography – GPC was used to determine the molecular weight and polydispersity of the polystyrene block in copolymers. This technique was not used to determine the polysiloxane molecular weight for reasons outlined in Moment's thesis[7]. A Waters Breeze gel permeation chromatography (GPC) system equipped with 2 Polymer Laboratories Plgel 5μm MIXED-C 300x7.5mm columns (200-2,000,000 MW range), a refractive index detector (Waters 2414), and an ultraviolet detector (Waters 2487, λ=254nm) was used for molecular weight

measurement relative to polystyrene standards. The system also contains a column heater (T=35°C) and an inline degasser, and uses Waters Breeze software. Tetrahydrofuran (THF) was the mobile phase and a flowrate of 1ml/min was used.

Nuclear Magnetic Resonance – ^{1}H NMR was used to determine the molecular weight of the PDMS and PVMS blocks as well as for general characterization of synthesis products. This was done on a Bruker Avance DPX-400 400MHz NMR Spectrometer.

Optical Microscopy – OM was used to determine the types of LC phases present as well as their transition temperatures. Different LC phases produce characteristic textures when viewed through cross polarizers. A Zeiss Axioskop 2 MAT optical microscope equipped with a Linkam THMS600 hotstage and Linkam TP94 controller was used to observe samples under crossed polarizers at different temperatures. Images of the samples were captured using an AxioCam MRc camera and AxioVision software.

Small Angle X-ray Scattering – SAXS was used to determine the shape and orientation of polymer features with dimensions on the order of 100Å (spheres, cylinders, lamellae, etc.). The shape determination was based on the relative scattering vector ratios of the peaks in the profile, while the LC spacing was based on the *d*-spacing of the first-order peak. SAXS also allowed us to determine how these features were oriented with respect to each other. A Molecular Metrology 2-D SAXS detector placed 1300mm from the sample was used to detect the scattering of Cu K_α x-rays at 45kV and 0.66mA produced by a Microsource x-ray generator. A Molecular Metrology hotstage with temperature controller was used for heating studies.

Transmission Electron Microscopy – TEM was used to obtain images of the phase-segregated morphology of the block copolymers. The type of morphology, grain size, and degree of ordering were determined with these images. Samples first were cryotomed before

using in the TEM. A RMC MT-X ultramicrotome with CR-X cryo attachment was used to section samples of ~50nm in thickness below room temperature. The diamond knife temperature was set at -75°C and the sample temperature set at -85°C. Films were transferred to copper grids and stained for 25 minutes with the vapor from OsO_4 4% aqueous solution. OsO_4 preferentially stains the liquid crystal polymer, making these regions appear dark in the TEM images. Samples were observed with a JEOL 200CX electron microscope operating at 200kV.

Wide Angle X-ray Scattering – WAXS was used to determine the types of liquid crystal phases present (S_C*, S_A, N, etc.). LC spacings with dimensions of 40Å and smaller were studied with this method. The same equipment used for SAXS was used for WAXS by moving the detector closer to the sample (sample-to-detector distance = 300mm).

Differential Scanning Calorimetry – DSC was used to determine the transition temperatures of the LC phases and the T_g values of both polymer blocks. Both heating and cooling scans were done in a TA Instruments Q1000 auto modulated DSC. All scans were conducted at heating and cooling rates of 10°C/min, and at least two heating and cooling ramps were done for each sample. Q Series and TA Universal Analysis software were used to control the DSC and analyze data.

Dynamic Mechanical Analysis – DMA was used to determine the transition temperatures of the BCP and to study stress-strain behavior. A TA Instruments Q800 DMA with cooling attachment machine was used. DMA was also used to stretch-align one of the samples. In this technique, a temperature ramp of 10°C/min was used with 20μm amplitude oscillation at 1Hz. The sample maintained mechanical integrity until approximately 70°C where it started to draw out. At T~115°C the material failed. Details on additional alignment techniques are discussed in Chapter 5.

Results

Materials Used

With the exception of the 10BPB4 mesogen, materials used in these studies were synthesized and characterized in the lab using the techniques described in Chapter 2. 10BPB4, however, was synthesized by Jawad Naciri at the Naval Research Laboratory and shared for use in these studies.

a. 10BPB4

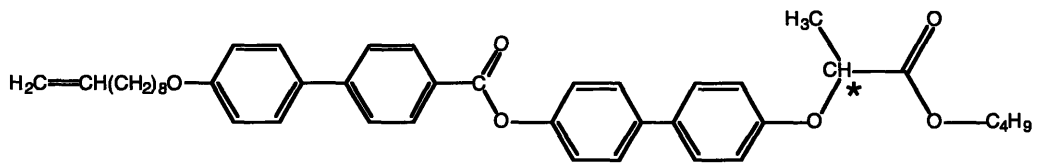

- DSC – G 71 N 87 I

b. 8BPP4

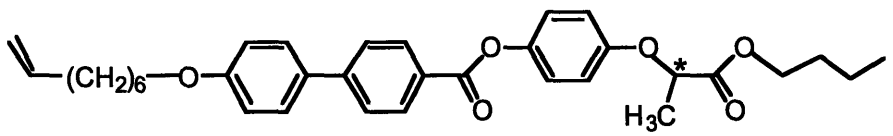

- DSC – G <0 S_X 30 S_C* 74 S_A 106 I

c. 4BPP4

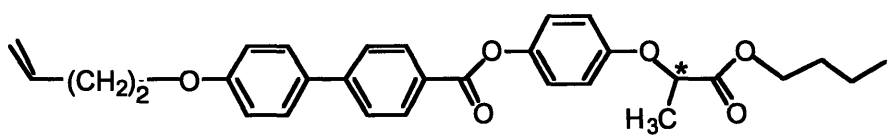

- DSC – G 50 S 97 N 120 I

Figure 4.2: Mesogens studied for use as ferroelectric actuators and their transition temperatures

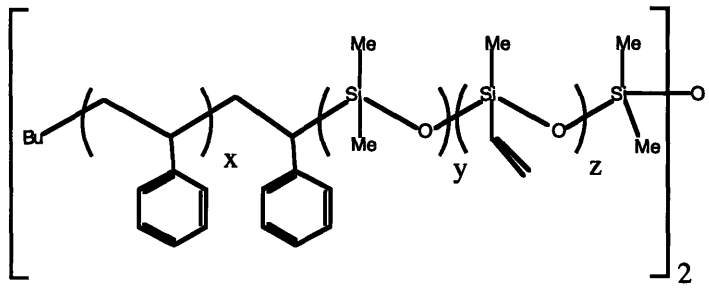

Figure 4.3: Chemical structure of the triblock copolymer. Mesogens were attached to the vinyl group on the PVMS block.

As a small molecule LC, 11BPP4[8] exhibited a spontaneous polarization as high as 300nC/cm^2. In a siloxane homopolymer, the value is still as high as 160nC/cm^2. The response times were also quite fast, at 3μs-30μs and 0.5ms-100ms for small molecules and homopolymers, respectively (both used fields of 8V/μm). While it was not studied in this research, Svensson, et al. also studied nitro-substituted mesogens and obtained P_S values as high at 700nC/cm^2. Even without the nitro substituents, these P_S values are significantly higher than what were determined in previous studies in this group[7]. Therefore, it is expected that in the current studies more favorable ferroelectric properties will be achievable compared to those observed in previous studies.

These three chiral mesogens were attached to two different polymer backbones. The calculated molecular weights of materials studied for ferroelectric actuators were given in Table 2.3 and the summary is given in Table 4.1.

Table 4.1: Summary of polymers synthesized for use as ferroelectric actuators

		POLYMER BACKBONES	
		PS27-PVMS16	**PS18-PVMS41-PS18**
MESOGENS	**10BPB4**		PS18-LCP_{10BPB4}297-PS18 (67%, 89%)
	4BPP4	PS27-LCP_{4BPP4}79 (55%, 75%)	
	8BPP4	PS27-LCP_{8BPP4}108 (73%, 80%)	

Key: Polymer Name (Mesogen attachment percentage, LCP weight percentage)

Functionalized polymers had total molecular weights of 106000g/mol-333000g/mol, PS blocks of 18000g/mol-27000g/mol, PDMS blocks of 400g/mol-1000g/mol, and PVMS-LC blocks of 79000g/mol-297000g/mol. Considering the short PDMS block to be part of the LCP and mesogen functionalization percentages of 55%-73%, this created polymers that ranged from 75wt% to 89wt% LCP. As mentioned in Chapter 3, previous studies on polysiloxane-based LCPs have shown that the critical degree of polymerization at which thermal transitions are no longer functions of molecular weight is ~10 repeat units[9]. Since all samples studied contain LCP blocks that are much larger than the critical weight, molecular weight should not impact these properties.

Thermal Transitions

Transition temperatures and phases for all polymers were determined using DSC, SAXS, WAXS and POM.

Table 4.2: Thermal transitions of polymers studied for use as ferroelectric actuators

	LCP T_g	**PS T_g**	**LC Transitions**
PS18-PVMS41-PS18	-60	82	

PS18-LCP$_{10BPB4}$297-PS18	-31	75	G -31 S 75 I
PS27-PVMS16	-60	84	
PS27-LCP$_{4BPP4}$79	-10	87	G -10 S_I 70 S_{II} 87 S_{III} 110 N >250 I
PS27-LCP$_{8BPP4}$108	-10	65	G -10 S_I 65 S_{II} 95 S_{III} 140 I

Data supporting these transition temperatures and phase determinations are shown in Figures 4.4 through 4.9. Transition temperatures were determined from DSC and phases from x-ray scattering. The samples did not exhibit characteristic LC textures in POM. Therefore, POM was primarily used for confirming transition temperatures, especially the clearing point.

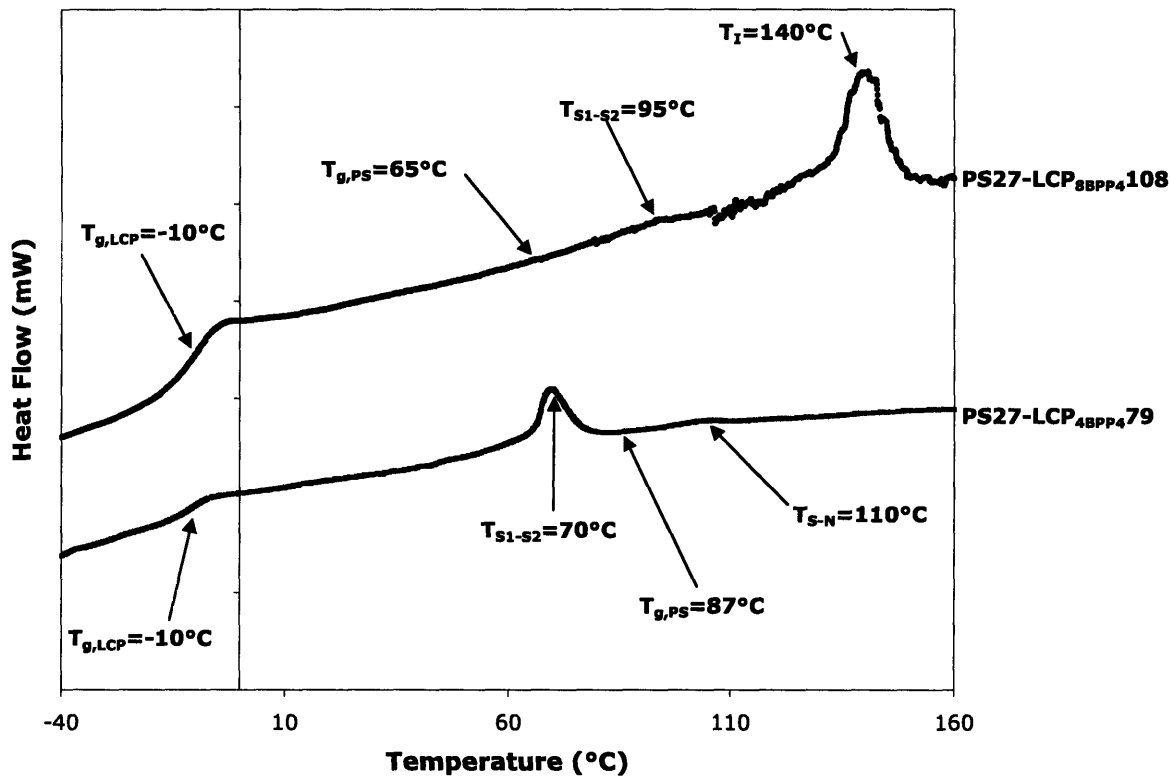

Figure 4.4: DSC thermographs of PS27-LCP$_{4BPP4}$79 and PS27-LCP$_{8BPP4}$108. Transition temperatures are indicated with arrows.

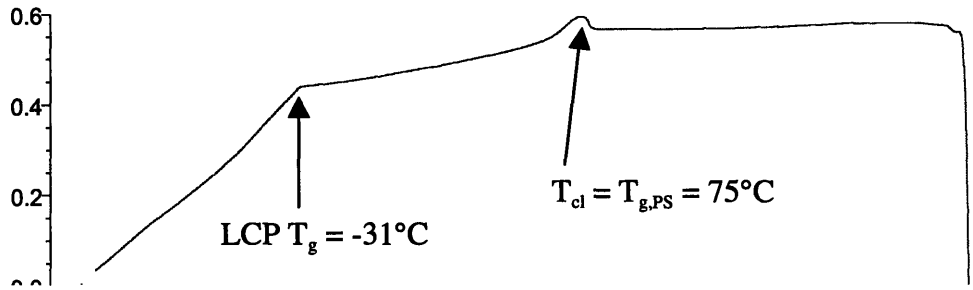

Figure 4.5: DSC thermograph of PS18-LCP_{10BPB4}297-PS18. Transition temperatures are indicated with arrows

Comparing thermal transitions for PS27-LCP_{8BPP4}108 and 8BPP4, one observes that both exhibit three LC phases. Further, all three phases are smectic. However, in PS27-LCP_{8BPP4}108, the transitions are shifted to temperatures that are 20°C-30°C higher than the transition temperatures determined for the mesogen. This indicates a stabilization of the smectic phases in the polymer, which is most likely due to interfacial effects from the BCP morphology.

In PS27-LCP_{4BPP4}79, LC phases are again present at higher temperatures compared to the 4BPP4 mesogen. In addition, the smectic phase is observed at temperatures as low as –10°C, significantly lower than what is observed for 4BPP4 (50°C). One similarity between PS27-LCP_{4BPP4}79 and the 4BPP4 mesogen is that both exhibit smectic and nematic phases, although in the polymer multiple smectic phases are observed instead of a single phase. Such additional phases are due to the increased interactions between the polymer backbone and LC mesogens, and those interactions will affect the phases observed.

In PS18-LCP_{10BPB4}297-PS18, only two phase transitions are observed, a LCP T_g at –31°C and a PS T_g that coincides with the LC clearing point at 75°C. In this case, it appears that the BCP is

not able to stabilize the smectic phase as the other functionalized polymers were able to do. Since the 10BPB4 unattached mesogen has thermal transitions at 71°C and 87°C, such an observation is similar to the 11MPOB samples reported in Chapter 3 in which $\chi_{eff}N$ drops below the critical value at the LC clearing point. Therefore, the clearing point causes an order-disorder transition.

As one observes from these data, the PS27-LCP_{4BPP4}79 sample has a higher PS T_g compared to the unfunctionalized PS27-PVMS19 backbone. This is indicative of increased phase segregation in the system caused by the rigid mesogen with a short spacer and agrees with what is expected based on previous studies with SCLCPs[7]. In the PS27-LCP_{8BPP4}108 sample, the PS T_g is significantly lower than its value in the unfunctionalized polymer. Such an observation indicates increased phase miscibility between the PS block and the LCP block. As discussed in Chapter 3, the shorter spacer minimizes the interaction between the side-chain LC mesogens and the PS block, thereby increasing the χ parameter above what it is in the unfunctionalized polymer backbone. However, in the system with a longer spacer, the mesogen is able to interact with the PS backbone and cause the two blocks to become co-miscible with each other.

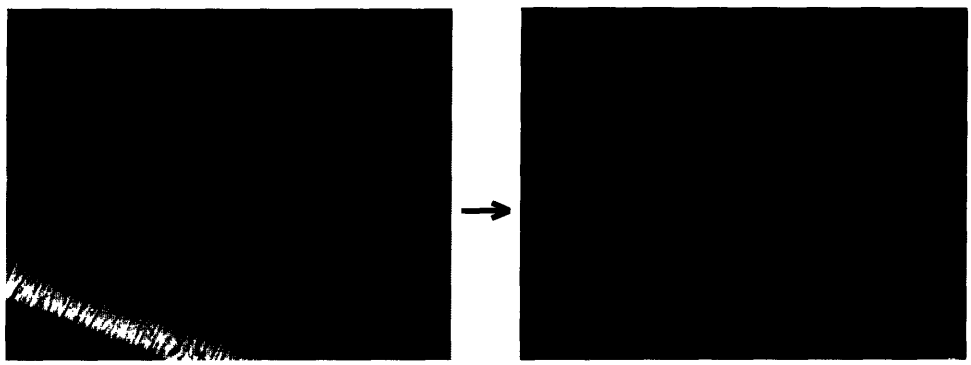

(a) (b)

Figure 4.6: POM images of PS27-LCP$_{8BPP4}$108 at (a) 25°C and (b) 156°C. These images indicate that the transition observed in DSC at T=140°C is a clearing point.

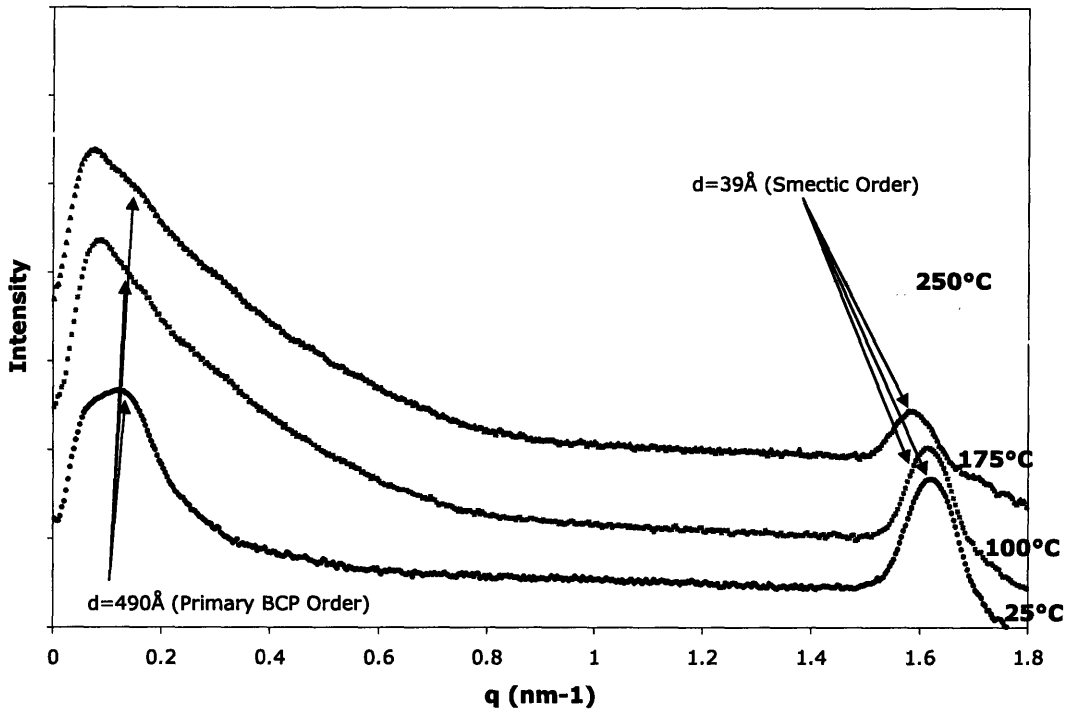

Figure 4.7: Temperature-dependent 1-D SAXS of PS27-LCP$_{8BPP4}$108. Peaks associated with the BCP order (d=490Å) and LC smectic order (d=39Å) are indicated with arrows. Since higher-order BCP peaks are not observed, a morphological determination could not be made from SAXS.

In Figures 4.6 and 4.7, thermal transitions and LC phases are observed for PS27-LCP$_{8BPP4}$108 in the POM and SAXS. From the POM images as the sample is heated, it can be determined that the thermal transition observed in the DSC at 140°C is indeed a LC clearing point because the material loses birefringence at that point. The identification of other LC phases using POM was

difficult because characteristic LC textures were not observed. Therefore, temperature-dependent SAXS was used to determine LC phases.

In temperature-dependent SAXS, smectic layers will generally be observed as peaks in the range of q~1.5-2nm^{-1}. Since mesogens do not align in layers in the nematic phase, the loss of a peak could indicate a smectic to nematic transition or a smectic to isotropic transition. In the case of PS27-LCP$_{8BPP4}$108 smectic peaks are observed at 25°C and 100°C at q=1.65nm^{-1}, which corresponds to smectic layers of 38.5Å. At higher temperatures, this peak shifts to a slightly lower q value, which corresponds to a spacing of 39.5Å. While this could be a change in the smectic tilt, it is small enough to be considered within instrument error. As the temperature is further increased, the smectic peak disappears. This is another indicator of LC clearing (smectic to isotropic transition) that is observed in POM and DSC. The temperatures from the different techniques are slightly different due to the different calibration standards used for them and the conditions under which the data were taken (vacuum vs. air vs. nitrogen).

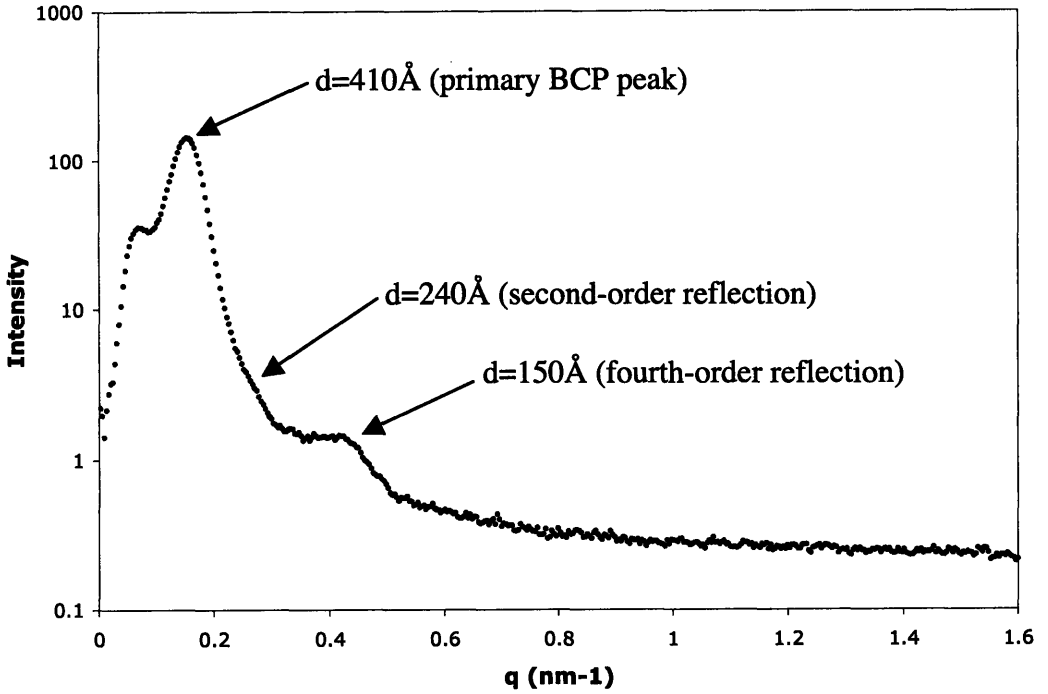

Figure 4.8: 1-D SAXS of PS27-LCP$_{4BPP4}$79. The primary peak for BCP order (d=410Å) and higher order reflections at d=240Å ($\sqrt{3}$, second-order) and d=150Å ($\sqrt{7}$, fourth-order) are indicated. This corresponds to cylindrical BCP morphology.

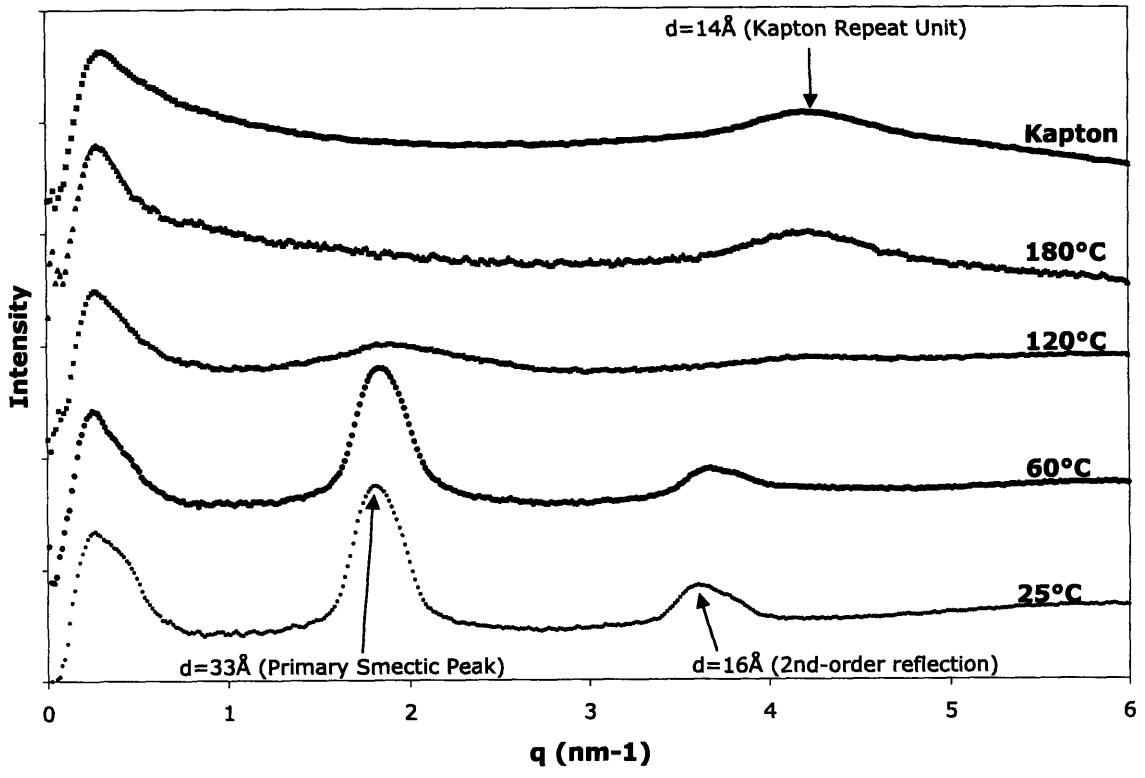

Figure 4.9: Temperature-dependent 1-D WAXS of PS27-LCP_{4BPP4}79. Note that peaks at q~4 at T=180°C are caused by the Kapton film holding the sample. Peaks associated with the LC smectic order (d=33Å) and Kapton peak are indicated.

In the temperature-dependent WAXS of PS27-LCP_{4BPP4}79 smectic peaks are observed at room temperature and at slightly elevated temperatures. However, around 120°C, the smectic peak is significantly smaller and, by 180°C, the smectic peak is gone. This indicates that the polymer has undergone a smectic to isotropic transition. It is also interesting to note that the PS27-LCP_{4BPP4}79 sample exhibits liquid crystallinity at high temperature (through ~325°C). In POM, the sample at that temperature appears to degrade and does not regain liquid crystalline properties as the temperature is lowered. Studies on mesogen-jacketed LC BCP systems have reported a similar phenomenon of $T_d<T_{cl}$[10]. Such LC stability is likely caused by the well-

ordered BCP morphology, which was observed in the SAXS data for that sample (Figure 4.8) and will be discussed further later.

From DSC (Figure 4.4) and temperature-dependent SAXS (Figure 4.7), it is interesting to note that in PS27-LCP_{8BPP4}108 the only LC phase observed is the smectic phase. In PS27-LCP_{4BPP4}79, however, both smectic and nematic phases are observed from the temperature-dependent WAXS data (Figure 4.9). This agrees well with previous studies that have shown that mesogens with longer spacers have tendencies to form smectic phases, while those with shorter spacers tend to stabilize nematic phases.

Physically, the PS18-LCP_{10BPB4}297-PS18 sample is quite elastomeric and can easily be stretched or sheared. The samples with the 4BPP4 or 8BPP4 mesogens are much more rigid at room temperature. Also, the nBPP4 samples have clearing points that are much higher than the polymer functionalized with 10BPB4. Since the mesogen substitution and polymer backbones are different between the 10BPB4 and nBPP4 systems, a suitable comparison is difficult to make. However, based on these and other studies, the differences that likely are contributing to these physical observations include the initial backbone composition, LCP weight percentage in the functionalized polymer[7], functionalized polymer total molecular weight[7], and mesogen spacer length and rigidity[7, 11].

In Chapter 3, the importance of the initial backbone composition and size of LCP block were shown to make the difference in some samples between having a viscous liquid product and a rubbery solid sample. In the nBPP4 system, the same LCP composition limit that was determined for the nMPOB system (~85wt%) might not hold. In the PS18-LCP_{10BPB4}297-PS18 sample, the backbone was initially 55wt% PVMS and the final product was elastomeric. However, the nBPP4 samples were attached to a polymer that was initially 60wt% PVMS and

were both quite rigid. Therefore, the nBPP4 samples perhaps will need polymers that are >50wt% PVMS initially in order to have a rubbery or elastomeric product. This agrees with results from Moment's studies[7], which used mesogens that were similar to 10BPB4 and the nBPP4 series. In addition, Moment found that the rubbery products he studied were samples that had large overall molecular weights. Since the PS18-LCP_{10BPB4}297-PS18 sample has a total molecular weight that is more than twice the molecular weight of either nBPP4-functionalized polymer, the molecular weight of the samples could be a cause of the significant difference in flexibility.

The choice of mesogen could also be a cause for the differences in elastomeric nature of the functionalized polymers. In previous studies, the mesogen spacer length and rigidity have been shown to impact the functionalized polymer properties. For instance, in Moment's work[7], some of the polymers with mesogen A were very rubbery. However, samples with Mesogen B were much more rigid. Further, Gray in 1982[11] reported that increasing mesogen rigidity can lead to higher T_gs and clearing points. These higher T_gs would make the materials less elastomeric.

Block Copolymer Morphology

From x-ray scattering, the BCP d-spacings and smectic LC spacings can be determined at room temperature as well as at elevated temperatures. Data from these studies were previously given in Figures 4.6 through 4.8, and Table 4.3 gives a summary of the room temperature results.

Table 4.3: X-ray scattering data on block copolymer and LC spacings for polymers functionalized with chiral mesogens. Both BCP and LC spacings decrease as the LCP molecular weight and volume fraction decrease.

	BCP Spacing (Å)	Observed LC Spacing (Å)
PS18-LCP$_{10BPB4}$297-PS18	-	54
PS27-LCP$_{4BPP4}$79	410	33
PS27-LCP$_{8BPP4}$108	490	39

It is interesting to note that the PS27-LCP$_{8BPP4}$108 sample retains BCP order at temperatures above the liquid crystal clearing point. This is observed in the temperature-dependent SAXS data from that sample (Figure 4.7). As these data show, the shoulder corresponding to BCP order is still evident at temperatures as high as 175°C, indicating an order-disorder transition well above the PS T_g. Such order has been observed in other studies with LC BCPs that use different LCP backbones and exhibit better phase segregation[12]. However, previous studies on similar polymer backbones[7] do not exhibit phase segregation above the PS T_g. This indicates that the currently studied systems have better phase segregation than those in previous studies. Such differences are likely caused by increased mesogen rigidity in the currently-studied mesogens (Figure 4.2) compared to those previously studied, especially Mesogen A (Figure 1.14).

In the room temperature SAXS of PS27-LCP$_{4BPP4}$79 we observe well-defined BCP peaks and reflections of the primary peak. The 1-D image of this sample was previously shown in Figure 4.7. In that figure, one observes a primary BCP peak at d=410Å, and reflections at d=240Å and d=150Å. These higher-order reflections correspond to ratios of $1:\sqrt{3}$ and $1:\sqrt{7}$ compared to the primary peak, which is indicative of a hexagonally-packed cylindrical morphology (peaks at ratios of $1:\sqrt{3}:2:\sqrt{7}$). In agreement with previously discussed data from DSC, the well-defined SAXS peaks also suggest a highly segregated BCP morphology for this sample.

While the PS27-LCP$_{4MPOB}$84 sample discussed in Chapter 3 exhibited a strong first-order peak in SAXS, PS27-LCP$_{4BPP4}$79 is the only sample characterized in these studies that exhibited

higher-order peaks. Such peaks indicate strong microphase segregation and well-ordered morphology in the sample. As observed in previous studies[12], PS cylinders in a LC matrix can stabilize the LC phase. Therefore, as previously discussed, the stable LC phase at high temperatures in PS27-LCP_{4BPP4}79 can be attributed to this effect.

TEM data can be compared with the SAXS-determined BCP spacings. Representative TEM images for PS27-LCP_{8BPP4}108 and PS27-LCP_{4BPP4}79 are shown in Figures 4.10 and 4.11, respectively. TEM data for PS18-LCP_{10BPB4}297-PS18 indicate phase segregation, but no regular morphology. Therefore, these images are not presented.

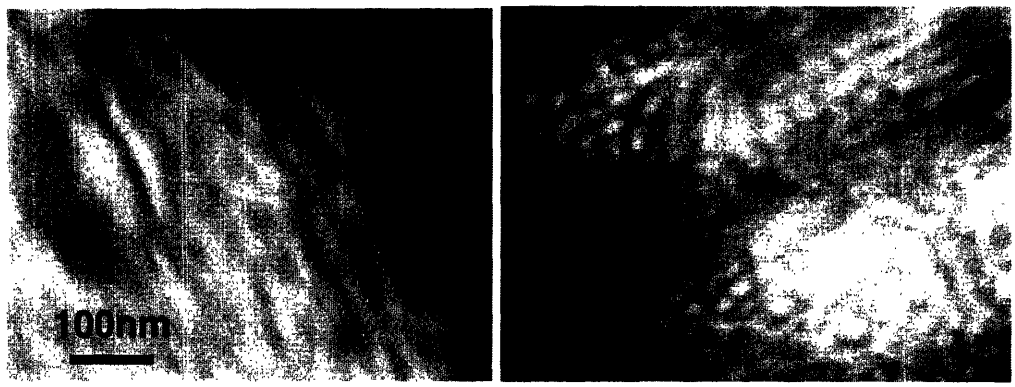

Figure 4.10: TEM images of PS27-LCP_{8BPP4}108. Weak BCP phase segregation and worm-like features are observed, indicating poorly ordered cylindrical morphology.

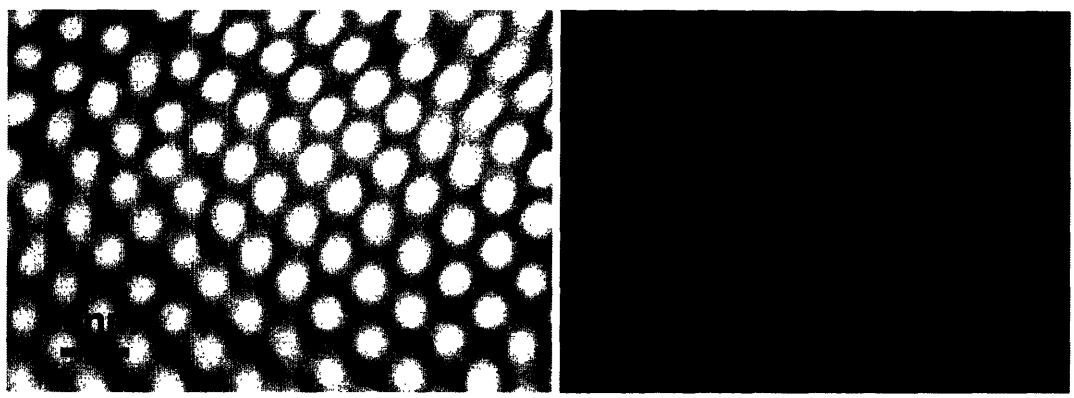

Figure 4.11: TEM images of PS27-LCP_{4BPP4}79. Strong phase segregation and cylindrical order are observed over a large area.

These TEM images agree with what is expected from other characterization techniques. In the PS27-LCP_{8BPP4}108 sample, there is weak phase segregation resulting in a significant interfacial area between the PS-rich and LCP-rich phases. This agrees with the significant lowering of the PS T_g observed in DSC and the weak shoulder in SAXS. Although phase segregation is observed, the lack of BCP order observed in the TEM images explains why the SAXS data did not exhibit reflections that would help to determine the actual BCP morphology.

On the other hand, the images of PS27-LCP_{4BPP4}79 exhibit an oriented and well-defined BCP morphology. This is expected because the SAXS data indicate a strongly segregated hexagonally close packed cylindrical morphology. In addition, DSC data show a PS T_g that is higher than that of the unfunctionalized backbone, again indicating enhanced phase segregation for the systems with shorter mesogens. The order is observed at lower magnifications and extends over a large area. Images of the sample at high magnification (Figure 4.11) show very well defined phase segregation.

As was discussed previously in Chapter 3, the block sizes determined from TEM micrographs can be compared to the theoretical domain sizes in a perfectly segregated hexagonally close-packed cylindrical morphology assuming a d-spacing determined by SAXS. As discussed in Chapter 3, the cross-sectional geometrical representation of the morphology is shown in Figure 4.12 and the equations used for such calculations are given in Equation 4.1.

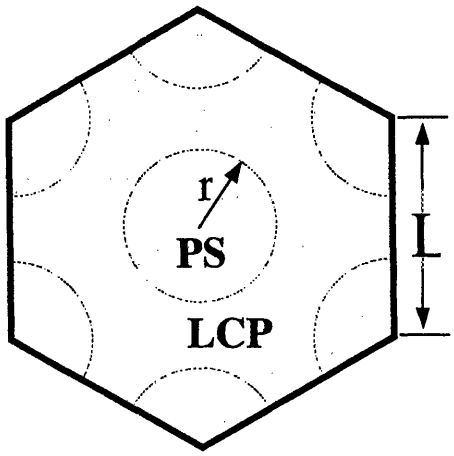

Figure 4.12: Geometric representation of cross-sectional morphology

$$\frac{V_{PS}}{V_{Total}} = \phi_{PS} = \frac{3A_{cs,PS}}{A_{cs,hex}} = \frac{3\pi r_{PS}^2}{\frac{3\sqrt{3}}{2}L^2} = \frac{2\sqrt{3}\pi r_{PS}^2}{3L^2}$$

$$d_{PS} = 2r_{PS} = \sqrt{\frac{2\sqrt{3}}{\pi}\phi_{PS}L^2}$$

$$L_{LCP} = L - d_{PS}$$

Equations 4.1: Equations to determine cylindrical diameter

$$\phi_{PS} = \frac{\frac{w_{PS}}{\rho_{PS}}}{\frac{w_{PS}}{\rho_{PS}} + \frac{w_{LCP}}{\rho_{LCP}}} \tag{3.3a}$$

$$\phi_{LCP} = 1 - \phi_{PS} \tag{3.3b}$$

Results of these calculations are given in Table 4.4. While results for the PS27-LCP$_{4BPP4}$79 system are in very good agreement with the experimental data, the PS27-LCP$_{8BPP4}$108 system at first glance shows different results compared to TEM data. These results for the 8BPP4 sample suggest that there is incomplete segregation between the PS and LCP phases. As was previously discussed, SAXS (Figure 4.7) and TEM (Figure 4.10) also indicate partial miscibility between the two phases. Further, Porod Analysis can be used to estimate an interfacial thickness for a strongly-segregated material[13, 14]. For the PS27-LCP$_{4BPP4}$79 sample, Porod Analysis gives a value

of 9.2Å (Figure 4.13). Similar analysis for PS27-LCP_{8BPP4}108 yields an interfacial thickness of 13Å. Considering calculations on the interfacial thickness and TEM measurement error, the theoretical results and the experimental results are actually in good agreement.

Table 4.4: Comparison of TEM measured domain dimensions with theoretical domain dimensions for perfect segregation in BPP4 systems. TEM measurements were done by hand using graphical software. All lengths are in Ångstroms.

	PS27-LCP_{4BPP4}79	**PS27-LCP_{8BPP4}108**
PS wt. Frac	0.255	0.200
LCP wt. Frac	0.745	0.800
ϕ_{LC}	0.733	0.789
ϕ_{PS}	0.267	0.211
L (SAXS)	410	490
Theor. L_{LCP} (SAXS)	187	254
Theor. d_{PS} (SAXS)	223	236
Interfacial Thickness (Porod)	9.2	13
Measured L (TEM)	350	450
Measured L_{LCP} (TEM)	120	140
Measured d_{PS} (TEM)	240	300

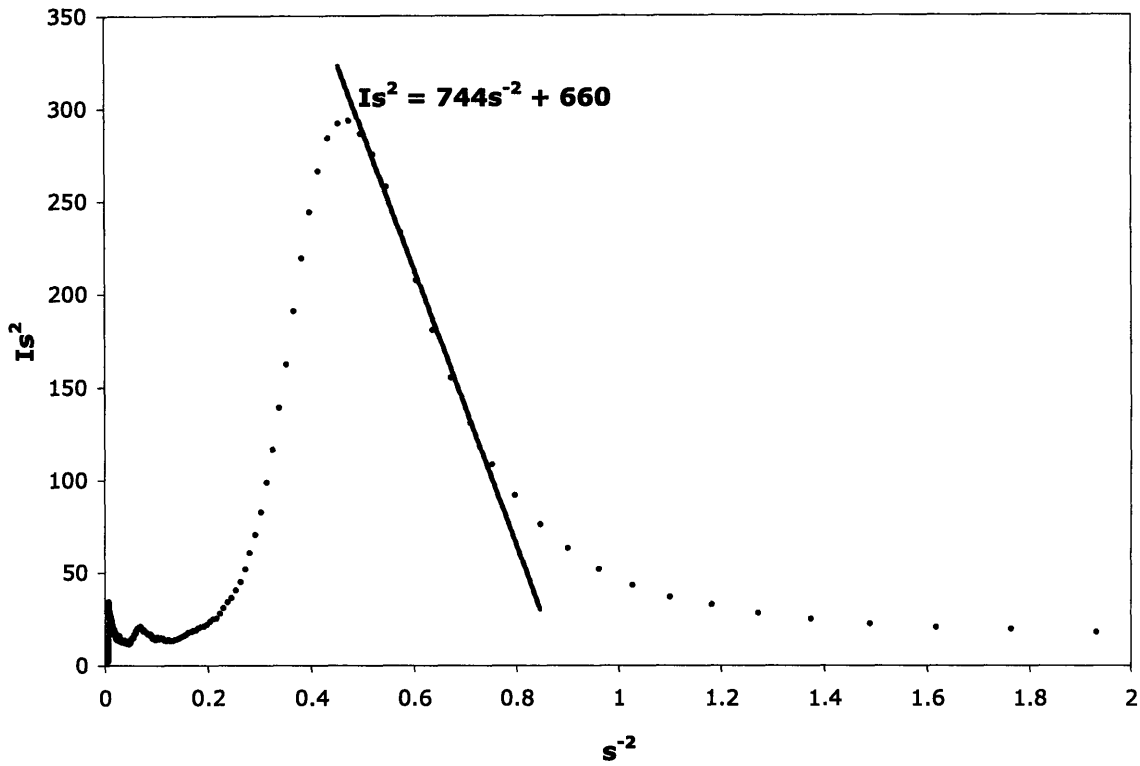

Figure 4.13: Porod Analysis on PS27-LCP$_{4BPP4}$79. The fit line for the Porod Region is shown along with the corresponding equation. This is used to determine interfacial thickness (ΔR) using the relationships $s^2 I = as^{-2} - 4a\pi\sigma^2$ and $\Delta R = 2\sqrt{3}\sigma$. Therefore, the slope of the fit line is the value "a" and the value for σ can be determined from $\sigma = \sqrt{\frac{b}{4a\pi}}$.

Liquid Crystal Properties

In addition to comparing the experimental BCP spacings with the theoretical spacings, the experimental liquid crystal smectic spacings can be compared with the theoretical values. A summary of these results is given in Table 4.5.

Table 4.5: Comparison of experimental LC smectic spacing with theoretical mesogen lengths

	Observed LC Spacing (Å)	Mesogen Length (Å)	Conclusion
PS18-LCP$_{10BPB4}$297-PS18	54	37	Smectic C bilayer, ~20° mesogen tilt
PS27-LCP$_{4BPP4}$79	33	25	Smectic C bilayer, ~25° mesogen tilt
PS27-LCP$_{8BPP4}$108	39	30	Smectic C bilayer, ~25° mesogen tilt

As defined in Chapter 3, the mesogen tilt angle is the angle between the LC director and the smectic layer normal. The pictorial representation of the bilayer was shown in Figure 3.13 and is reprinted in Figure 4.14.

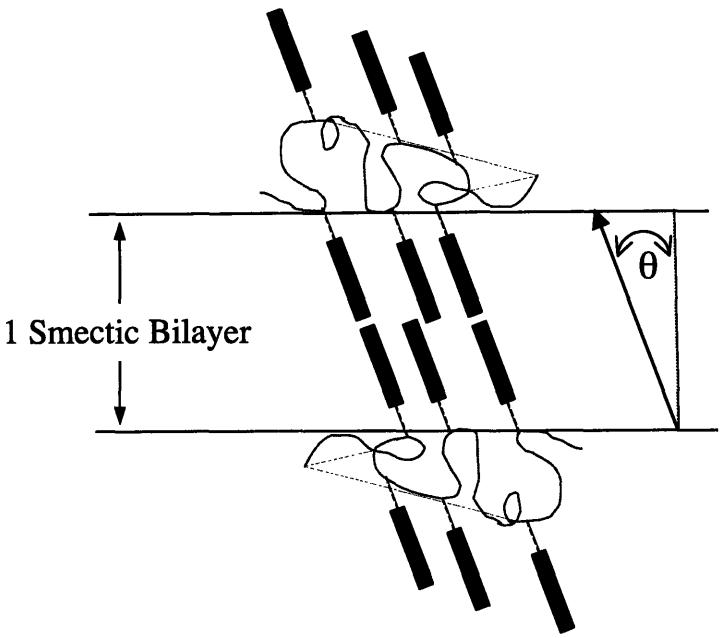

Figure 4.14: Smectic bilayer in LCP region. θ = Mesogen tilt angle, which is the angle between smectic director and layer normal.

The calculated tilts in all three samples are quite reasonable considering previous polymer studies using similar mesogens[8] and using other S_C* mesogens[15-17]. Studies on 11BPP4-functionalized polysiloxane materials by Svensson, et al.[8] reported a tilt angle of ~30°-37°.

In addition to a tilt, in these samples some discrepancy between the theoretical spacing and the experimentally-observed spacing could be caused by interdigitation of the mesogens. This has been observed in research by Clingman, et al.[18]. In that study it was found that such interdigitation is non-negligible for mesogens with decyl endgroups, but generally small for those with methyl endgroups. Since the mesogens studied in the current work have butyl endgroups, some interdigitation is expected. However, it should be minimal. Further, studies using time-resolved FT-IR to examine polymer structure and dynamics have shown that spacers can have tilt angles that are different than the mesogen tilt angle[19]. Therefore, while the calculated tilt angles are reasonable, some error remains.

Initial Processing Studies

Since the polymers functionalized with chiral mesogens exhibit useful phase-segregation and LC properties, processing has begun on these samples to determine if better alignment of the mesogens and orientation in the BCP morphology can be achieved. In POM, it is observed that the PS18-LCP_{10BPB4}297-PS18 sample when it is solvent-cast exhibits a lack of birefringence. However, it does exhibit birefringence upon stretching or shearing by hand. Images of the unsheared and sheared samples are in Figure 4.15.

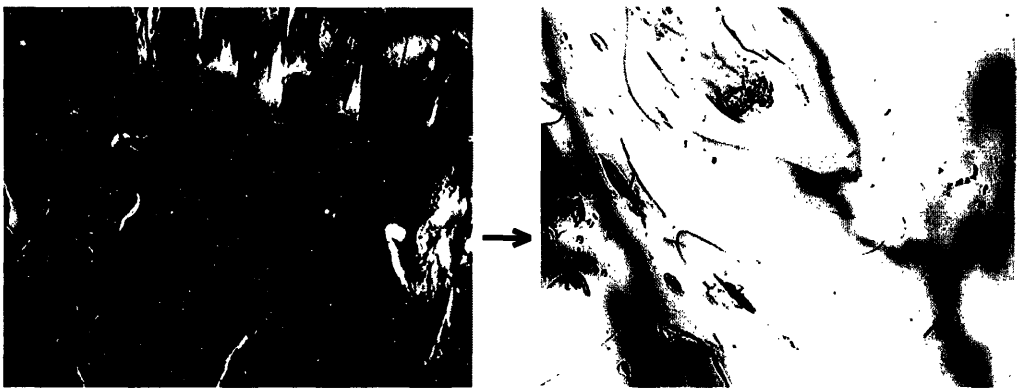

(a) (b)

Figure 4.15: Unsheared (a) and hand-sheared (b) POM images of PS18-LCP_{10BPB4}297-PS18. The as-cast sample lacks birefringence, but birefringence is observed in the sheared sample.

This mechanical orientation persists over long time periods. It cannot be recovered, however, when the sample is heated above the PS T_g and cooled back to room temperature. Heating allows for more mobility in the polymer and LC mesogens. Therefore, they can reorient at high temperatures to assume a more stable arrangement. These observations indicate that the most stable state for the sample at room temperature is not the sheared orientation. However, an extremely slow relaxation time for the material will allow mechanical alignment to be possible below the PS T_g. Similar observations have been made by other groups using freely-suspended liquid crystalline gels[20]. In that research, electric fields were used to orient the LC gel. After a LC texture is formed, the authors reported only being able to erase the texture by heating to a temperature above the gelling point and subsequent cooling into the gel state.

In the less elastomeric PS27-LCP_{4BPP4}79 sample, the mesogens may be aligned using the DMA as described in the Experimental Section of this chapter. In this situation, the sample is

stretched at an elevated temperature until it breaks or slips. From this study, Figure 4.16 shows the 2-D WAXS data obtained from the original sample and the stretched sample.

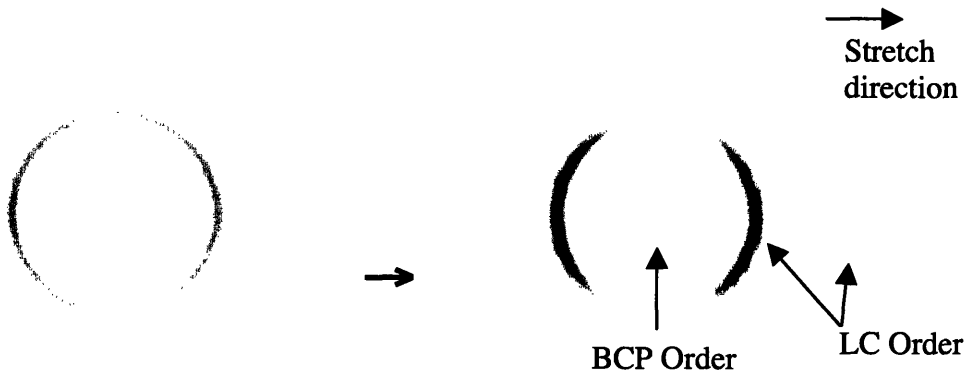

(a) (b)

Figure 4.16: 2-D WAXS data from PS27-LCP_{4BPP4}79 solvent-cast sample (a) and the stretched sample (b). The initial sample exhibits uniform LC scattering, while the stretched sample exhibits anisotropic LC scattering indicative of aligned mesogens.

As one will observe from the primary scattering ring in WAXS, the liquid crystals do not display significant orientation in the solvent-cast sample. However, by stretching the sample in the DMA at elevated temperatures (70°C-115°C), the liquid crystals are better oriented and this results in a higher anisotropy in the system. It should also be noted that, in the stretched samples, a comparison of the inner scattering ring (BCP order) to the outer scattering ring (LC order) indicate smectic liquid crystal layers that are perpendicular to the block copolymer ordering. This means that the mesogens are oriented parallel to the PS cylinders, and the desired orientation and confinement are achieved.

The primary drawback of this processing technique is that the temperature was too high, leading to block copolymer order that is not as defined in the stretched sample compared to the solvent-cast sample. This loss of order is not observed in SAXS (Figure 4.17), but it is observed in TEM (Figure 4.18).

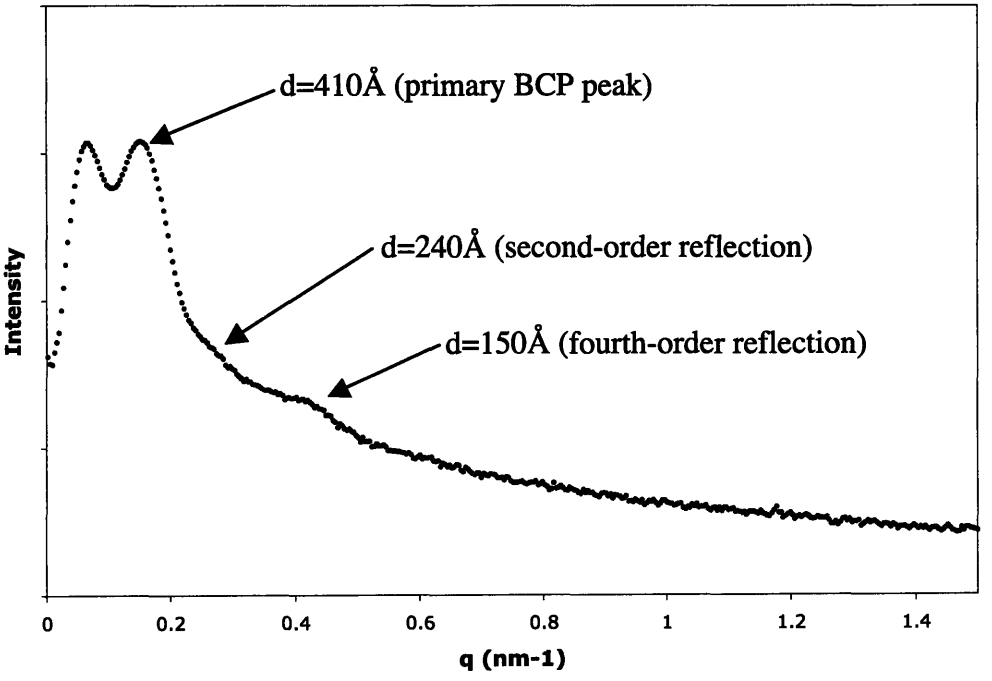

Figure 4.17: 1-D SAXS of stretched PS27-LCP_{4BPP4}79. Arrows indicate the primary BCP peak (d=410Å), second-order peak (d=240Å, $\sqrt{3}$), and fourth-order peak (d=150Å, $\sqrt{7}$).

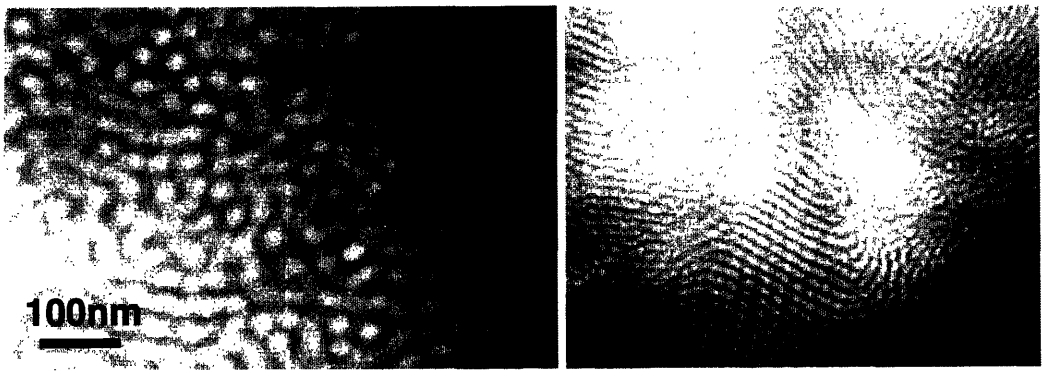

Figure 4.18: TEM images of stretched PS27-LCP_{4BPP4}79. Phase segregation is observed, but a larger interface is visible and the worm-like features are not as ordered as in the solvent-cast sample.

Comparing these figures to those of the solvent-cast sample (Figures 4.8 and 4.11), a few obvious differences are observed. First, in SAXS the peaks of the stretched sample are neither as strong nor as defined as those for the solvent-cast sample. Since sample thickness will affect the intensity of the peaks, the different appearances are likely caused by the thickness instead of weakened BCP morphology. Through the TEM data, however, it is visually observed that there is an interfacial region between the PS-rich and LCP-rich regions. Additionally, the TEM shows a lower overall order in the stretched sample compared to that of the original film. As was previously shown, the solvent-cast sample had very well-defined features and they were oriented on a regular lattice. This is not the case in the stretched sample, and it leads to the conclusion that the stretching temperature used was too high, which allowed for the PS and LCP blocks to become miscible. Further data on the processing studies on PS27-LCP_{4BPP4}79 will be discussed in Chapter 5.

Chapter 4 Summary

In this Chapter, results from studies on three polymers containing chiral mesogens have been given. The primary conclusion is that, as was concluded in Chapter 3, the mesogens with shorter spacers give rise to better phase segregation and BCP morphology in functionalized BCPs. All

samples exhibit enhanced LC phase stability due to the BCP cylindrical morphology. In addition, the shorter spacers allow for higher clearing points and multiple phase transitions.

However, polymers with shorter spacers were not elastomers. Therefore, future studies should use materials with larger polymer backbones and/or larger LCP content. This could be accomplished through synthesizing a polymer backbone of larger molecular weight, increasing the mesogen attachment percentage, or increasing the PVMS volume fraction in the initial polymer backbone. Finally, processing such as shearing and stretching has been successfully used to orient the liquid crystals in functionalized polymers. Chapter 5 will further discuss these techniques and will also discuss additional processing techniques that have been attempted.

References

1. Garg, D. P.; Zikry, M. A.; Anderson, G. L., Current and potential future research activities in adaptive structure: an ARO perspective. *Smart Materials and Structures* **2001,** 10, 610-623.

2. Brehmer, M.; Zentel, R.; Wagenblast, G.; Siemensmeyer, K., Ferroelectric Liquid Crystalline Elastomers. *Macromolecular Chemistry and Physics* **1994,** 195, (6), 1891-1904.

3. Lehmann, W.; Skupin, H.; Tolksdorf, C.; Gebhard, E.; Zentel, R.; Kruger, P.; Losche, M.; Kremer, F., Giant lateral electrostriction in ferroelectric liquid-crystalline elastomers. *Nature* **2001,** 410, (6827), 447-450.

4. Lehmann, W.; Gattinger, P.; Keck, M.; Kremer, F.; Stein, P.; Eckert, T.; Finkelmann, H., The inverse electromechanical effect in mechanically oriented S-C* elastomers examined by means of an ultra-stable Michelson interferometer. *Ferroelectrics* **1998,** 208, (1-4), 373-383.

5. Lehmann, W.; Hartmann, L.; Kremer, F.; Stein, P.; Finkelmann, H.; Kruth, H.; Diele, S., Direct and inverse electrmechanical effect in ferroelectric liquid crystalline elastomers. *Journal of Applied Physics* **1999,** 86, (3), 1647-1652.

6. Roy, S. S.; Lehmann, W.; Gebhard, E.; Tolksdorf, C.; Zentel, R.; Kremer, F., Inverse piezoelectric and electrostrictive response in freely suspended FLC elastomer film as detected by interferometric measurements. *Molecular Crystals and Liquid Crystals* **2002,** 375, 253-268.

7. Moment, A. The Synthesis and Characterization of Polystyrene Liquid Crystalline Siloxane Block Copolymers. Doctoral, Massachusetts Institute of Technology, Cambridge, MA, 2000.

8. Svensson, M.; Helgee, B.; Sharp, K.; Andersson, G., Effects of nitro substituents on the properties of a ferroelectric liquid crystalline side chain polysiloxane. *Journal of Materials Chemistry* **1998,** 8, (2), 353-362.

9. Plate, N. A.; Shibaev, V. P., In *Comb-Shaped Polymers and Liquid Crystals*, Cowie, J. M. G., Ed. Plenum: New York, 1987.

10. Yi, Y.; Fan, X.; Wan, X.; Li, L.; Zhao, N.; Chen, X.; Xu, J.; Zhou, Q.-F., ABA Type Triblock Copolymer Based on Mesogen-Jacketed Liquid Crystalline Polymer: Design, Synthesis, and Potential as Thermoplastic Elastomer. *Macromolecules* **2004,** 37, (20), 7610-7618.

11. Gray, G. W., In *Polymer Liquid Crystals*, Ciferri, A.; Krigbaum, W. R.; Meyer, R. B., Eds. Academic Press: New York, 1982; pp 1-33.

12. Anthamatten, M. L. Massachusetts Institute of Technology, Cambridge, MA, 2001.

13. Todo, A.; Hashimoto, T.; Kawai, H., Small-Angle X-ray Scattering from Block Copolymers as an Ideal Model System for a Pseudo Two-Phase Solid Texture. *Journal of Applied Crystals* **1978,** 11, 558-563.

14. Tyagi, D.; McGrath, J. E.; Wilkes, G. L., Small Angle X-ray Studies of Siloxane-urea Segmented Copolymers. *Polymer Engineering and Science* **1986,** 26, (20), 1371-1398.

15. Blinov, L. M.; Chigrinov, V. G., *Electrooptical Effects in Liquid Crystal Materials.* Springer-Verlag: New York, 1994.

16. Anthamatten, M. L.; Hammond, P. T., A SAXS Study of Microstructure Ordering Transitions in Liquid Crystalline Side-Chain Diblock Copolymers. *Macromolecules* **1999,** 32, 8066-8076.

17. Anthamatten, M. L.; Zheng, W. Y.; Hammond, P. T., A Morphological Study of Well-Defined Smectic Side-Chain LC Block Copolymers. *Macromolecules* **1999,** 32, 4838-4848.

18. Clingman, S. R.; Mao, G.; Ober, C. K.; Colby, R. H.; Brehmer, M.; Zentel, R.; Bignozzi, M.; Laus, M.; Angeloni, A.; Gillmor, J. R., Effect of polymer architecture on self-diffusion of LC polymers. *Journal of Polymer Science Part B-Polymer Physics* **1999,** 37, (5), 405-414.

19. Shilov, S. V.; Skupin, H.; Kremer, F.; Gebhard, E.; Zentel, R., Segmental orientation and mobility of ferroelectric liquid crystal polymers. *Liquid Crystals* **1997,** 22, (2), 203-210.

20. Li, J. J.; Stannarius, R.; Tolksdorf, C.; Zentel, R., Hydrogen bonded ferroelectric liquid crystal gels in freely suspended film geometry. *Physical Chemistry Chemical Physics* **2003,** 5, (5), 916-923.

Chapter 5 – Processing of Polymers for Use as Ferroelectric Actuators

Motivation and Background

Processing can make a significant difference in the ordering of the BCP and the alignment of mesogens. Some processing techniques that have been used include annealing[1], stretching, use of magnetic fields[2], and various types of shearing[3-6]. These techniques can be used to mechanically orient the sample or take advantage of shifting the equilibrium state of order in the material. In annealing, studies have shown that the chosen temperature, time, and film thickness all impact the final morphology and order of the sample[1]. In shearing, the temperature, amplitude, and frequency have an impact on the final properties[4, 6].

In groups that study LC homopolymers for use as actuators, mechanical stretching has been used to align mesogens. In studies by Lehmann, et al.[7], the material was exposed to stretching three times in different directions. The stretching was followed by chemical crosslinking to create the final sample that would be studied. Since the currently studied polymers form physical crosslinks, this final chemical crosslinking step is unnecessary. However, the stretching technique Lehmann used has been considered for our systems and a high temperature uniaxial stretch has been attempted to observe the effect on mesogen alignment and BCP order. Results from that stretched sample were discussed in Chapter 4.

Roll-casting is another technique that has been used in this group and others to align BCP samples[8-12]. In this technique, a sample is dissolved into an appropriate solvent and placed between two countercurrent rollers, one of which is coated with Teflon. The roller speed and spacing can be used to enhance BCP order based on the desired morphology and concentration. Roll-casting has been attempted in this project on two polymers, but was not successful due to

solvent choice and/or quantity of material. Therefore, since it has been quite successful in orienting samples in previous projects, future work will include determining the proper conditions for roll-casting the currently studied samples.

This chapter examines the effect on BCP ordering and LC alignment when PS27-LCP_{4BPP4}79 is subjected to stretching, shearing, and annealing. In order to use the material as an actuator, the BCP morphology should be well-ordered PS cylinders in a LCP matrix and grainless. Further, the LCP block should be confined by the BCP morphology and there should be one overall, uniform S_C* director for all mesogens. TEM and SAXS were used to determine the BCP morphologies, DSC was used to determine thermal transitions, and WAXS was used to study the anisotropy of the mesogens as various processing techniques were performed on the sample.

Experimental

Small Angle X-ray Scattering – SAXS was used to determine the shape and orientation of polymer features with dimensions on the order of 100Å (spheres, cylinders, lamellae, etc.). The shape determination was based on the relative scattering vector ratios of the peaks in the profile, while the LC spacing was based on the *d*-spacing of the first-order peak. SAXS also allowed us to determine how these features were oriented with respect to each other. A Molecular Metrology 2-D SAXS detector placed 1300mm from the sample was used to detect the scattering of Cu K_α x-rays at 45kV and 0.66mA produced by a Microsource x-ray generator. An extended sample holder allowed for a sample-to-detector distance of 1100mm was used to simultaneously monitor BCP order and primary LC order in some samples.

Transmission Electron Microscopy – TEM was used to obtain images of the phase-segregated morphology of the block copolymers. The type of morphology, grain size, and degree of ordering were determined with these images. Samples first were cryotomed before using in the TEM. A RMC MT-X ultramicrotome with CR-X cryo attachment was used to section samples of ~50nm in thickness below room temperature. The diamond knife temperature was set at -75°C and the sample temperature set at -85°C. Films were transferred to copper grids and stained for 25 minutes with the vapor from OsO_4 4% aqueous solution. OsO_4 preferentially stains the liquid crystal polymer, making these regions appear dark in the TEM images. Samples were observed with a JEOL 200CX electron microscope operating at 200kV.

Wide Angle X-ray Scattering – WAXS was used to determine the types of liquid crystal phases present (S_C*, S_A, N, etc.). LC spacings with dimensions of 40Å and smaller were studied with this method. The same equipment used for SAXS was used for WAXS by moving the detector closer to the sample (sample-to-detector distance = 300mm).

DMA Stretch – In this technique, a temperature ramp of 10°C/min was used with 20μm amplitude oscillation at 1Hz frequency. The sample maintained mechanical integrity until approximately 70°C where it started to draw out. At T~115°C the material failed.

DMA Shear – An amplitude of 50μm, frequency of 10Hz, and temperature of 80°C were chosen. The sample thickness was 0.4 mm and the shear sandwich mode was used for 40 min. Later, this process was repeated at a temperature of 45°C to determine how temperature would affect the final properties.

Annealing – Annealing was done at two conditions to determine the appropriate temperature and time. Initially, samples were annealed in a vacuum oven at 80°C for 2 days. This temperature was chosen because it is close to the PS T_g and allowed for almost complete

mobility in the polymer sample. However, the temperature fluctuated somewhat and it reached a maximum of ~100°C for ~1hr. Later, additional samples were annealed at 70°C for 3-5 days. This lower temperature was chosen because it was ~15°C below the PS T_g. Therefore, the LCP regions will be mobile without the two phases becoming miscible. Some annealed samples were quenched using liquid nitrogen to freeze in the morphology, while others were allowed to cool slowly under ambient conditions.

Results

As in Chapter 4, the 4BPP4 chiral mesogen was attached to a diblock copolymer backbone and used in these processing studies.

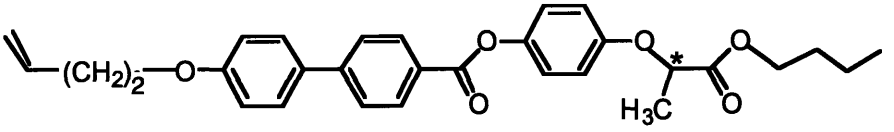

- DSC – G 50 S 97 N 120 I

Figure 5.1: 4BPP4 chiral mesogen used in processing studies

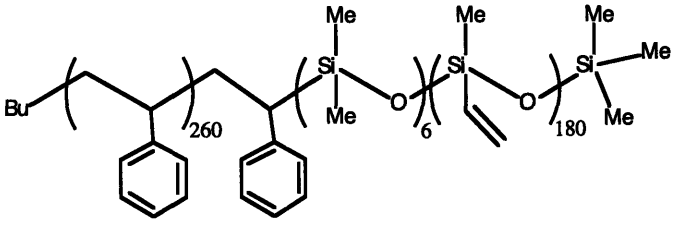

Figure 5.2: Diblock copolymer backbone (PS27-PVMS16) to which 4BPP4 was attached

Table 5.1 summarizes the solvent-cast sample characteristics of the 4BPP4-functionalized BCP used for these studies

Table 5.1: Summary of properties in solvent-cast PS27-LCP$_{4BPP4}$79

Mesogen Attachment	55%
LCP wt%	75%
LCP T_g	-10°C
PS T_g	87°C
Thermal Transitions	G -10 S_I 70 S_{II} 87 S_{III} 110 N >250 I
BCP d-spacing	410Å (HCP)
LC Smectic Spacing	33Å

This material when solvent-cast from toluene exhibits a very well-defined HCP morphology as shown in Figure 4.10 and again in Figure 5.3.

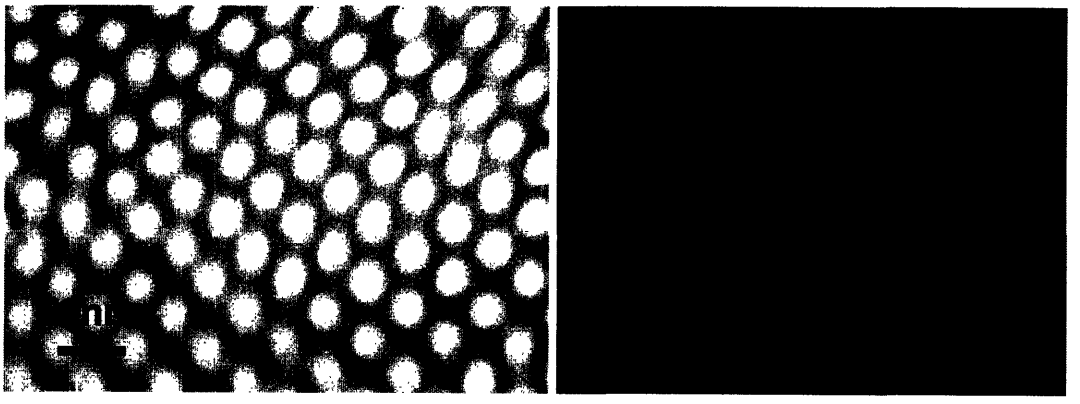

Figure 5.3: TEM images of PS27-LCP$_{4BPP4}$79

As one observes from the low-magnification image, the order is fairly uniform over a large area. As discussed in Chapter 4, this well-defined order allows for good mesogen confinement and a stable smectic phase at high temperatures. The mesogen confinement is caused by the BCP spacing in the sample that confines the LCP phase to a space of ~150Å, which is significantly smaller than the S_C* pitch of ~3-5μm. However, mesogen alignment is poor, as indicated by the 2-D x-ray scattering pattern given in Figure 5.4. Therefore, processing

techniques will be studied as ways to align the LC mesogens. While aligning the mesogens, care must be taken to also maintain the high BCP order displayed in the solvent-cast sample.

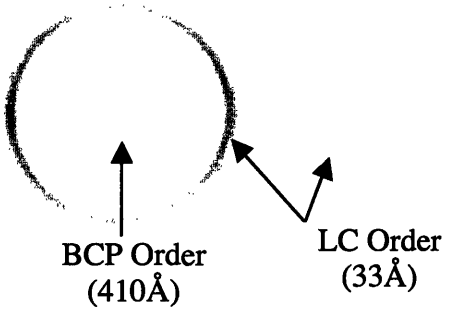

Figure 5.4: 2-D WAXS data from PS27-LCP_{4BPP4}79 solvent-cast sample. Arrows indicate the scattering associated with BCP and LC order.

Thermal Transitions and Block Copolymer Morphology

As discussed in Chapter 4, stretching this sample in the DMA at high temperatures has been successful in aligning the LC mesogens in the material, as indicated by higher anisotropy in the 2-D WAXS data. The stretched sample, however, lacks the same high order of BCP orientation as exhibited in the solvent-cast sample. TEM images of this sample are shown in Figure 5.5.

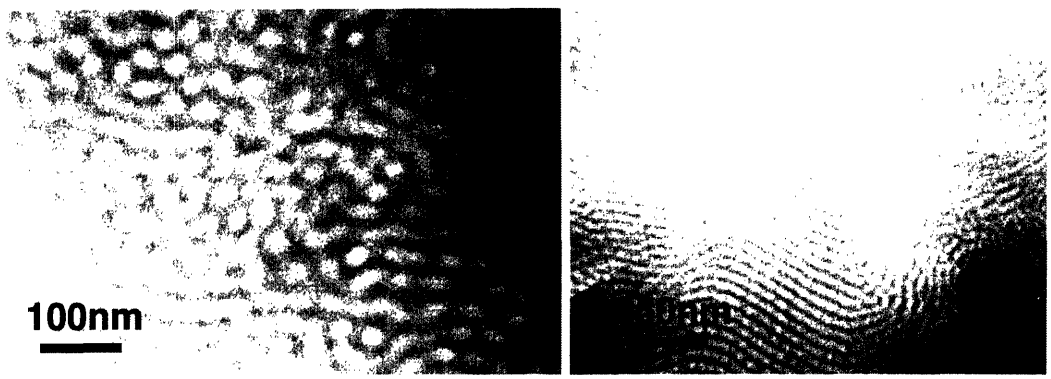

Figure 5.5: TEM images of stretched PS27-LCP_{4BPP4}79. Phase segregation is observed, but a larger interface is visible and the worm-like features are not as ordered as in the solvent-cast sample.

Since this sample was stretched during a temperature ramp up to ~115°C, it underwent LC and BCP phase transitions, including a PS T_g. These higher temperatures allow for enhanced mobility and increased interaction between the two polymer phases because the χ parameter is lowered at higher temperatures. This increased interaction (lower χ) would allow for the lowering of phase segregation observed in the TEM images. In addition, the lower-magnification image exhibits side-on cylinders that swirl to form a pattern that resembles the characteristic focal conic texture indicative of smectic phases. Previous studies have shown that the LC order can affect the BCP order, especially at high LC volume fraction and low polymer molecular weight[12, 13]. Figure 5.6 gives a pictorial representation of the focal conic texture. Such control over ordering is similar to observations in other studies in which thermotropic and lyotropic LCPs were used to influence alignment in nanoparticles[14, 15].

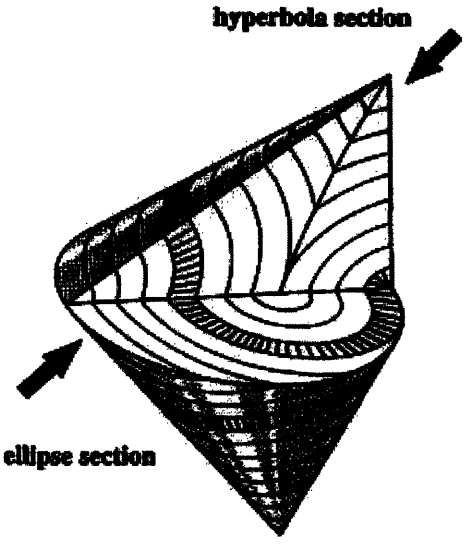

Figure 5.6: Focal conic diagram[13]

Since neither the solvent-cast sample nor the stretched sample exhibits the ideal combination of BCP orientation and LC alignment, shearing and annealing were also studied to determine if under different conditions the desired morphology could be obtained. In annealing, the purpose is to affect the mobility of the two blocks in such a way as to increase phase segregation. It is also important to remember that the χ parameter is an inverse function of temperature such that

$$\chi = a + \frac{b}{T} \tag{5.1}$$

a and b are constants that vary based on the polymer blocks used. This inverse relationship is caused by increased entropy at higher temperatures, which will allow the LCP block to mix with the PS block above a critical temperature.

DSC and SAXS data from the processed samples are shown in Figures 5.7 and 5.8, respectively.

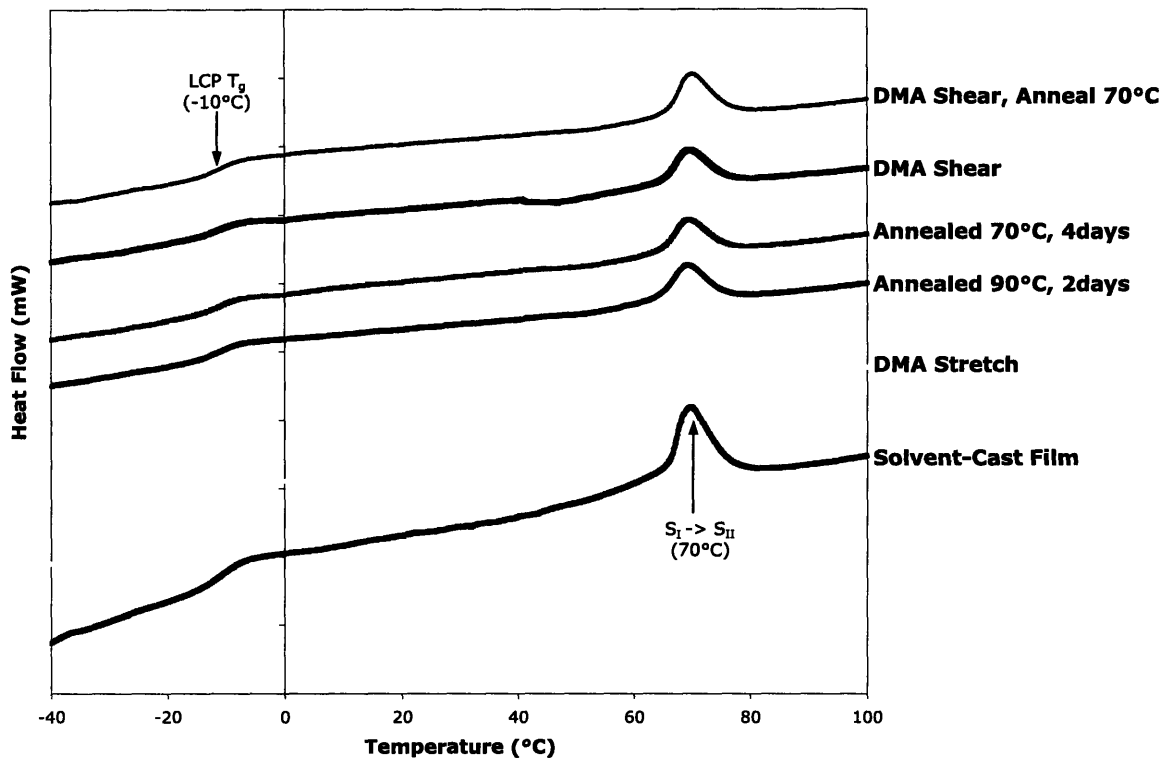

Figure 5.7: DSC data from processed samples. The T_gs and LC phase transitions remain constant for all samples, indicating similar ordering regardless of processing.

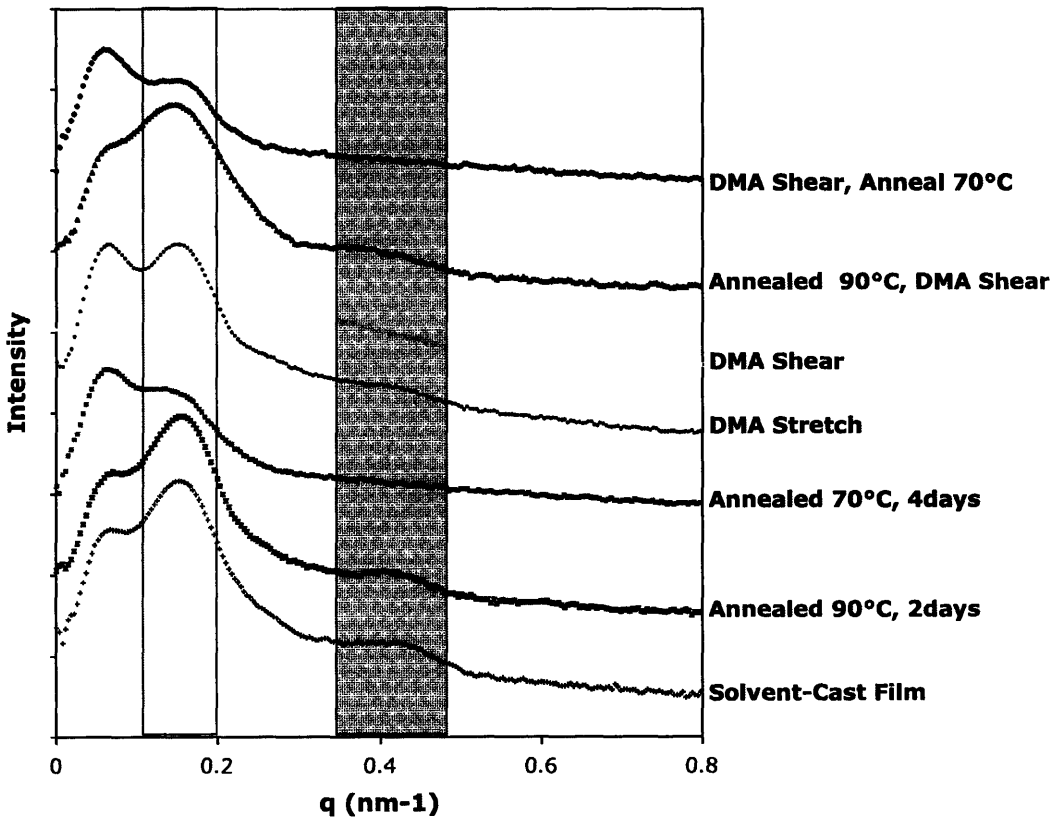

Figure 5.8: SAXS data from processed samples, highlighting the first-order peak (410Å, light grey box) and the most prominent reflection peak (150Å, $\sqrt{7}$ fourth-order peak, darker grey box)

From these data, it is observed that all the processed samples exhibit a strong thermal transition at 70°C, a LCP T_g at –10°C, and strong phase segregation. These thermal transitions are also observed in the original sample, indicating little change in the BCP order and phase segregation upon processing. Most processed samples also retained the well-ordered HCP morphology and domain spacings (410Å) exhibited in the solvent-cast sample. However, in the case of samples that were annealed at 70°C, the reflection peak is not observed. Since this annealing temperature

occurs near the end of a $S_I \rightarrow S_{II}$ phase transition for the material and is close to the PS T_g, the reduction of order is likely caused by the LC phase transition. As previously discussed, at high temperatures LC transitions have been shown to affect BCP order in previous studies[12, 13]. This leads to focal conic BCP textures as shown in Figure 5.4, and in some cases has been shown to induce transitions from one BCP morphology to another as reported in the literature. Therefore, near such a transition, order may be lost somewhat in order to allow for rearrangement to occur.

In order to visually study the BCP changes that occurred from the various processing techniques, TEM was used. Images from the samples are shown in Figures 5.9 through 5.13.

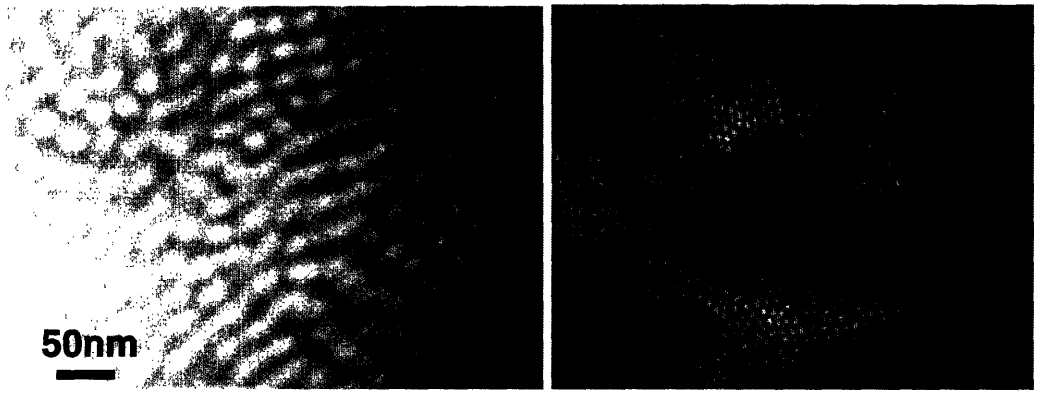

Figure 5.9: TEM of DMA-sheared PS27-LCP_{4BPP4}79 (A=50μm, f=10Hz, T=80°C). Cylindrical morphology is observed as indicated by circular and worm-like features.

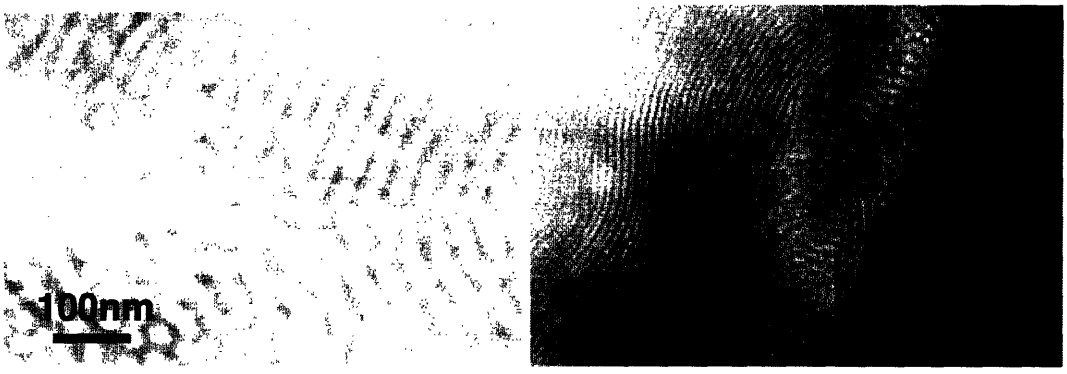

Figure 5.10: TEM of 90°C-annealed (2days) PS27-LCP_{4BPP4}79. A long-range focal conic texture is clearly observed. An interfacial region is observed at higher magnifications.

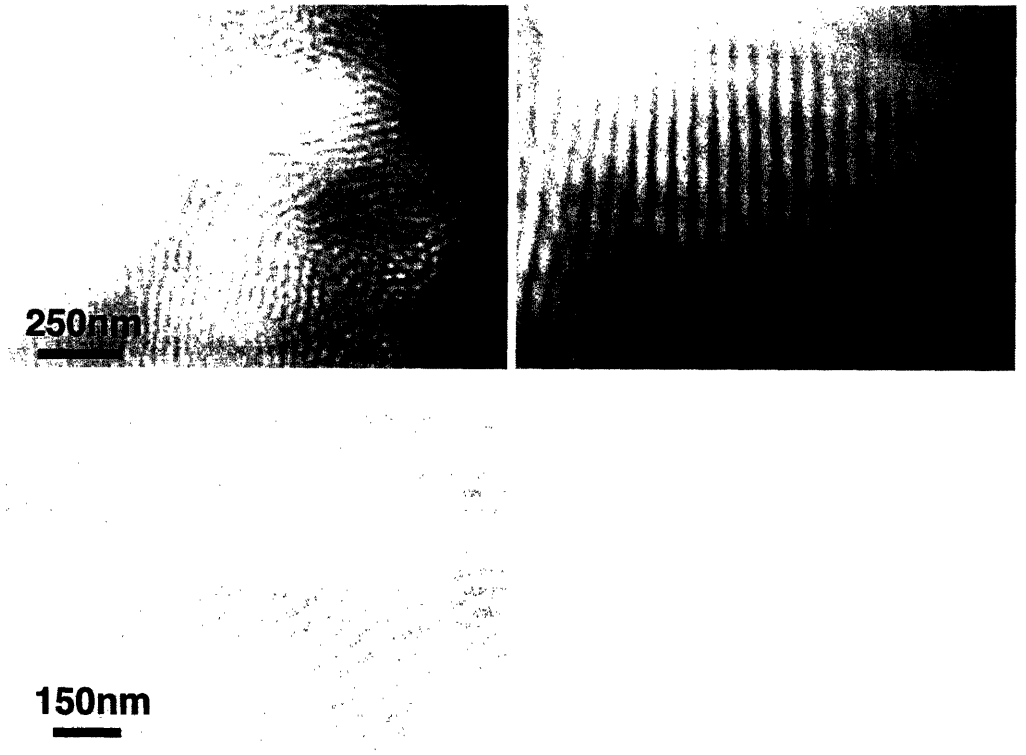

Figure 5.11: TEM of 90°C-annealed (2days) then DMA-sheared PS27-LCP_{4BPP4}79 (A=50μm, f=10Hz, T=80°C). Short-range, well-ordered cylindrical morphology with a narrow interface is observed at high magnifications. However, an unordered phase-segregated morphology is observed over the long-range in low-magnification images.

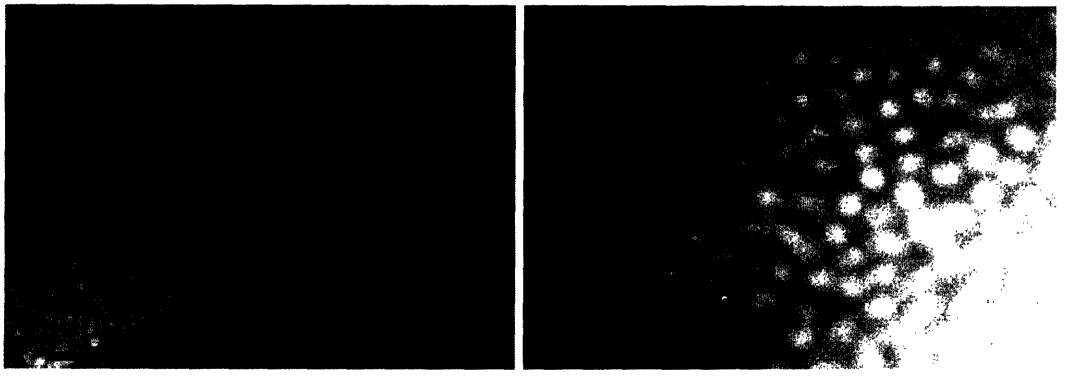

Figure 5.12: TEM of 70°C-annealed (4days) PS27-LCP_{4BPP4}79. Circular and worm-like features are observed, as well as an interfacial region at higher magnifications.

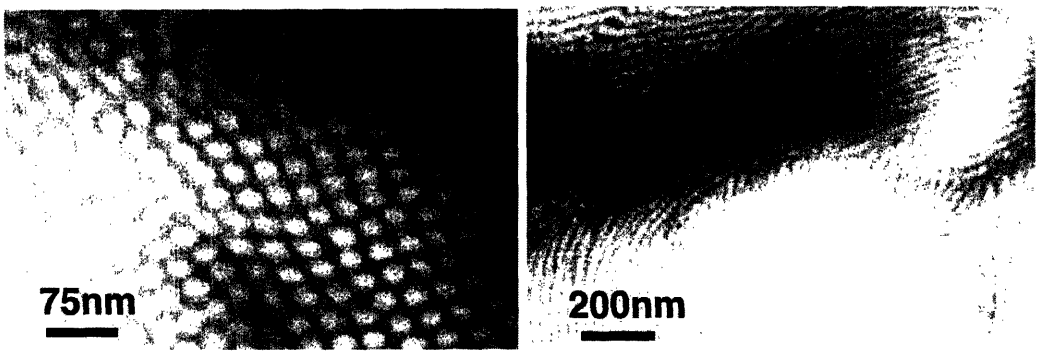

Figure 5.13: TEM of DMA-sheared (A=50μm, f=10Hz, T=80°C) then 70°C-annealed (4days) PS27-LCP_{4BPP4}79. Cylindrical morphology is observed, as well as some worm-like features. This is likely due to mesogen rearrangements at the nearby phase transition.

As observed in these images, all still have BCP order, as expected from the SAXS data. However, some samples exhibit large interfaces between the LCP and PS blocks. In addition, a strong focal conic texture is observed indicative of a smectic phase. This is reasonable since the annealing was performed above the PS T_g and both blocks of the material were very mobile. Further, the material was slowly cooled to room temperature instead of being quenched in an extremely cold atmosphere. This allowed the sample to continue rearranging at cooler temperatures before taking data. Therefore, the mesogens were able to significantly impact the BCP order due to the enhanced mobility and the ability to maintain a pseudo-equilibrium state while cooling.

It is interesting to note that shearing the 90°C-annealed sample helped it to regain much of the order lost upon annealing at such a high temperature, while some order appears to be lost upon shearing the solvent-cast sample. Since both shears were done at the same time and under identical conditions, as described in the Experimental section of this chapter, polymer mobility

can be ruled out as the cause. However, orientation of the polymer in the sample holder could affect it. Since the initial orientation of the cylinders was not known when shearing occurred, those of the solvent cast sample may have been aligned at an angle to their ideal orientation. Therefore, at an elevated temperature and under a shear field, the cylinders might have been forced to significantly rearrange. For the sample that was initially annealed at 90°C, the cylinders were already oriented in non-uniform directions. Therefore, forcing such shear-induced rearrangements could be easier than in the solvent-cast film, no matter how the film was oriented on the sample holder. While the annealed and sheared film is more-ordered than the precursor annealed film, it does still exhibit remnants of a focal conic texture.

Liquid Crystal Ordering

In addition to studying the BCP order in these processed samples, it is important to study the LC alignment because that is essential to obtaining ferroelectric actuation. In order to study this, samples were studied in SAXS employing a shorted sample-to-detector distance by using an extended sample holder (distance~1100mm). 1-D and 2-D data from these studies are shown in Figures 5.14 through 5.19:

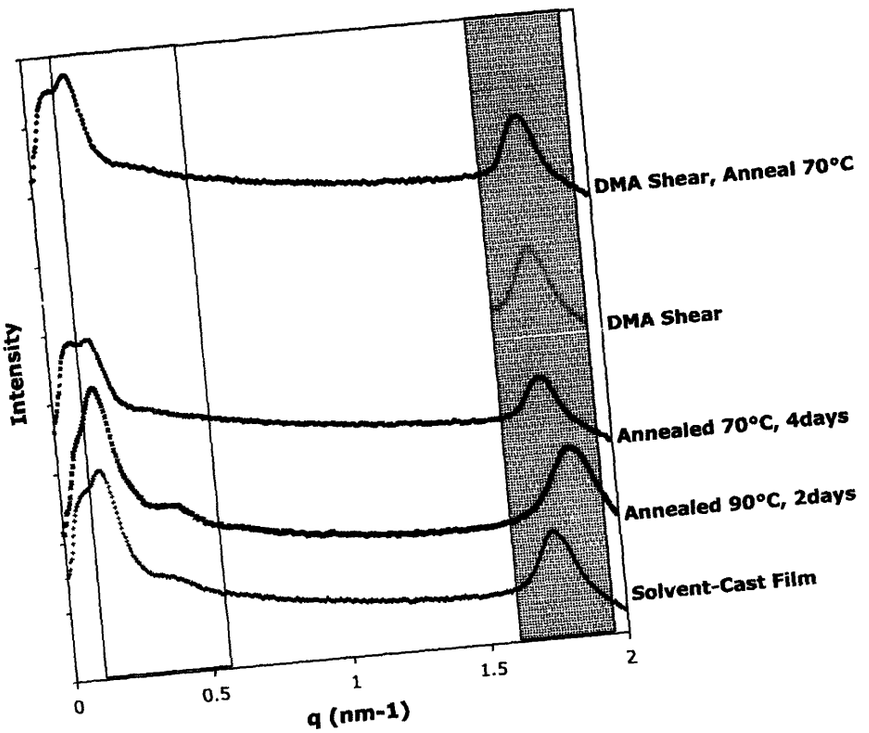

Figure 5.14: 1-D SAXS of processed samples using extended sample holder. The light grey box indicates BCP order (410Å), while the darker grey box highlights LC order (31Å-33Å). In the 90°C-annealed sample, a lowering of the smectic spacing is observed. This is perhaps from an increased tendency toward mesogen interdigitation at higher temperatures.

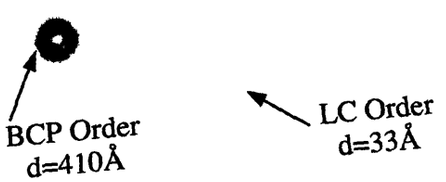

Figure 5.15: 2-D SAXS of solvent-cast PS27-LCP_{4BPP4}79 in extended sample holder. BCP ordering is observed as indicated by the anisotropy in the inner BCP scattering ring.

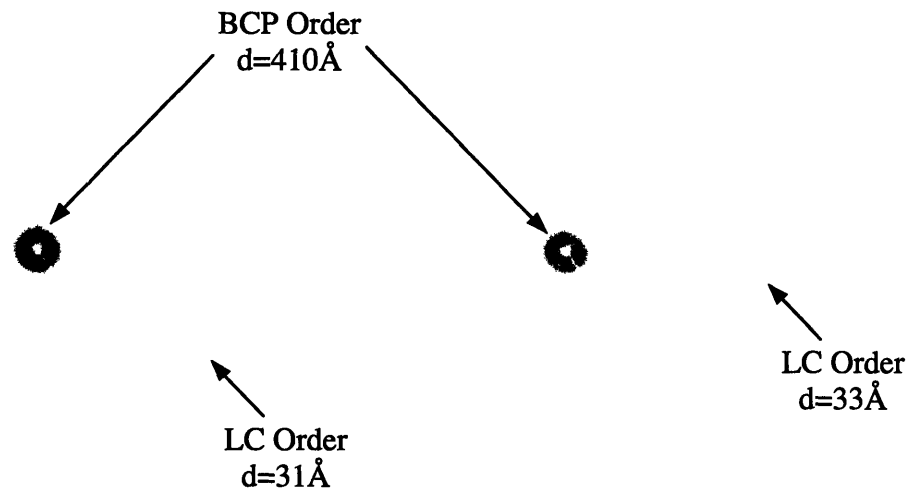

Figure 5.16: 2-D SAXS of 90°C-annealed (a) and 70°C-annealed (b) PS27-LCP_{4BPP4}79 in extended sample holder. Ordered BCP morphology is observed in the inner BCP scattering ring of the 70°C-annealed sample.

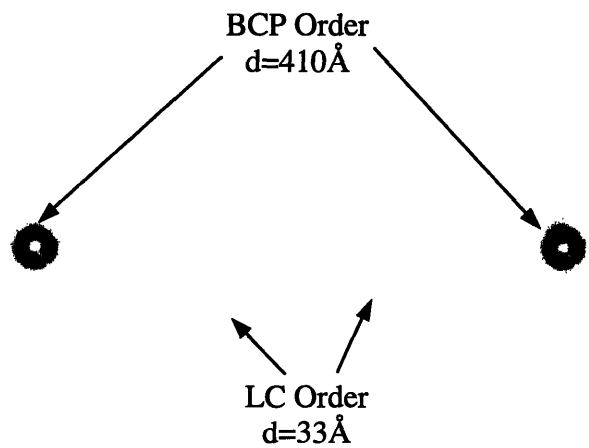

Figure 5.17: 2-D SAXS of 90°C-annealed (a) and 70°C-annealed (b) PS27-LCP_{4BPP4}79 quenched in liquid nitrogen in extended sample holder. Ordered BCP morphology is observed in the inner BCP scattering ring of the 70°C-annealed sample.

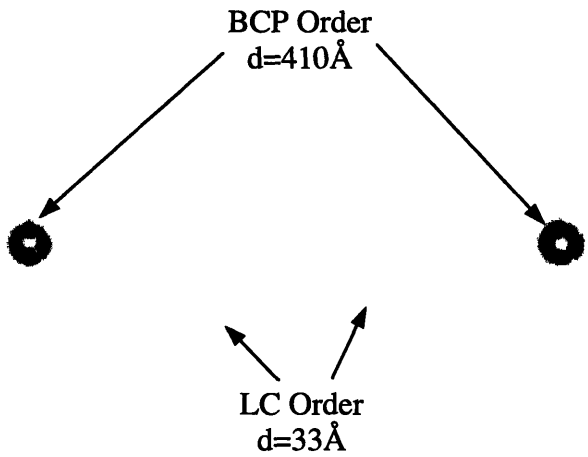

Figure 5.18: 2-D SAXS of 80°C-sheared (a) and 40°C-sheared (b) PS27-LCP$_{4BPP4}$79 in extended sample holder. Ordered BCP morphology is observed in the inner BCP scattering ring of the 80°C-sheared sample.

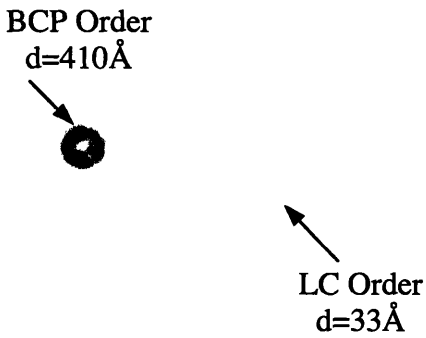

Figure 5.19: 2-D SAXS of DMA-sheared then 70°C-annealed PS27-LCP$_{4BPP4}$79 in extended sample holder. Ordered BCP morphology is observed in the inner BCP scattering ring.

As is observed in these images, all processed samples exhibit smectic scattering at q~1.8-1.9 (d~31Å-33Å). This is consistent with what is observed in the solvent-cast sample and indicates a very broad smectic C range from below room temperature to above 90°C. Some samples also indicate well-oriented BCP segregation morphology as observed from the inner scattering rings. It is interesting that none of the processed samples exhibits LC alignment, except the DMA-stretched sample. A 2-D WAXS image for that sample was shown in Figure 4.11 and is reprinted in Figure 5.20.

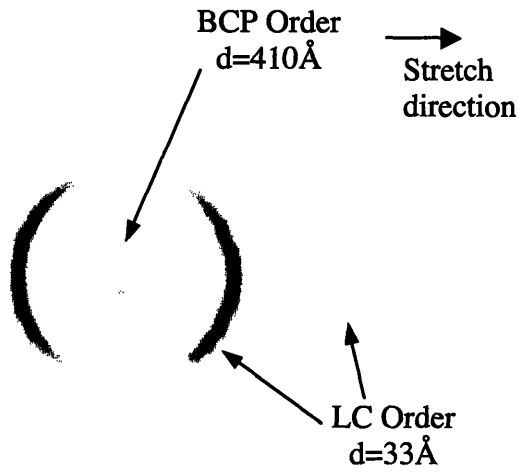

Figure 5.20: 2-D WAXS data from DMA-stretched PS27-LCP$_{4BPP4}$79. Anisotropy is observed in the BCP scattering as well as the LC scattering, indicating LC layers that are perpendicular to the PS cylinders.

As was previously discussed, this sample indicated aligned mesogens as well as an oriented BCP morphology. Further, since smectic layers are perpendicular to the PS cylinders, the mesogens are aligned parallel to the PS cylinders. This arrangement is necessary for ferroelectric actuation.

All other processing techniques lacked such LC alignment, making these materials less-desirable.

In samples processed at 70°C and above, the lack of LC alignment could be caused by the lack of orientation in the PS cylinders. Previous studies[16] have suggested that the PS orientation becomes trapped upon vitrification below the PS T_g. Therefore, any lack of order in the PS phase or defects in its ordering that occur upon cooling will adversely affect alignment of the LC phase.

The annealing time can also have an impact on the final order observed. The 70°C samples were annealed for 4days, while 90°C samples were annealed for 2days. Since longer annealing times are necessary for annealing at lower temperatures[1], a longer annealing time at 70°C perhaps would allow for a system with higher order. In addition, the sample thickness was not uniform throughout the film. This has also been shown to impact the order observed[1].

Chapter 5 Summary

BCP ordering and LC alignment have been studied on the PS27-LCP_{4BPP4}79 sample using stretching, shearing, and annealing. The solvent-cast sample exhibited a well-ordered hexagonally close-packed BCP morphology, but lacked LC alignment. With one exception, processing the sample adversely affects the BCP order and does not improve the LC alignment. In the case of the DMA-stretched sample, mesogen alignment has been significantly enhanced. Annealing the solvent-cast sample at 90°C followed by shearing at 80°C did allow for some recovery of the initial BCP order. Processing techniques performed at high temperatures produced samples that exhibited focal conic textures in the BCP morphology observed in TEM.

References

1. Guarini, K. W.; Black, C. T.; Yeung, S. H. I., Optimization of Diblock Copolymer Thin Film Self Assembly. *Advanced Materials* **2002,** 14, (18), 1290-1294.

2. Osuji, C.; Ferreira, P. J.; Mao, G.; Ober, C. K.; Vander Sande, J. B.; Thomas, E. L., Alignment of Self-Assembled Hierarchical Microstructures in Liquid Crystalline Diblock Copolymers Using High Magnetic Fields. *Macromolecules* **2004,** 37, (26), 9903-9908.

3. Coles, M. J.; Carboni, C.; Coles, H. J., A highly bistable fast-shear aligned polymer dispersed ferroelectric liquid crystal device. *Liquid Crystals* **1999,** 26, (5), 679-684.

4. de Moel, K.; Mäki-Ontto, R.; Stamm, M.; Ikkala, O.; ten Brinke, G., Oscillatory Shear Flow-Induced Alignment of Lamellar Melts of Hydrogen-Bonded Comb Copolymer Supramolecules. *Macromolecules* **2001,** 34, (9), 2892-2900.

5. Stein, P.; Aßfalg, N.; Finkelmann, H.; Martinoty, P., Shear modulus of polydomain, mono-domain and non-mesomorphic side-chain elastomers: Influence of the nematic order. *The European Physics Journal E* **2001,** 4, 255-262.

6. Ansari, I. A.; Castelletto, V.; Mykhaylyk, T.; Hamley, I. W.; Lu, Z. B.; Itoh, T.; Imrie, C. T., Hierarchical Order in a Side-Group Liquid Crystalline Block Copolymers. *Macromolecules* **2003,** 36, 8898-8901.

7. Lehmann, W.; Hartmann, L.; Kremer, F.; Stein, P.; Finkelmann, H.; Kruth, H.; Diele, S., Direct and inverse electrmechanical effect in ferroelectric liquid crystalline elastomers. *Journal of Applied Physics* **1999,** 86, (3), 1647-1652.

8. Albalak, R. J.; Thomas, E. L., Roll-Casting of Block-Copolymers and of Block Copolymer-Homopolymer Blends. *Journal of Polymer Science Part B-Polymer Physics* **1994,** 32, (2), 341-350.

9. Albalak, R. J.; Thomas, E. L., Microphase Separation of Block Copolymer Solutions in a Flow Field. *Journal of Polymer Science Part B-Polymer Physics* **1993,** 31, (1), 37-46.

10. Zheng, W. Y.; Albalak, R. J.; Hammond, P. T., Mesogen Orientation within Smectic C* Side Chain Liquid Crystalline Diblock Copolymers. *Macromolecules* **1998,** 31, (8), 2686-2689.

11. Moment, A. The Synthesis and Characterization of Polystyrene Liquid Crystalline Siloxane Block Copolymers. Doctoral, Massachusetts Institute of Technology, Cambridge, MA, 2000.

12. Anthamatten, M. L. Massachusetts Institute of Technology, Cambridge, MA, 2001.

13. Zheng, W. Y.; Hammond, P. T., Phase Behavior of New Side Chain Smectic C* Liquid Crystalline Block Copolymers. *Macromolecules* **1998,** 31, (3), 711-721.

14. Hamley, I. W., Nanotechnology with Soft Materials. *Angewandte Chemie, International Edition* **2003,** 42, 1692-1712.

15. Mitov, M.; Bourgerette, C.; de Guerville, F., Fingerprint patterning of solid nanoparticles embedded in a cholesteric liquid crystal. *Journal of Physics: Condensed Matter* **2004,** 16, S1891-S1988.

16. Hamley, I. W.; Castelletto, V.; Lu, Z. B.; Imrie, C. T.; Itoh, T.; Al-Hussein, M., Interplay between Smectic Ordering and Microphase Separation in a Series of Side-Group Liquid-Crystal Block Copolymers. *Macromolecules* **2004,** 37, (13), 4798-4807.

Chapter 6 – Conclusions and Future Project Directions

Summary of Current Research

In this research, the potential for ferroelectric and nematic actuation in elastomeric liquid crystal block copolymers was studied. First, PS-PVMS-PS triblock copolymer synthesis techniques were examined and diblock coupling was successfully used to make one triblock copolymer. In addition, PVMS homopolymers and PS-PVMS diblock copolymers were synthesized for comparison. Four achiral and three chiral mesogens were attached to polymer backbones of varying molecular weight and composition.

In block copolymers functionalized with achiral and chiral mesogens, the only morphology observed was PS cylinders in a LCP matrix. The shorter spacers were shown to exhibit the most desirable phase segregation for such applications (i.e. $\chi_{PS\text{-}LCP}$ decreases as spacer length decreases). In addition, the LC clearing point increased as the mesogen spacer length decreased and, in PS27-LCP_{4BPP4}79, the material actually degraded before the LC clearing point was reached. Such stabilization in the LC phase was enhanced by the observed well-ordered and strongly segregated cylindrical morphology in that sample. LC phases were also stabilized by in PS27-LCP_{8BPP4}108 and in PS27-LCP_{4MPOB}84, as observed by the ~40°C increase in LC clearing point in the BCPs when compared to the clearing point of the LC mesogens.

Miscibility between the LCP and PS blocks was greater for polymers with achiral mesogens compared to those functionalized with chiral mesogens. It was also noted that the polymers functionalized with achiral mesogens formed viscous liquids when the LCP weight fraction was greater than ~85wt%. Therefore, the initial goal of a BCP with ~80wt%-90wt% LCP block is

too large for these systems. Such a limit on LCP size was not observed for polymers functionalized with chiral mesogens based on the materials that were studied.

In polymers with chiral mesogens, the shorter spacers led to more rigid materials, which was undesirable. This increase in rigidity with a decrease in spacer length could be influenced by the overall size of the polymer as well as the LCP composition in the polymer. Therefore, future studies should consider polymers that are larger and/or contain a LCP block that is a larger fraction of the total polymer size.

The final studies in this project included attempting various techniques to process polymers functionalized with chiral mesogens. In stretching and shearing experiments on the elastomeric PS18-LCP_{10BPB4}248-PS18, it was shown that the LC alignment can be mechanically manipulated as observed in POM. Stretching, annealing, and shearing studies on the more rigid PS27-LCP_{4BPP4}79 indicated that it was difficult to both obtain BCP order and LC alignment after processing. In high-temperature stretching studies, the LC mesogens were observed to align parallel to the PS cylinders based on WAXS data. However, high temperatures adversely affected the BCP order. A focal conic texture developed in the BCP morphology, which was indicative of a smectic phase that developed during processing or upon cooling. Other samples exhibited focal conic textures when observed in TEM, but did not exhibit LC alignment in WAXS studies.

Future Directions

While this project has made significant strides toward determining a material that can be used as an actuator, some tasks are remaining before that goal can be realized. Using the same polymer backbone and mesogens, additional processing techniques as well as ferroelectric and piezoelectric measurements must be done. Since phase segregation was not ideal in any system, studying different backbones and the synthesis of well-defined PS-PVMS-PS triblock have also been considered. In addition to changing the backbone, investigating new mesogens should be considered because alternatives have been reported that exhibit higher P_S values and broad S_C^* phases. Finally, molecular modeling of the materials will be an option in order to better understand and predict the affect of backbone and mesogen variations on the final properties (i.e. structure-property relationships).

Processing Methods

As discussed in Chapter 5, processing studies have begun on one of functionalized polymers. While some promising results were observed, none of the techniques was able to both orient the BCP morphology and align LC mesogens was determined. In addition to continuing studies on shearing and annealing, there are three techniques that are currently under consideration in order to accomplish this: roll-casting, extruding, and embedding of nanoparticles.

Roll-casting[1] – This technique was discussed in Chapter 1 and a diagram was given in Figure 1.13. This diagram is reprinted in Figure 6.1.

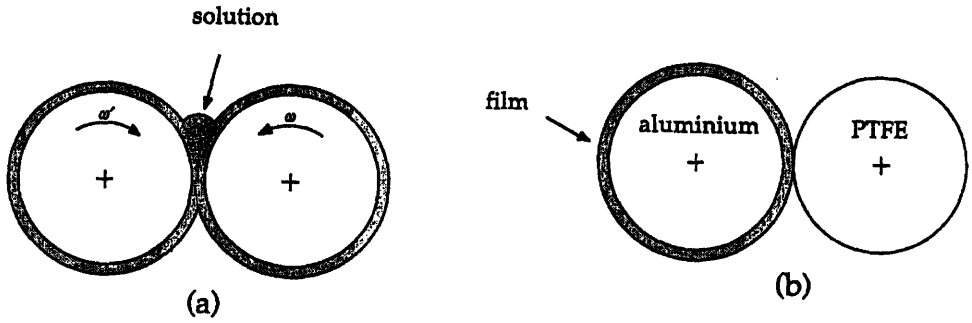

Figure 6.1: Diagram of the roll-cast technique[1]

The roll-cast technique was developed in the Thomas Lab[1, 2] of the Materials Science and Engineering Department and has been used in previous studies in our group[3]. This technique has been shown to produce phase segregated materials that are grainless. While initial studies on this technique were attempted in this project, suitable materials were not produced due to the small quantity of material available and the choice of solvent. Therefore, before roll-casting is attempted again, a larger amount of material must be synthesized. Additionally, a suitable roll-casting solvent must be determined.

Extrusion – In this technique, a polymer melt is pushed through a die and cooled. This will form a sheet in the shape of the die opening. Figure 6.2 shows the die that was fabricated by the machine shop for this purpose.

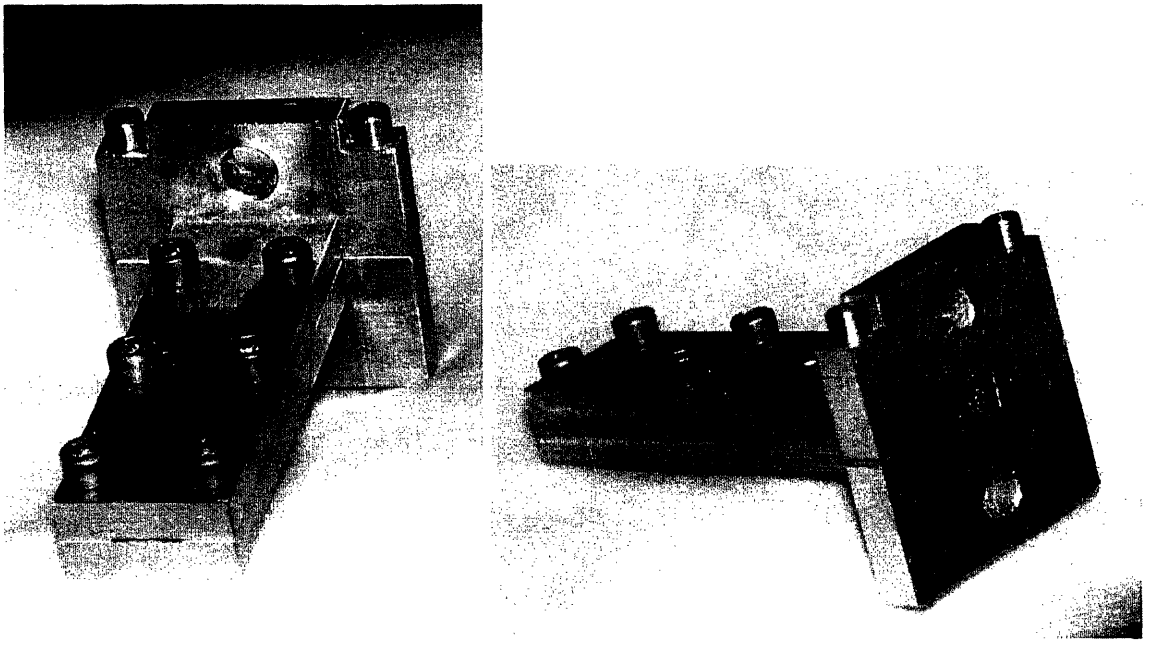

(a) (b)

Figure 6.2: Pictures of the (a) outlet and (b) inlet of the extrusion die that has been made

Previous studies with this technique have shown that it is very successful at orienting the BCP morphology and aligning the LC mesogens[4]. For our purposes, the S_C* LC mesogens must align parallel to the PS cylinders (i.e. smectic layers are perpendicular to the cylinders). Initial studies using the previously shown die and equipment in the Cohen Lab indicate that in the extruded PS27-LCP_{4BPP4}79 the proper BCP ordering and LC alignment are achieved. However, future work on determining the proper temperature and flow rate are necessary to optimize the process.

Embedding Nanoparticles – In addition to mechanical ordering and alignment of the BCP and LC mesogens, some groups have used the addition of particles to the BCP in order to enhance actuator properties. Recently, Courty, et al.[5], reported the use of carbon nanotubes in nematic actuators as a method to increase the electromechanical strain. In these studies, CNT concentrations of ~0.01% have been shown to enhance the material properties. Therefore, the

use of similar embedded nanoparticles in the LC BCPs studied in this project could allow for larger LC anisotropy in the system and stronger ferroelectric properties.

Ferroelectric and Piezoelectric Measurements

In order for the polymers synthesized to be useful in actuator-type applications, they must exhibit ferroelectric properties. Ferroelectric tested was initially planned for this project. However, the LC mesogens must first be aligned and such alignment was not achieved in the current systems. Therefore, future work must include such studies. Standard techniques for measuring electro-optical properties may be used to determine whether the materials exhibit ferroelectric properties and, if so, what the switching speed is.

Since these materials are being studied for use as actuators, it is especially important that the materials exhibit piezoelectric properties. Specifically, it is necessary for the LC material to produce a strain upon application of an electric field in order for the material to flex in actuator applications. There is no standard technique for studying piezoelectric properties. Therefore, the first step in this process was to develop a technique based on what other groups have used. The initial idea was something similar to the setup shown in Figure 6.3.

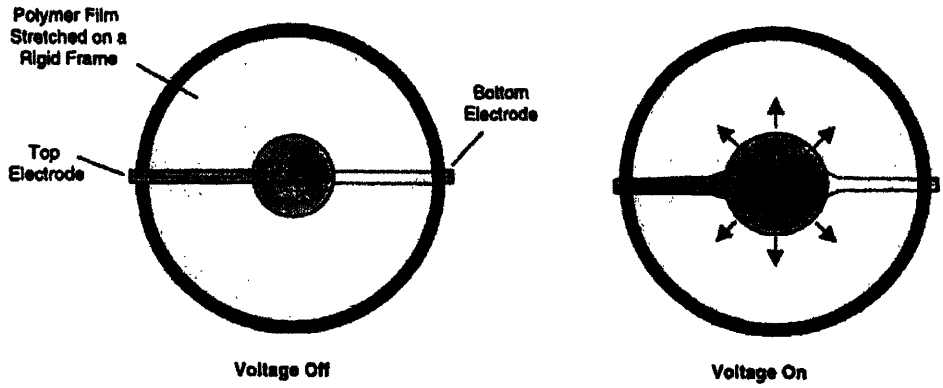

Fig. 2. Experimental setup (top view).

Figure 6.3: Initial concept for piezoelectric measurement equipment[6]

For this measurement a disk of the polymer would be placed in a larger circular dish. A voltage could then be applied to the polymer and the amount of strain can be measured.

Through the ISN, researchers on this project learned about the Hunter Group and their techniques for measuring actuator properties. In their studies, an electrode-equipped DMA has been used to study actuator properties of conductive polymers in electrolyte solution. In this technique, the electrical field can be controlled externally and the mechanical deformation of the material can be measured very accurately. While this setup is not suitable for the LC BCPs studied in this research, a modified version that can be used on small solid polymeric films in air will be used for the initial piezoelectric studies on our materials.

Polymer Backbones

While studies of PS-PVMS-PS-based LC BCPs has begun and results from polymers using this backbone were reported, a technique to routinely synthesize such polymer backbones was not determined. Therefore, only one triblock backbone was used in the current studies. As

previously described in Chapter 2, the triblock was synthesized using anionic polymerization and diblock coupling. However, recently a technique was developed in which a difunctional PVMS homopolymer is synthesized and terminated using an endgroup that can be used to terminate a living PS chain. While improvements are still being made, this technique appears very promising and has already been used to synthesize PS-PVMS-PS triblock copolymers.

One of the initial ideas for this project was to investigate the effect on end properties caused by variations on the polymer backbone. In such a study, the amorphous block or the LC block may be varied. The polyacrylate backbone for the LC block was considered because the technique was already known to this group[7,8]. The T_g of polyacrylate is above room temperature, so it is expected that the properties with this backbone will be noticeably different from the properties of the polymers with the very low T_g PVMS backbone.

In previous studies, such polymers did not exhibit properties that were as desirable as those for the PS-PVMS-based LC BCPs. Therefore, this backbone variation was not attempted. However, the idea of using a polymethacrylate backbone for the amorphous block was recently considered. In this case, the LCP backbone could still be PVMS and the high-T_g/low-T_g combination would be maintained. However, by changing the amorphous block, a different type of ordering and level of phase segregation could be achieved.

Since only one polymer sample in the current study exhibited significant phase segregation and BCP ordering, studies on other amorphous blocks in LC BCPs could allow for enhanced BCP and LC properties. Watanabe[9] reported observing a significant change in transition temperatures when amorphous blocks of various T_g values were studied with the same LC block. Using a low T_g amorphous block proved to bring about electro-optic properties in a study by Hikmet[10]. However, a low-T_g block would adversely impact mechanical properties. Therefore, it

would be interesting to determine the impact that variations in the amorphous block would have on the polymers in this study.

Through the MIT Institute for Soldier Nanotechnologies, a collaboration has developed between this project and a project in the Schrock group in the MIT Chemistry Department. This project seeks to use ring-opening metathesis polymerization to synthesize a methyltetracyclododecene-polynorbornene backbone with side-chain LC mesogens attached to the polynorbornene. Structures of the ROMP initiator and the polymer are shown in Figure 6.4.

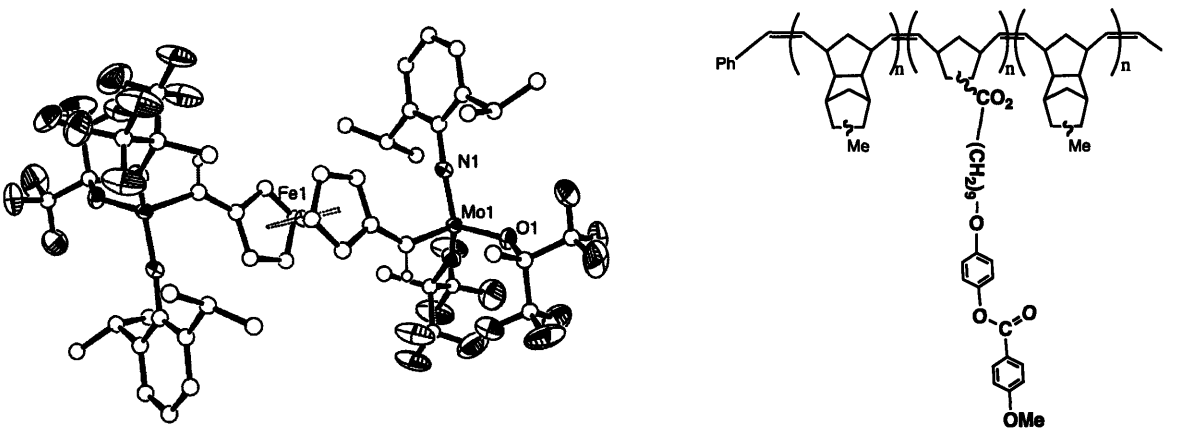

(a) (b)

Figure 6.4: (a) ORTEP plot of $[(R_{F6}O)_2(ArN)MoCH_2(C_5H_4)]_2Fe$ difunctional initiator. (b) ABA triblock copolymer synthesized where A = methyltetracyclododecene (MTD), B = monomer with liquid crystal mesogen

Initial studies on this type of LC BCP indicate favorable properties. The polymer is extensible (~100% strain before break) and exhibits strong phase segregation as observed in DSC. SAXS and TEM studies have yet to be done in order to better quantify and qualify BCP phase segregation and morphology.

Mesogens

While the chiral mesogens studied in this project exhibit P_S values that are significantly higher than those in Moment's work[11], mesogens with even higher P_S values have been reported. Therefore, in future studies, those mesogens should be considered as a way to obtain a quicker and larger ferroelectric or piezoelectric response. As mentioned in Chapter 2, the Cooray group[12] developed a mesogen with a higher P_S than the values for the mesogens studied in this project.

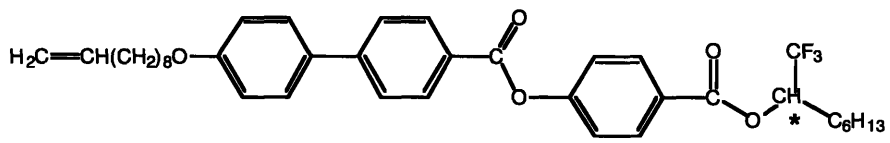

Siloxane Homopolymer Studies:

M_n=7000 PDI=1.1 τ=0.51ms (T=T_c-10°C=90.3°C)

Phases observed: P_s=122nC/cm^2 (T=T_c-30°C=70.3°C)

I 134.8 S_A 100.3 S^*_C <20

Figure 6.5: Cooray ferroelectric mesogen[12]

In this mesogen, the enhanced P_S value is caused in part by the trifluoromethyl group attached to the chiral center.

In addition to the Cooray mesogen, in research by the Svensson group[13] mesogens with $-NO_2$ groups have been studied. These mesogens are similar to the 8BPP4 and 4BPP4 mesogens studied in this project.

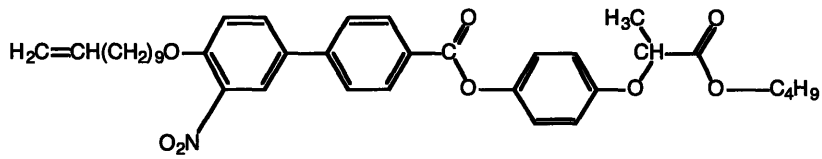

Figure 6.6: Svensson mesogen with nitro substituent[13]

This mesogen exhibits a very high P_S value in small molecule studies (~700nC/cm^2). Therefore, it is expected that it would enhance the ferroelectric and piezoelectric properties of materials studied in this project. Alternately, some studies have shown that using dopants can increase the P_S value in a ferroelectric liquid crystal[14-16]. Therefore, using the same mesogens that were studied in this project, higher P_S values could be possible using suitable dopants.

Molecular Modeling of LC BCPs

Previous studies in this group have developed a model for predicting morphologies in LC-amorphous block copolymers[8, 17]. While initial ideas for this project included using that model, due to time constraints this did not happen. However, some initial studies using the Biosym software package were done in order to determine interaction parameters between the PS block and the LCP block in the currently studied LC BCP systems. These studies allowed us to treat one polymer as the solvent and the other an as unconnected polymer in the solvent. However, this is not the actual situation and will not allow for the proper interfacial effects that are used to stabilize the BCP morphology and LC alignment.

Therefore, in future modeling studies, it could be beneficial to develop a collaboration with another group at MIT or elsewhere that regularly does molecular modeling and simulations of similar polymeric materials. Such modeling could aid in the molecular understanding of certain observations, such as miscibility and phase transitions. Additionally, since the amount of

mesogen has been the limiting factor in the amount of materials available to study, modeling could minimize the number of samples that would be studied because it would narrow down the region of interest in the phase diagram.

References

1. Albalak, R. J.; Thomas, E. L., Roll-Casting of Block-Copolymers and of Block Copolymer-Homopolymer Blends. *Journal of Polymer Science Part B-Polymer Physics* **1994,** 32, (2), 341-350.

2. Albalak, R. J.; Thomas, E. L., Microphase Separation of Block Copolymer Solutions in a Flow Field. *Journal of Polymer Science Part B-Polymer Physics* **1993,** 31, (1), 37-46.

3. Zheng, W. Y.; Albalak, R. J.; Hammond, P. T., Mesogen Orientation within Smectic C* Side Chain Liquid Crystalline Diblock Copolymers. *Macromolecules* **1998,** 31, (8), 2686-2689.

4. Phatak, A.; Macosko, C. W.; Bates, F. S.; Hahn, S. F., Extrusion of triblock and pentablock copolymers: Evolution of bulk and surface morphology. *Journal of Rheology* **2005,** 49, (1), 197-214.

5. Courty, S.; Mine, J.; Tajbakhsh, A. R.; Terentjev, E. M., Nematic elastomers with aligned carbon nanotubes: New electromechanical actuators. *Europhysics Letters* **2003,** 64, (5), 654-660.

6. Pelrine, R.; Kornbluh, R.; Joseph, J.; Heydt, R.; Pei, Q.; Chiba, S., High-field deformation of elastomeric dielectrics for actuators. *Materials Science and Engineering C* **2000,** 11, 89-100.

7. Zheng, W. Y.; Hammond, P. T., Phase Behavior of New Side Chain Smectic C* Liquid Crystalline Block Copolymers. *Macromolecules* **1998,** 31, (3), 711-721.

8. Anthamatten, M. L. Massachusetts Institute of Technology, Cambridge, MA, 2001.

9. Yamada, M.; Itoh, T.; Hirao, A.; Nakahama, S.-I.; Watanabe, J., Side-chain LC block copolymers with well defined structures prepared by living anionic polymerization. 2: Effect of the glass transition temperature of amorphous segments on the phase behavior and structure of the LC segment. *High Performance Polymers* **1998,** 10, 131-138.

10. Omenat, A.; Hikmet, R. A. M.; Lub, J.; van der Sluis, P., Synthesis, Characterization, and Physical Properties of New Ferroelectric Liquid Crystalline Materials: Block Copolymers. *Macromolecules* **1996,** 29, (21), 6730-6736.

11. Moment, A. The Synthesis and Characterization of Polystyrene Liquid Crystalline Siloxane Block Copolymers. Doctoral, Massachusetts Institute of Technology, Cambridge, MA, 2000.

12. Cooray, N. F.; Kakimoto, M.; Imai, Y., Novel Fluorine-Containing Ferroelectric Side Chain Liquid-Crystalline Polysiloxanes Showing Bistable Fast Switching. *Macromolecules* **1994,** 27, (6), 1592-1596.

13. Svensson, M.; Helgee, B.; Sharp, K.; Andersson, G., Effects of nitro substituents on the properties of a ferroelectric liquid crystalline side chain polysiloxane. *Journal of Materials Chemistry* **1998,** 8, (2), 353-362.

14. Hartley, C. S.; Wang, R. Y.; Lemieux, R. P., Ferroelectric liquid crystals induced by atropisomeric bipheyl dopants: Correlation between the sign of induced polarization and the absolute configuration. *Chemistry of Materials* **2004,** 16, (25), 5297-5303.

15. Hartley, S.; Lemieux, R., Ferroelectric liquid crystals induced by atropisomeric bipheyl dopants: the effect of chiral perturbations on achiral dopants. *Liquid Crystals* **2004,** 31, (8), 1101-1108.

16. Maly, K. E.; Zhang, P.; Wand, M. D.; Buncel, E.; Lemieux, R. P., Reversible photocyclization of achiral dithienylperfluorocyclopentene dopants in a ferroelectric liquid crystal: bistable SSFLC photoswitching. *Journal of Materials Chemistry* **2004,** 14, (18), 2806-2812.

17. Anthamatten, M. L.; Hammond, P. T., Free-energy model of asymmetry in side-chain liquid-crystalline diblock copolymers. *Journal of Polymer Science Part B-Polymer Physics* **2001,** 39, (21), 2671-2691.